

*“To my dear parents and you who helped!”*

**“献给我亲爱的父母及所有帮助过我的你们！”**

## ACKNOWLEDGEMENT

Any words that I write will not be sufficient to express the gratitude that I feel towards those who have encouraged me, believed in me, inspired me, and stayed by my side. This has not always been easy.

I am most thankful to my supervisor Prof. Jakub Wiener for his guidance, support and encouragement. My gratitude for his leadership, enormous patience, kindness, and trust is immense. I would also like to thank Dr. Rajesh Mishra and my co-supervisor Dr. Jaromír Marek for their kind advice and guidance.

My thanks to Dr. Dana Křemenáková the, Dean Dr. Jana Drašarová, Vice Dean Dr. Gabriela Krupincová and Dr. Pavla Těšínová for their continuous support. I thank Ing. Hana Musilová Bohumila Keilová Kateřina Štruplová, Kateřina Nohýnková, and Ing. Hana Cesarová Netolická for always being there helping. Thanks also to my lab mates with whom I have fulfilled all my experiments and measurements correctly. I am grateful to SGS grants (2013 - 48012 & 2014 - 21040) for providing funding for my study.

Thank you to my parents who instilled in me a strong sense of the importance of doing something you can be proud of, and the discipline to do it. Thank you, Mom, for believing I can do anything, pushing me to become a better me. Thank you, Dad, for your steadfast support throughout this transformation process to a PhD. You are the best parents in the world. No doubt.

Special thanks to all my friends here who give friendship meaning beyond measure.

And last, but certainly not least, thank you Prof. Jiří Militký. Thank you for always supporting me at very difficult points, imagining that I could do this, and taking me in. I cannot thank you more for your continuous support at the various stages of my life here at TUL.

There are so many people who reached out their hands while I needed still left unnamed here, thank you all with all my heart.

## ABSTRACT

Since first synthesized and introduced in 1935, the polyamides' production quantities grow tremendously and polyamides' applications increased numerously. Polyamide 6 fibers are one of the widely used synthetic fibers in textile area due to its outstanding properties. As a sorbent to dyes, heavy metal ions, pesticides etc., the adsorption properties of polyamide 6 fibers assemblies have been studied for some extent. However, as the rapid development of nanotechnology including both electrospinning and nanoparticles technologies is changing people's life in all areas, how does nanofibers assembly behavior became an important question. A systematical study for adsorption properties of polyamide 6 nanofibers assembly will be realized in this work.

Prior to initiation of research, a detailed literature review was conducted to understand and identify their gaps to address in this work. The theories of solid-liquid sorption, thermodynamics, and photocatalysis were studied, the application of polyamide nanofibers and Titanium dioxide nanoparticles were reviewed. This comparison of dye removing methods was expected to provide insights into optimal conditions for dye removal.

In this work, nanotechnologies including electrospun nanofibers and nanoparticles were implemented for further study of adsorption properties of polyamide 6 nanofibers assembly. Dye was chosen to be a model as the sorbed material for investigating the adsorption properties. Dye static and dynamic sorption properties of polyamide 6 nanofibers assembly were detected, kinetic and thermodynamic considerations were studied, and Titanium dioxide nanoparticles deposition and steam process were applied as surface modification methods for polyamide 6 nanofibers.

Static sorption and thermodynamics study revealed that Langmuir isotherm and Pseudo-second order equations fitted the sorption experimental data well, and the sorption process of acid dye on polyamide 6 nanofibers assembly was a feasibility, spontaneous, entropy-driven, and sorption. Steam treatment with temperature over 120 °C encouraged the static sorption of acid dyes on polyamide 6 nanofibers assembly.

Dynamic sorption study showed that nanofibers have superior dye removal properties than conventional fibers, and hormone and dye sorption capacity of polyamide 6 nanofibers showed a positive relationship with the specific surface area.

TiO<sub>2</sub> nanoparticles photocatalysis self-cleaning treatment with concentration over 18 mg/m<sup>2</sup> and over 90 minutes under UV light could help improving the dye self-cleaning effect, and TiO<sub>2</sub> nanoparticles photocatalysis was proved to be one method for improving the dynamic sorption capacity of Acid Orange 7 on polyamide 6 nanofibers. Decolorization of wastewater containing soluble dyes would be one of the potential applications for this method.

**Keywords:** Sorption; Nanofibers; Dye; Surface modification

## ABSTRAKT

Polyamidy byly syntetizovány poprvé v roce 1935 a od té doby jejich počet i výroba prudce roste. Vlákna z polyamidu 6 jsou v důsledku svých vynikajících vlastností jedním z široce používaných syntetických vláken v textilní oblasti. Vlákna z polyamidu 6 jsou studována jako sorbenty barviv, iontů těžkých kovů, pesticidů atd. Nicméně s růstem rychlosti rozvoje nanotechnologií, včetně elektrického zvláknování a dalších technologií přípravy nanočástic, se mění život lidí ve všech oblastech a chování nanovláknenných soustav se stává důležitou otázkou. Systematický výzkum sorpční vlastnosti systémů polyamidových nanovláken je podstatou této práce.

Před začátkem výzkumu byl proveden podrobný přehled literatury, pro identifikaci mezer v současných znalostech této problematiky, které budou doplněny v této práci. Byly studovány zejména teorie sorpce v systémech tuhá látka-kapalina, termodynamika sorpce, fotokatalýza, použití polyamidových nanovláken a nanočástic oxidu titaničitého. Zejména při využití sorpce a fotokatalýzy se očekává, že umožní optimální odstranění organických látek z vodných systémů.

V této práci byly nanotechnologie implementovány do reálné studie adsorpčních vlastností soustav nanovláken na bázi polyamidu 6. Jako modelový sorbent pro sledování adsorpčních vlastností bylo vybráno organické barvivo. Byly stanoveny statické a dynamické sorpční vlastnosti soustavy nanovláken z polyamidu 6, byly využity kinetické a termodynamické modely, depozice nanočástic oxidu titaničitého a parní aktivace polyamidových nanovláken.

Statická sorpční studie odhalila, že termodynamická Langmuirova izoterma a kinetická rovnice pseudodruhého řádu dobře vyhovuje při popisu sorpce pro experimentální data ze spontánní sorpčního procesu kyselého barviva do struktury nanovláken z polyamidu 6. Parní aktivace polyamidu při teplotě nad 120°C vedla ke zvýšení statické sorpce kyselého barviva do soustavy nanovláken z polyamidu 6.

Studie dynamické sorpce ukázala, že nanovláknena mají lepší sorpční vlastnosti vůči barvivům barviva než konvenční vlákna. Sorpční kapacita nanovláken z polyamidu 6 vůči hormonům i barvivům vykazovaly přímou úměru ke specifickému povrchu vláken.

Fotokatalytické nanočástice  $\text{TiO}_2$  vykazovaly samočisticí schopnosti při koncentraci

nad  $18 \text{ mg/m}^2$  a době ozařování UV světlem vyšší než 90 minut. Sorpce barviva do nanovlákného sorbentu ovlivnila samočisticí efekt a fotokatalytické  $\text{TiO}_2$  nanočástice se ukázaly být jednou z metod pro zlepšení snížení koncentrace barviva Acid Orange 7 v roztoku. Odbarvování odpadní vody s obsahem rozpustných barviv by být jedním z možných aplikací této metody.

**Klíčová slova:** sorpční; nanovlákná; barvivo; povrchová úprava

## TABLE OF CONTENTS

<b>CHAPTER 1. INTRODUCTION.....</b>	<b>17</b>
1.1 BACKGROUND.....	17
1.2 OBJECTIVES AND SOLUTIONS .....	17
<b>CHAPTER 2. LITERATURE REVIEW.....</b>	<b>19</b>
2.1 CHARACTERIZATION OF POLYAMIDE 6.....	19
2.1.1 Formation of polyamide 6.....	19
2.1.2 Application of polyamide 6 .....	20
2.2 STUDY OF ADSORPTION .....	21
2.2.1 Definitions.....	21
2.2.2 Types of adsorption.....	23
2.2.3 Application of adsorption principles.....	23
2.2.4 Adsorption on nanofibers assembly.....	24
2.2.5 Adsorption modes of solid-gas & solid-liquid interface.....	24
2.2.6 Kinetics .....	28
2.2.7 Thermodynamics.....	31
2.3 NANOTECHNOLOGY .....	32
2.3.1 Electrospinning technology .....	32
2.3.2 Nanoparticle technology .....	35
2.3.3 Surface modification for nanofibrous membrane .....	38
2.3.4 Nanophotocatalysis .....	38
<b>CHAPTER 3. MATERIALS AND METHODS.....</b>	<b>41</b>
3.1 MATERIALS AND APPRATUS .....	41
3.1.1 Sorbent .....	41
3.1.2 Sorbed material .....	48
3.1.3 Other materials.....	51
3.2 DYNAMIC SORPTION STUDY APPARATUS ASSEMBLING .....	51
3.2.1 Vacuum sorption apparatus .....	51
3.2.2 Constant influent apparatus.....	52
3.2.3 On-line testing constant flow apparatus.....	53
3.2.4 Dynamic sorption photocatalysis apparatus.....	54
3.2.5 Crossflow dynamic sorption apparatus .....	55

3.3	METHODS .....	55
3.3.1	Batch experimental methods.....	55
3.3.2	Dynamic sorption experimental methods .....	57
3.3.3	Surface modification methods .....	58
<b>CHAPTER 4. RESULT AND DISCUSSION .....</b>		<b>61</b>
4.1	ANALYSIS OF DYE SORPTION ONTO POLYAMIDE 6 NANOFIBROUS MEMBRANE....	61
4.1.1	Factors influencing sorption of dyes by polyamide 6.....	61
4.1.2	Equilibrium modeling .....	65
4.1.3	Kinetic modeling.....	69
4.1.4	Thermodynamic considerations .....	74
4.2	ANALYSIS OF DYNAMIC SORPTION.....	76
4.2.1	General comparison on dynamic sorption efficiency .....	76
4.2.2	Factors influencing dye sorption capacity and fouling of PNM .....	81
4.3	SURFACE MODIFICATION ON POLYAMIDE 6 NANOFIBROUS MEMBRANE .....	89
4.3.1	Steam treatment .....	89
4.3.2	Nanophotocatalysis to implement self-cleaning of PNM .....	91
4.3.3	Dynamic sorption process with nanophotocatalysis .....	99
<b>CHAPTER 5. CONCLUSIONS .....</b>		<b>103</b>
<b>REFERENCES.....</b>		<b>105</b>
<b>RESEARCH OUTPUTS .....</b>		<b>117</b>



## LIST OF SYMBOLS AND ABBREVIATIONS

Symbol	Unit	Description
$a$	mg/(g min)	initial sorption rate
$A$	1/s	Arrhenius factor
$A_S$	--	slope
$b$	g/mg	desorption constant
$c$	--	BET constant
$C_A$	mol/g	amount of sorbed material on sorbent of the solution at equilibrium
$C_L$	mg/L	remained solution concentration
$C_S$	mg/L or mol/L	equilibrium concentration of the sorbed material in the solution
$E_1$	J	heat of adsorption for the first layer
$E_a$	kJ/mol	Arrhenius activation energy of adsorption
$E_{bg}$	--	band gap energy
$e_{cb}^-$	--	conduction band electrons
$E_L$	J	heat of adsorption for the second and higher layers
$\Delta G^\circ$	kJ/mol	Gibbs free energy change
$\Delta H^\circ$	kJ/mol	enthalpy change
$h_{vb}^+$	--	valence band holes
$I$	--	y-intercept
$k_2$	g/(mmol min)	rate constant of pseudo-second order sorption
$K_C$	--	sorption equilibrium constant
$K_f$	(mg/g)(L/g) <sup>n</sup>	constant of Freundlich isotherm
$K_L$	L/mg	affinity between sorbed material and sorbent
$m$	mg or g	mass
$N$	1/mol	Avogadro's number
$1/n$	--	heterogeneity factor
$p$	Pa	pressure
$p_0$	Pa	gas pressure required for saturation
$q_0$	mg/g	maximum amount of dye adsorbed
$q_{cal}$	mg/g or mmol/g	predicted data
$q_e$	mmol/g	adsorption capacity at equilibrium

$q_{\text{exp}}$	mg/g or mmol/g	experimental data
$q_t$	mg/g or mmol/g	adsorption capacity at time $t$
$R$	J/(mol K)	gas constant, equals to 8.314.
$R^2$	--	square of correlation coefficient
$R_l^2$	--	square of correlation coefficient of linear regression fitting
$s$	$\text{m}^2$	adsorption cross section of the adsorbing species
$\Delta S^\circ$	J/(mol K)	entropy change
$S_{\text{BET}}$	$\text{m}^2/\text{g}$	specific surface area
$S_{\text{total}}$	$\text{m}^2$	total surface area
$t$	min	time
$T$	K or $^\circ\text{C}$	solution temperature
$v$	mL	gas volume adsorbed at pressure $p$
$V$	$\text{m}^3/\text{mol}$	molar volume of Nitrogen gas
$v_m$	mL	volume of gas required for a single molecular layer over the entire adsorbent surface

<b>Abbreviation</b>	<b>Description</b>
AA	Ascorbic acid or the samples prepared with ascorbic acid
AB41	C.I. Acid Blue 41
Ag	Silver
AO7	C.I. Acid Orange 7
AR73	C.I. Acid Red 73
Au/Pd	Gold/Palladium
AY11	C.I. Acid Yellow 11
AY36	C.I. Acid Yellow 36
BB	Samples prepared without ascorbic acid
BET	Brunauex-Emmett-Teller
Cd	Cadmium
CuO	Copper oxide
DSC	Differential scanning calorimetry
ED	17 $\beta$ -Estradiol
FTIR	Fourier transform infrared spectroscopy
HCl	Hydrochloric acid
HEPA	High-efficiency particulate air filter
MgO	Magnesium oxide

NaOH	Sodium Hydroxide
NPsUV	Sample treated with nanoparticles and UV light
NpslUV	Sample treated with nanoparticles and longtime UV light
P	Pollutant
PAN	Polyacrylonitrile
PNM	Polyamide 6 nanofibrous membrane
SB	Spunbond nonwoven
SEM	Scanning electron microscopy
<i>SSE</i>	Sum of error squares
<i>SST</i>	Sum of total error square
TiO <sub>2</sub>	Titanium dioxide
UV	Ultraviolet or sample treated with only UV light
UV-Vis	Ultraviolet-visible spectroscopy
W	Woven fabrics
ZnO	Zinc oxide

## LIST OF FIGURES

Fig. 2-1 Basic terms of adsorption [36].	22
Fig. 2-2 Characteristic adsorption isotherms [56].	25
Fig. 2-3 Schematic diagram of set up of electrospinning apparatus: a) typical vertical set up; b) horizontal set up of electrospinning apparatus [82].	33
Fig. 2-4 Electrospun nanofibers and mats application fields: a) targeted by US patents; b) potential applications of electrospun polymer nanofibers [83].	34
Fig. 2-5 Illustration demonstrating the effect of the increased surface area provided by nanostructured materials [92].	35
Fig. 2-6 Major photocatalytic pathways of C.I. Acid Orange 7, a representative azo dye for phenyl-azonaphthol chemical group, based on the identification of by-products from previous reported degradation studies [104-106].	37
Fig. 2-7 Photo-induced formation mechanism of electron-hole pair in a semiconductor TiO <sub>2</sub> particle with the presence of water pollutant (P) [125].	39
Fig. 3-1 SEM images of nanofibrous membranes surface.	42
Fig. 3-2 SEM images of nanofibrous membranes cross section.	43
Fig. 3-3 BET testing result of polyamide 6 nanofibrous membranes. a) BET plots of two membranes; b) Quantity adsorbed of Nitrogen versus relative pressure applied during BET test.	44
Fig. 3-4 FTIR spectrum of polyamide nanofibrous membranes.	45
Fig. 3-5 Heat flow endo result from DSC test.	45
Fig. 3-6 Chemical structures of polyamide 6 (a) and polyacrylonitrile (b).	46
Fig. 3-7 SEM images of filters: a) PNM with areal density of 0.5 g/m <sup>2</sup> , b-f) SB with areal density of 20, 40, 50, 70, and 100 g/m <sup>2</sup> ; g) PAN with areal density of 0.4 g/m <sup>2</sup> .	48
Fig. 3-8 The molecular structures of selected dyestuffs.	49
Fig. 3-9 Light absorbance spectrum in wavelength of AY11, AY36, AR73, and AB41.	50
Fig. 3-10 Light absorbance of different dye solution concentrations and the function of linear fitting for each dye.	50
Fig. 3-11 Dynamic sorption unit used for sorption study on nanofibrous membrane: 1) funnel; 2) sorbent; 3) sorbent supporting unit; 4) vacuum pressure port; 5) vacuum flask.	52
Fig. 3-12 Constant influent apparatus: a) Structure of the apparatus: 1- beaker with	

influent, 2- peristaltic pump, 3- sorbent, 4- sorbent supporting unit, 5- funnel; b) Picture of the assembled apparatus. ....	52
Fig. 3-13 On-line testing constant flow apparatus: a) the sketch of testing apparatus: 1) container with original solution; 2) & b) isocratic pump; 3) sorbent; 4) & c) sanitary in-line stainless steel holder; 5) & d) UV-Vis variable wavelength detector. ....	53
Fig. 3-14 Apparatus for dynamic sorption process with UV lighting. 1) funnel; 2) sorbent; 3) sorbent supporting unit; 4) vacuum pressure port; 5) vacuum flask; 6) container with original solution; 7) peristaltic pump; 8) UV lighting system. ....	54
Fig. 3-15 Crossflow filtration apparatus. a) Setting up method; b) Crossflow filtration unit; 1) Polypropylene (PP) web; 2) PNM1.3; 3) Glass rod. ....	55
Fig. 3-16 Spiral wound filter after using. ....	55
Fig. 4-1 PNM1.3 exhaustion of dye AB41 under different temperatures. ....	61
Fig. 4-2 The effect of initial pH on the sorption capacity of dye AB41 by PNM1.3 and PNM2.9. ....	62
Fig. 4-3 Absorbance and dye removal capacity change of dye solution by PNM sorption according to time. ....	63
Fig. 4-4 Effect of dosage of PNM1.3 on sorption capacity $C_s$ and exhaustion of AB41. ....	64
Fig. 4-5 Batch experimental data comparison between sorbents Woven and PNM1.3. ....	65
Fig. 4-6. Freundlich isotherm model applied on batch experiment results of PNM1.3: a) Freundlich isotherm linear fitting; b) The experimental data compared with Freundlich isotherm model. ....	66
Fig. 4-7 Langmuir isotherm model applied on batch experiment results of PNM1.3: a) Langmuir isotherm linear fitting; b) The experimental data compared with Langmuir isotherm model. ....	67
Fig. 4-8 Comparison among Experimental data and two isotherm models. ....	68
Fig. 4-9 Sorption capacity change of AY36 on different membranes under 30 and 50 °C. ....	69
Fig. 4-10 Elovich and Pseudo-Second Order equation fitting for comparison under different bath temperature: a) linear fitting of Elovich equation; b) linear fitting of Pseudo-Second Order equation; c) Elovich equation curve and experimental data; d) Pseudo-Second Order equation curve and experimental data. ....	72
Fig. 4-11 Elovich and Pseudo-Second Order equation fitting for comparison different	

dyestuff: a) linear fitting of Elovich equation; b) linear fitting of Pseudo-Second Order equation; c) Elovich equation curve and experimental data; d) Pseudo-Second Order equation curve and experimental data.....	74
Fig. 4-12 Arrhenius plot for the adsorption of AB41 onto PNM1.3.....	75
Fig. 4-13 Van't Hoff plots for determination of thermodynamic parameters for the adsorption of AB41 onto PNM1.3. ....	75
Fig. 4-14 Morphology of fiber mats after 1 L dye solution sorption: a) PNM1.3; b) PNM2.9; c) SB20; d) SB40; e) SB50; f) SB100.....	77
Fig. 4-15 Dye sorption capacity of PNM and SB fiber mats: (a) PNM with areal density 0.5, 1.3, and 2.9 g/m <sup>2</sup> , (b) SB with areal density 20, 40, 50, 70, and 100 g/m <sup>2</sup> ; (c) Comparison of dye sorption capacity at 5 mL and 1 L sorption among all fiber mats; (d) The curve between dye sorption capacity and volume of PNMs at the initial stage. ....	79
Fig. 4-16 Dye sorption capacity of mats with different areal densities. ....	80
Fig. 4-17 Dye sorption capacity of polyamide 6 and polyacrylonitrile. ....	81
Fig. 4-18 Accumulated mass per mass of fibrous membrane and flux changing during the dynamic sorption process with dye solution concentration 0.03 g/L: a) adsorption capacity of membranes versus volume; b) flux versus volume. ....	82
Fig. 4-19 Accumulated mass and flux changing during the dynamic sorption process by membrane with PNM1.3: a) accumulated mass versus volume; b) flux versus volume.....	83
Fig. 4-20 SEM images of PNM1.3 after dynamic sorption process: a, c, & e) first layer membrane after dynamic sorption process with concentration of 0.01, 0.02, and 0.03 g/L respectively; b, d, & f) second layer membrane after dynamic sorption process with concentration of 0.01, 0.02, and 0.03 g/L respectively. ....	85
Fig. 4-21 Absorbance curves of effluents regarding to time with different feeding dye solution concentrations: a) 0.01 g/L; b) 0.02 g/L; c) 0.03 g/L.....	86
Fig. 4-22 Dye removal rate by PNM1.3 regarding to time with different feeding dye concentrations: a) 0.01 g/L; b) 0.02 g/L; c) 0.03 g/L.....	88
Fig. 4-23 Dye removal capacity changes according to steaming temperature. ....	89
Fig. 4-24 FTIR spectra.....	90
Fig. 4-25 Surface morphology of PNM coated by TiO <sub>2</sub> nanoparticles (1000×, 10000×, 25000×).....	92
Fig. 4-26 Dye removal rate change according to TiO <sub>2</sub> nanoparticles concentration	

under different UV light treating time. ....	94
Fig. 4-27 Stain removal efficiency shown as dye removal rate at different point of UV light treating time. ....	95
Fig. 4-28 Linear regressions for samples with different concentrations of TiO <sub>2</sub> nanoparticles: a-e) 0, 9, 18, 44, and 88 mg/m <sup>2</sup> ; f) time dependent index result of all samples. ....	97
Fig. 4-29 3D plot of dye removal rate versus TiO <sub>2</sub> concentration and UV light treating time: a) samples deposited with different concentration of TiO <sub>2</sub> nanoparticles; b) samples deposited with different concentration of TiO <sub>2</sub> nanoparticles with the presence of ascorbic acid. ....	99
Fig. 4-30 Dye removed amount comparison of different samples: a) comparison among control sample, UV, and NPsUV; b) samples with different UV treating time. ....	100
Fig. 4-31 Sorption capacity comparison of different samples: a) comparison among control sample, UV, and NPsUV; b) samples with different UV treating time. ....	101

## LIST OF TABLES

Table 3-1 Testing results from BET test on two nanofibrous membranes. ....	44
Table 3-2 Description of samples with different areal densities used in this experiment. .....	46
Table 3-3 Physical and chemical characteristics of 17 $\beta$ -estradiol. ....	48
Table 3-4 The physical and chemical characteristics of selected dyestuffs. ....	51
Table 3-5 Sample code of TiO <sub>2</sub> nanoparticles deposited onto PNM1.3. ....	59
Table 3-6 Sample code of dynamic sorption experiment with TiO <sub>2</sub> nanophotocatalysis. .....	59
Table 4-1 Equilibrium isotherm constants at room temperature.....	68
Table 4-2 Result comparison about bath temperature of linear Elovich and Pseudo-second order equation fitting.....	70
Table 4-3 Result of linear Elovich equation and Pseudo-second order equation fitting on PNM2.9 under 50 °C.....	72
Table 4-4 Thermodynamic parameters of AB41 dye adsorption on PNM1.3. ....	75
Table 4-5 17- $\beta$ Estradiol dynamic sorption result by PNM with different areal densities.....	76
Table 4-6 Dye removal values comparison while the dynamic sorption process reaches 13 minutes.....	88
Table 4-7 Scanning images of UV treated samples with different treating time-AA group. ....	93
Table 4-8 Scanning images of UV treated samples with different treating time-BB group. ....	93



## CHAPTER 1. INTRODUCTION

### 1.1 BACKGROUND

All thermoplastic polyamides are characterized by excellent toughness and flexibility at low temperature in the absence of plasticizer, low density, high dimensional stability, ease of conventional thermoplastic processing, good chemical resistance, good environmental stress cracking resistance, good elastic recovery, and good dynamic properties [1]. Therefore, polyamides are widely used in many areas such as: technical parts, bearings, gear wheels, rollers, screws, gaskets, fittings, coverings, housings, automotive parts, houseware, sports goods, membranes, foils, packing, blow-molded parts, fibers, tanks [2].

Polyamide 6, whose main form is polymorphic monoclinic [3], is a very important engineering resin manufactured in large quantities for film, fiber and plastic applications due to its high strength, high ductility, excellent resistance to short-term heat exposure and excellent resistance to chemical solvents [4, 5]. Polyamide 6 fibers are one of the most commonly used fibers in the world, and polyamide 6 nanofibers have been widely studied as nanotechnology progressed fast nowadays.

Adsorption properties of many different substances on conventional scale polyamide 6 have been studied numerously. However, systematic study of adsorption properties on polyamide 6 nanofibers assembly has rarely found. Which factors affect the adsorption properties on polyamide 6 nanofibers assembly and how do they affect has to be studied further.

### 1.2 OBJECTIVES AND SOLUTIONS

The aim of this research is to study the adsorption properties of which dyestuff as a model onto polyamide 6 nanofibers assembly. The sorption equilibrium, the sorption kinetics, the thermodynamics, and the dynamic sorption efficiency of dyestuff and hormone onto polyamide 6 nanofibers assembly from aqueous solution will be investigated. Meanwhile, the surface modifications on nanofibers such as sterilization with steam and photocatalysis with immobilization of Titanium dioxide nanoparticles will be applied and inspected.

Sorbent performance is the critical factor in the design and operation of an adsorption system. The sorption isotherms, and kinetics equations will be applied to the experimental data, and thermodynamic parameters will be calculated. The correlation between experimental conditions such as temperature, pH, waste concentration, membrane dosage, and membrane fiber scale will be discussed;

For dynamic adsorption, the effects of structural parameters (specific surface area and pore size) on performances (efficiency, capacity, dye removal rate and life span of utilization) of nanofibers assembly will be investigated.

For surface modification, steam sterilization will be used as a surface etching method and the dye sorption capacity will be discussed under different steam temperatures. TiO<sub>2</sub> nanoparticles will be immobilized onto nanofibers assembly, the self-cleaning performance of nanofibrous membrane will be investigated under different conditions in terms of temperature, content of TiO<sub>2</sub> nanoparticles, time under UV, and catalyst. Dynamic sorption process with TiO<sub>2</sub> nanoparticles photocatalysis will be performed.

The results will be useful in their application to the design of polyamide 6 nanofibers assembly sorption systems.

## CHAPTER 2. LITERATURE REVIEW

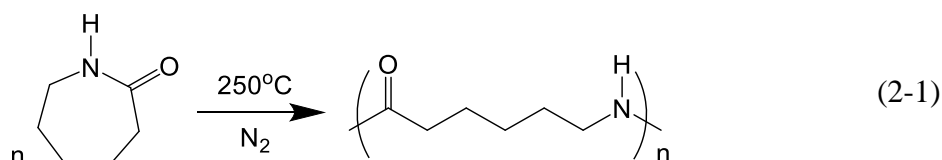
### 2.1 CHARACTERIZATION OF POLYAMIDE 6

Polyamides played an important role as speciality thermoplastics of particular use in engineering applications, and by far the bulk of polyamide materials are implemented in the form of fibers. The U. S. Federal Trade Commission defines polyamide fibers as “a manufactured fiber in which the fiber forming substance is a long chain synthetic polyamide in which less than 85% of the amide linkages (–CO–NH–) are attached directly to two aliphatic groups [6].” Among the many synthetic fibers, polyamides are one of the most important [7]. And the fiber-forming polyamides and their immediate chemical derivatives and copolymers are often referred to as nylons [8].

In 1935 spring, after extensive researches into condensation polymerization, W. H. Carothers and his colleagues first synthesized polyamide 66 [9, 10]. Du Pont Company commercialized it after 3 years. Paul Schlack invented after the polyamide 6 in Germany. Today polyamide 66 and 6 account for nearly all the polyamides produced for fiber applications.

#### 2.1.1 Formation of polyamide 6

Polyamide 6 is made by the self-condensation of 6-amino-caproic acid or its lactam, caprolactam [11, 12]. Both batch and continuous processes have been used for the manufacture of polyamide 6. In a typical batch process the caprolactam, water (which acts as a catalyst) and reacted under a nitrogen blanket at 250 °C for about 12 hours. The product consists of about 90% high polymer and 10% low molecular weight material such as the monomer. Low molecular weight materials may be removed by leaching and/or vacuum distillation [13]. Below the equation showed the chemical reaction of the open ring process:



The monoclinic form of polyamide 6 crystal is referred to as the  $\alpha$  form and is believed to have fully extended antiparallel chains. A second stable form, the  $\gamma$  form,

with a somewhat shorter *c*-axis repeat, is observed in melt-spun fibers, particularly at high spinning speeds and draw-down ratios. Drawing or annealing gives the  $\alpha$  form [8, 14].

### 2.1.2 Application of polyamide 6

As for wastewater cleaning, researchers reported that polyamide 6 nanofibers has the potential ability for removing heavy metal ions such as Cd (II) with some modifications [15, 16]. Meanwhile, polyamide 6 nanofibers have been used for direct dyes wastewater recycling [17]; In [18], polyamide nanofibers were made under steady state conditions with the insertion of chemicals and Ag nanoparticles, and the nanofibrous membranes functionalized with the bactericides exceed the normal removal efficiencies obtained by microfiltration membranes. Consider dyeing polyamides, acid dye, metal-complex dye, and disperse dye can be used, which means these dyes have good affinity with polyamides [19]. Dyes for polyamides normally form ionic bonds (see Eq. (2-2)) within the polymer matrix. In this case dyes bearing a negative (anionic) charge are used because polyamides carry a positive (cationic) charge-especially during the dyeing process [20]. This means polyamide has a potential function as dyestuff wastewater cleaning, especially the acid dye, metal-complex dye, and disperse dye [21]. Ummartyotin [22] used ZnO spin-casted polyamide 6 for dyestuff methylene blue, and it is noted that polyamide 6 and its compound deposited with ZnO exhibited a good potential for use of its self-cleaning and antibacterial properties in the textile industry. Polypyrrole/polyamide nanofibers were used as the sorbent for microextraction in packed syringe to analyze some selected organophosphorous pesticides [23].



As for air filtration, Shi [24] used solution blown polyamide 6 nanofiber mats, and result showed high filtration efficiency of 83.10-93.45 % for 0.3  $\mu$ m particles filtration and extremely low pressure drop of 15.37-30.35 Pa which indicates potential application of high efficiency and low resistance filter. An electrospun polyamide 6 filter (mean fiber diameter: 100 nm) shows a much lower pressure drop performance relative to the commercial HEPA filter media when the filtration efficiency of the polyamide 6 nanofilter and the HEPA filter are over 99.98% with test particles of

0.02–1.0  $\mu\text{m}$  in diameter [25].

Polyamide 6 nanofibers was proved to be antibacterial nanofibers [26]. As for protective clothing, Dhineshabu [27, 28] prepared MgO/polyamide 6 hybrid nanofibers for cotton fabrics coating, the fire retardancy and antibacterial activity were studied.

In the area of biotechnology, for affinity sorption, polyamide is a useful polymer phase for hydrophobic interaction chromatography in biomacromolecule processing as it has an alkyl backbone, while the amide functionality is hydrophilic (in fact ionic) in nature [29-32]. Polyamide 6 has played an important role as a base polymer for infinity membrane forming in purification of the papain [33, 34] and pentachlorophenol sorption [35].

## 2.2 STUDY OF ADSORPTION

### 2.2.1 Definitions

Adsorption is a phase transfer process that is widely used in practice to remove substances from fluid phases (gases or liquids). It can also be observed as natural process in different environmental compartments. The most general definition describes adsorption as an enrichment of chemical species from a fluid phase on the surface of a liquid or a solid [36].

The solid material that provides the surface for adsorption is referred to as adsorbent; the species that will be adsorbed are named adsorbate. An adsorbent media is a media containing adsorbents removing liquid and soluble contaminants from fluid streams by surface adsorption, i.e. the contaminants are attracted to the surfaces of the medium and held there by physical chemical effects [37].

By changing the properties of the liquid phase (e.g. concentration, temperature, pH) adsorbed species can be released from the surface and transferred back into the liquid phase. This reverse process is referred to as desorption. Over the last few decades, adsorption has gained paramount importance in industry and environmental protection. Adsorption processes are widely applied for separation and purification because of the high reliability, energy efficiency, design flexibility, technological maturity and the ability to regenerate the exhausted adsorbent.

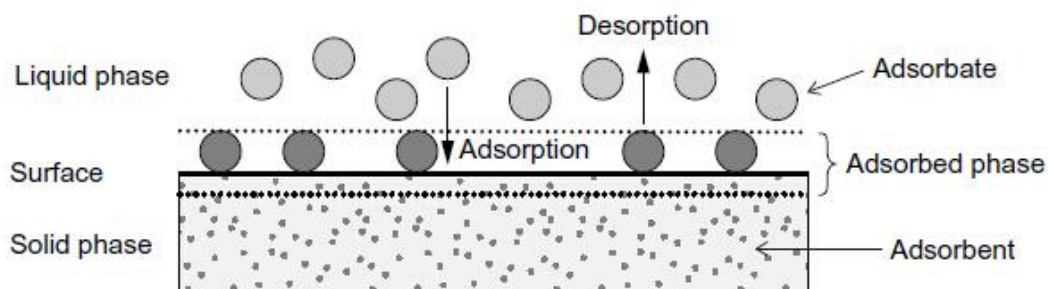


**Fig. 2-1** Basic terms of adsorption [36].

Adsorption works on the principle of adhesion. The process of adsorption involves separation of a substance from one phase accompanied by its accumulation or concentration at the surface of another. The process can take place in any of the following systems: liquid-gas, liquid-liquid, solid-liquid, and solid-gas [38, 39].

Most of the solid adsorbents possess a complex porous structure that consists of pores of different sizes and shapes. In terms of the science of adsorption, total porosity is usually classified into three groups: micropores (smaller than 2 nm), mesopores (in the range of 2 to 50 nm) and macropores (larger than 50 nm). The adsorption in micropores is essentially a pore-filling process, because sizes of micropores are comparable to those of adsorbate molecules. All atoms or molecules of the adsorbent can interact with the adsorbate species. That is the fundamental difference between adsorption in micropores and larger pores like meso- and macropores. Thus, the size of the micropores determines the accessibility of adsorbate molecules to the internal adsorption surface. The pore size distribution of micropores is another important property for characterizing adsorptivity of adsorbents [38, 39].

In the case of mesopores whose walls are formed by a great number of adsorbent atoms or molecules, the boundary of interphases (adsorbent surface area) has a distinct physical meaning. The action of adsorption forces occurs at a close distance from mesopores walls. Therefore, the mono- and multilayer adsorption takes place successively on the surface of mesopores, and their final fill proceeds according to the mechanism of capillary adsorbate condensation [40]. The basic parameters characterizing mesopores are specific surface area, pore volume and pore-size of pore-volume distribution. Mesopores, like macropores, play also an essential role in the transport of adsorbate molecules inside the micropore volume. The mechanism of

adsorption on the surface of macropores does not differ from that which occurs on flat surfaces. Since the specific surface area of macroporous solids is very small, adsorption on this surface is usually neglected. Similarly, the capillary adsorbate condensation does not occur in macropores.

### 2.2.2 Types of adsorption

Depending on the nature of attractive forces existing between the adsorbate and adsorbent, adsorption can be classified as Physical adsorption and Chemical adsorption. In physical adsorption, the forces of attraction between the molecules of the adsorbate and the adsorbent are of the weak van der Waals' type. Since the forces of attraction are weak, the process of physical sorption can be easily reversed by heating or decreasing the pressure of the adsorbate.

In chemisorption, the forces of attraction between the adsorbate and the adsorbent are very strong; the molecules of adsorbate form chemical bonds with the molecules of the adsorbent present in the surface.

### 2.2.3 Application of adsorption principles

Adsorption separation plays a significant role in the environmental pollution control and life supporting systems or planetary bases, where adsorbents may be used to process the habitat air or to recover useful substances from the local environments. Adsorption processes are good candidates for separation and purification by virtue of the high reliability, energy efficiency, design flexibility, technological maturity and the ability to regenerate the process by regenerating the exhausted adsorbent.

Development and application of adsorption principles cannot be considered separately from development of technology used to manufacture adsorbents applied on both laboratory and industrial scales, the adsorbents can take a broad range of chemical forms and different geometrical surface structures.

A larger specific surface area of adsorbent pores provides a large adsorption capacity. The creation of a large internal surface area in a limited volume inevitably gives rise to large numbers of small sized pores between adsorption surfaces.

#### 2.2.4 Adsorption on nanofibers assembly

The separation efficiency, in general, increases linearly with decreasing membrane thickness and increasing applied pressure. Thus, we can take advantage of the unique properties of electrospun membranes consisting of very-small-diameter fibers. Electrospun nonwoven nanostructure (a) has interconnected pores, (b) with pore sizes of the order of only a few times to a few ten times the fiber diameter, and (c) the pore space to material ratio is on the order of 3:1 or even higher [41].

Numerous adsorption properties of water vapors, dyes, iodine, and lipase on conventional polyamide 6 fibers, fabrics, films, or matrix have been studied [42-50]. Despite research publications and references in this field, there are still numerous open questions about the adsorption processes at the interfaces solid (fiber)/liquid (process solution), especially in nanoscale [46]. Wang [51] revealed that nanoscale polyamide 6 can improve the efficiencies of rejection of divalent cations, removal of basic dyes and selective separation of mixed cations on novel positively charged thin film composite nanofiltration membrane. The polyamide 6/chitosan nanofibers used in [52] proved to be a suitable carrier for immobilized and modified laccase, also efficient in the removal of a mixture of endocrine disrupting chemicals by adsorption examinations. Hekmati [53] studied the effect of nanofiber diameter on water absorption properties of polyamide 6 nanofibers. In study [54], compared with bulk: film of the same polymer, polyamide nanofibers show a considerable increase in the polar component of the surface free energy. Chemical surface analysis using X-ray photoelectron spectroscopy provided evidence for enhanced availability of polar oxygen groups at electrospun nanofiber surface relative to the film, which therefore confirm chemical group orientation at the electrospun polyamide nanofiber surface that promotes availability of polar groups for enhanced wetting behavior.

#### 2.2.5 Adsorption modes of solid-gas & solid-liquid interface

In adsorption systems, the mass transfer of solute or sorbed material onto and within the sorbent particle directly affects the adsorption rate. It is important to study the rate at which the solute is removed from aqueous solution in order to apply adsorption by solid particles to industrial uses. There are essentially four stages in the adsorption process:



- a. Transport of sorbed material from the bulk of the solution to the exterior film surrounding of the adsorbent;
- b. Movement of sorbed material across the liquid film to external surface sites;
- c. Migration of sorbed material within the pores of the sorbent;
- d. Sorption of sorbed material at internal surface sites.

All these processes may be involved in the control of the sorbed material removal rate. However, in a fully mixed agitated tank, mass transport from the bulk solution to the external surface is usually fast. The transport of sorbed material from the bulk of the solution to the exterior film surrounding the adsorbent is usually neglected. In addition, the adsorption of sorbed material at surface sites (step d) is usually rapid. Thus, these processes usually are not considered as the rate-limiting steps in the sorption process.

Three phenomena may be involved in physical adsorption [55]:

- a. Monomolecular adsorption;
- b. Multimolecular adsorption;
- c. Condensation in pores or capillaries.

Frequently, there is overlapping of these phenomena, and the interpretation of adsorption studies can be complicated.

According to Brunauer's classification of adsorption isotherms, five characteristic types of adsorption isotherms were shown in Fig. 2-2.

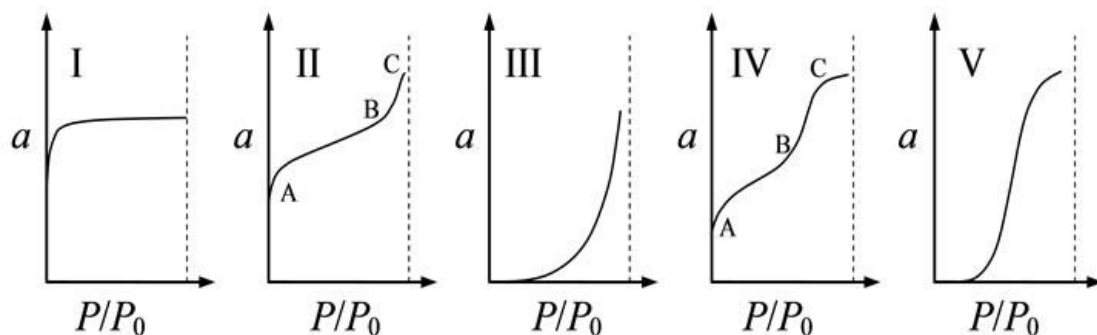


Fig. 2-2 Characteristic adsorption isotherms [56].

### 2.2.5.1 Brunauer–Emmett–Teller (BET) theory

BET theory aims to explain the physical adsorption of gas molecules on a solid surface and serves as the basis for an important analysis technique for the measurement of the specific surface area of a material. In 1938, Stephen Brunauer, Paul Hugh Emmett, and Edward Teller published the first article about the BET theory in the *Journal of the American Chemical Society* [57, 58].

Based on Langmuir's one layer molecules adsorption equation, Brunauer, Emmett, and Teller derived the BET equation (Eq. (2-3)) from multimolecular adsorption theory that provided for calculating the number of adsorbate molecules in a monolayer.

$$\frac{1}{v[(p_0/p)-1]} = \frac{c-1}{v_m c} \left( \frac{p}{p_0} \right) + \frac{1}{v_m c} \quad (2-3)$$

where  $v$  is the gas volume adsorbed at pressure  $p$ ,  $v_m$  is the volume of gas required for a single molecular layer over the entire adsorbent surface,  $p_0$  is the gas pressure required for saturation at the temperature of the experiment.  $c$  is the BET constant,

$$c = \exp\left(\frac{E_1 - E_L}{RT}\right) \quad (2-4)$$

where  $E_1$  is the heat of adsorption for the first layer, and  $E_L$  is that for the second and higher layers and is equal to the heat of liquefaction. Specific surface area and the properties of the pores were calculated according to [57, 59-61].

Eq. (2-3) shows an adsorption isotherm which can be plotted as a straight line with  $1/v[(p_0/p)-1]$  on the y-axis and  $p/p_0$  on the x-axis according to experimental results. This plot is called a BET plot. The linear relationship of this equation is maintained only in the range of  $0.05 < p/p_0 < 0.35$ . The value of the slope  $A_S$  and the y-intercept  $I$  of the line are used to calculate the monolayer adsorbed gas quantity  $v_m$  and the BET constant  $c$  [59].

The following equations can be used:

$$v_m = \frac{1}{A_s + I} \quad c = 1 + \frac{A_s}{I} \quad (2-5)$$

The total surface area  $S_{total}$  and the specific surface area  $S_{BET}$  are given by:

$$S_{total} = \frac{(v_m N s)}{V} \quad (2-6)$$

$$S_{BET} = \frac{S_{total}}{m} \quad (2-7)$$

where  $v_m$  is in units of volume which are also the units of the molar volume of the Nitrogen gas,  $N$  is Avogadro's number,  $s$  the adsorption cross section of the adsorbing species,  $V$  the molar volume of Nitrogen gas, and  $m$  the mass of the sample.

#### 2.2.5.2 Freundlich isotherm

The concave isotherm ('L' or 'H' isotherms) is the most widely met isotherm. The first model is empirical (Van Bemmelen, 1888; Freundlich, 1909) [62] and is based on the following relation between the adsorbed quantity  $C_s$  and the remained solute concentration  $C_L$ :

$$C_s = K_f C_L^{1/n} \quad (2-8)$$

with  $K_f$  ((mg/g)(L/g)<sup>n</sup>) and  $1/n$  (heterogeneity factor, dimensionless) being two constants. The constant  $n$  may be either greater or less than unity, leading to isotherms which are either concave or convex to the bulk concentration axis [63]. This equation is easily linearizable (Eq. (2-9))[64, 65].

$$\lg C_s = \lg K_f + 1/n(\lg C_L) \quad (2-9)$$

The Freundlich equation predicts that the dye concentrations on the adsorbent will increase so long as there is an increased in the dye concentration in the liquid [66].

#### 2.2.5.3 Langmuir isotherm

Another very common model is based on reaction hypotheses (Langmuir, 1918) [62,

67]. The Langmuir isotherm equation is:

$$C_s = \frac{q_0 K_L C_L}{1 + K_L C_L} \quad (2-10)$$

where  $C_s$  is the sorption capacity of mass of dye per mass of fiber (mg/g),  $K_L$  is the affinity between sorbed material and sorbent (L/g),  $C_L$  is the concentration in liquor (g/L),  $q_0$  is the maximum amount of dye that can be adsorbed (mg/g). It can be linearized by Eq. (2-11) [64].

$$\frac{1}{C_s} = \frac{1}{q_0 K_L} \cdot \frac{1}{C_L} + \frac{1}{q_0} \quad (2-11)$$

The Freundlich isotherm types are most often observed for adsorption from solution onto solids while the Langmuir isotherm is common to both liquid-solid and liquid-gas systems [63]. Langmuir isotherm is useful for adsorption onto specific sites by chemisorption.

#### 2.2.5.4 Determination of isotherms

Two isotherms have been used to determine the best fitting equation, which correlates the theoretically predicted data with the experimental data. The best fitting isotherm will be determined by choosing the equation resulting in the lowest sum of error squares (SSE) or highest value of the square of correlation coefficient ( $R^2$ ), such that:

$$R^2 = 1 - \frac{SSE}{SST} \quad (2-12)$$

$$SSE = \sum (q_{\text{exp}} - q_{\text{cal}})^2 \quad (2-13)$$

$$SST = \sum \left( q_{\text{exp}} - \frac{\sum q_{\text{exp}}}{n} \right)^2 \quad (2-14)$$

where  $SSE$  is the sum of error square,  $SST$  is the Sum of total error square,  $q_{\text{exp}}$  is experimental data (mg/g or mmol/g), and  $q_{\text{cal}}$  is predicted data (mg/g or mmol/g).

#### 2.2.6 Kinetics

The mechanism of acid dye sorption onto various sorbents has been subjected to

extensive research, debate and controversy for decades. Numerous researches are based on a reaction kinetic sorption process in which reaction rate constants are determined as key parameters describing the process. In the present work, two kinetic models will be tested to determine the reaction order of the sorption process of acid dyes onto polyamide 6 nanofibrous membrane; the models are Elovich Equation and Pseudo-Second Order Equation.

#### 2.2.6.1 The Elovich equation

The Elovich equation has general application to chemisorption kinetics. The equation has been proved satisfactorily applicable to most chemisorption data and will cover a large range of slow adsorption. A detailed report to interpret the use of this equation in the kinetics of chemisorption of gases on solids was demonstrated by Low [68, 69].

The Elovich equation is formulated as:

$$\frac{dq_t}{dt} = a^{-bq_t} \quad (2-15)$$

Where  $q_t$  is adsorption capacity at time  $t$  (mg/g),  $a$  is the initial sorption rate (mg/(g min)) and  $b$  is the desorption constant (g/mg) during any one experiment. Integration of Eq. (2-15) with boundary conditions  $q=0$  at  $t=0$  and  $q=q_t$  at  $t=t$ , gives [70, 71]

$$q_t = b \ln(ab) + b \ln(t) \quad (2-16)$$

Thus, a linear plot of Eq. (2-16)  $q_t$  versus  $\ln(t)$ , yields both constants  $a$  and  $b$  from the intercept and the slope. Equation (2-16) will be used to test the applicability of the Elovich equation to the kinetics of sorption.

#### 2.2.6.2 Pseudo-second order equation

If the rate of sorption is a second order mechanism [72], the pseudo-second order chemisorption kinetic rate equation may be expressed as:

$$\frac{dq_t}{dt} = k_2 (q_e - q_t)^2 \quad (2-17)$$

Where  $q_e$  and  $q_t$  are the adsorption capacity (mmol/g) at equilibrium and at time  $t$ , respectively, and  $k_2$  is the rate constant of pseudo-second order sorption (g/mmol/min).

For the boundary conditions  $t=0$  to  $t=t$  and  $q=q_i$ ; the integrated form of Eq. (2-17) becomes:

$$\frac{1}{(q_e - q_t)} = \frac{1}{q_e} + k_2 t \quad (2-18)$$

Which is the integrated rate law for a pseudo-second order reaction. Equation (2-18) can be rearranged to obtain:

$$q_t = t / \left( \frac{1}{k_2 q_e^2} + \frac{t}{q_e} \right) \quad (2-19)$$

Which has a linear form:

$$\frac{t}{q_t} = \frac{1}{k_2 q_e^2} + \frac{1}{q_e} t \quad (2-20)$$

If pseudo second-order kinetics is applicable, the plot of  $t/q_t$  against  $t$  of Eq. (2-20) should give a linear relationship, from which  $q_e$  and  $k_2$  can be determined from the intercept and slope of the plot.

### 2.2.6.3 Determination of the kinetic model

Two kinetic models have been used to determine the best fitting equation, which correlates the theoretically predicted data with the experimental data. The best fitting kinetic model will be determined by choosing the equation resulting in the lowest sum of error squares (SSE).

The parameters of the Elovich equation and the Pseudo-second order equation were determined by the linear regression analysis of those equations to obtain the highest value of the square of correlation coefficient ( $R^2$ ), such as shown in Eq. (2-12).

Furthermore, Pseudo kinetic models are based on the solid phase adsorbent loading,  $q_e$  and  $q_t$ , and these are dependent on the initial dye concentration,  $C_0$ . Consequently, the Pseudo rate constants are dependent on  $C_0$  as well. Each kinetic model is now analyzed.

### 2.2.7 Thermodynamics

Adsorption is generally accompanied by release of energy, that is, most adsorption processes are exothermic in nature. Adsorption is a spontaneous process; therefore its Gibbs free energy change is negative ( $\Delta G^\circ < 0$ ). However, the entropy change associated with adsorption is generally negative because the adsorbate molecules lose their translation freedom when they get attached to the surface of the adsorbent. Therefore, in order for  $\Delta G^\circ$  to be negative, the enthalpy change ( $\Delta H^\circ$ ) must be sufficiently negative, such that,  $(\Delta G^\circ = \Delta H^\circ - T\Delta S^\circ) < 0$ . This explanation accounts for exothermic adsorption processes. In cases, where endothermic adsorption occurs as in the case of hydrogen adsorption on glass, the entropy change  $\Delta S^\circ$  is sufficiently positive such that  $\Delta G^\circ$  remains negative. Enthalpy of adsorption, which is the enthalpy change for the adsorption of one mole of an adsorbate on an adsorbent surface, is usually in the range of 20 to 40 kJ/mole, while for chemisorption, the values are an order of magnitude high, that is, 200 to 400 kJ/mole.

The pseudo-second order rate constant can be expressed as a function of temperature by the following Arrhenius type relationship:

$$\ln k_2 = \ln A - \frac{E_a}{RT} \quad (2-21)$$

where  $E_a$  is the Arrhenius activation energy of adsorption,  $A$  is the Arrhenius factor,  $R$  is the gas constant and is equal to 8.314 J/(mol K) and  $T$  is the operating temperature. A linear plot of  $\ln k_2$  vs  $1/T$  can be constructed to generate the activation energy from the slope ( $-E_a/R$ ). The magnitude of activation energy gives an idea about the type of adsorption, which is mainly physical or chemical. Low activation energies (5-40 kJ/mol) are characteristics for physisorption, while higher activation energies (40-800 kJ/mol) suggest chemisorptions [73, 74].

In order to determine the thermodynamic feasibility and the thermal effects of the sorption, the Gibbs free energy ( $\Delta G^\circ$ ) the entropy  $\Delta S^\circ$  and the enthalpy ( $\Delta H^\circ$ ) were calculated. For the determination of  $\Delta H^\circ$  and  $\Delta S^\circ$ , the relationship between sorption equilibrium constant  $K_C$  and Gibbs free energy was considered at any temperature [75]:

$$K_C = C_A/C_S \quad (2-22)$$

$$\ln K_C = \frac{\Delta S^\circ}{R} - \frac{\Delta H^\circ}{RT} = -\frac{\Delta G^\circ}{RT} \quad (2-23)$$

where  $K_C$  is the equilibrium constant,  $C_A$  is the amount of the sorbed material on the sorbent of the solution at equilibrium (mol/g),  $C_S$  is the equilibrium concentration of the sorbed material in the solution (mol/L). The  $q_e$  of the Pseudo-Second Order model was used to obtain  $C_A$  and  $C_S$ .  $T$  is the solution temperature (K) and  $R$  is the gas constant which equals to 8.314 J/(mol K).

The plot of  $\ln K_C$  as a function of  $1/T$  should give a linear relationship with slope of  $-\Delta H^\circ/R$  and an intercept of  $\Delta S^\circ/R$ . Then  $\Delta G^\circ$  is obtained at any temperature from the following equation:

$$\Delta G^\circ = \Delta H^\circ - T\Delta S^\circ \quad (2-24)$$

The  $\Delta G^\circ$  is the fundamental criterion to determine if a process occurs spontaneously. For a given temperature, a phenomenon is considered to be spontaneous if the  $\Delta G^\circ$  has a negative value. Moreover, if  $\Delta H^\circ$  is positive, the process is endothermic and if it is negative, the process is exothermic [75].

## 2.3 NANOTECHNOLOGY

Nanotechnology has the potential to significantly affect society. It is already used for instance by the information and communications sectors. It is also used in cosmetics and sunscreens, in textiles, in coatings, in some food and energy technologies, as well as in some medical products and medicines. Moreover, nanotechnology could also be used in reducing environmental pollution [76]. Nanotechnology is already having an impact in many spheres of chemical and materials science. It would seem that only our imagination would limit the widespread application of nanotechnology [77].

### 2.3.1 Electrospinning technology

#### 2.3.1.1 Present situation of electrospinning technology

Electrospinning is an old technique. It was first observed by Rayleigh [78] in 1897,



studied in detail by Zeleny [79] in 1914 (on electrospraying), and patented by Formhals [80] in 1934. In particular, the work of Taylor and others on electrically driven jets has laid the groundwork for electrospinning [81]. This technique has been known for over 60 years in the textile industry for manufacturing non-woven fiber fabrics.

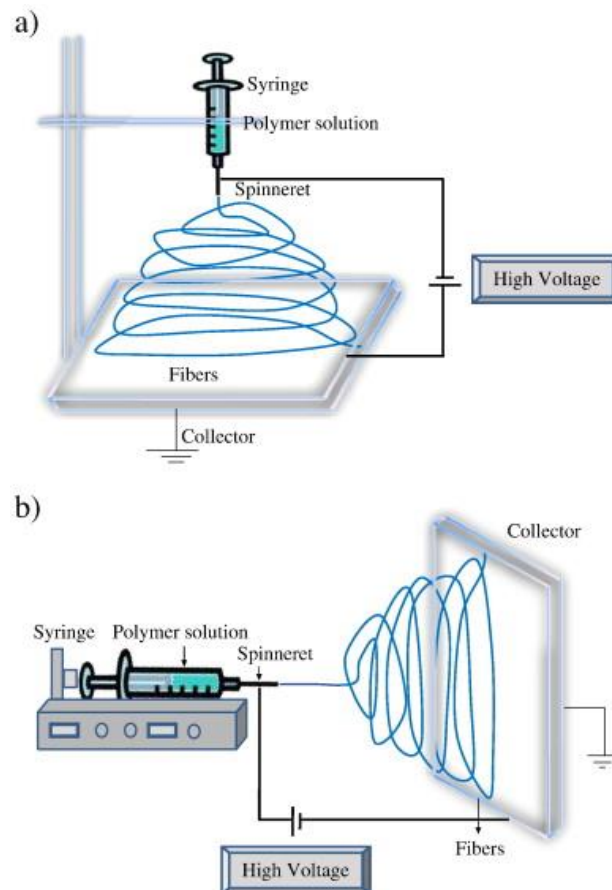


**Fig. 2-3** Schematic diagram of set up of electrospinning apparatus: a) typical vertical set up; b) horizontal set up of electrospinning apparatus [82].

An electrospinning system consists of three major components: a high voltage power supply, a spinneret, and a grounded collecting plate [83]. The typical set up of electrospinning apparatus is shown in Fig. 2-3. In the electrospinning process, a polymer solution held by its surface tension at the end of a capillary tube is subjected to an electric field and an electric charge is induced on the liquid surface due to this electric field. When the electric field applied reaches a critical value, the repulsive electrical forces overcome the surface tension forces. Eventually, a charged jet of the solution is ejected from the tip of the Taylor cone and a rapid whipping of the jet occurs in the space between the capillary tip and collector which leads to evaporation

of the solvent, leaving a polymer behind [82, 84].

### 2.3.1.2 Application of nanofibers

Fiber materials with diameters within the nanometer range when compared with microscale materials have several important characteristics, such as a large surface area to volume ratio (a nanofiber can be as large as  $10^3$  times that of a microfiber), tunable porosity, pore size ranging from 10 nm to several micrometers, flexibility in surface functionalities, good mechanical performance, and malleability to construct a wide variety of fiber sizes and shapes. These outstanding properties make nanofibers the desirable candidates for many important applications [85].

Due to several advantages such as high specific surface area and very high porosity, etc., the electrospun nanofibers and mats are broadly applied in biomedical applications, filtration, environmental engineering, defense and security, energy storage and generation, and in various researches that are ongoing [82, 86-89].

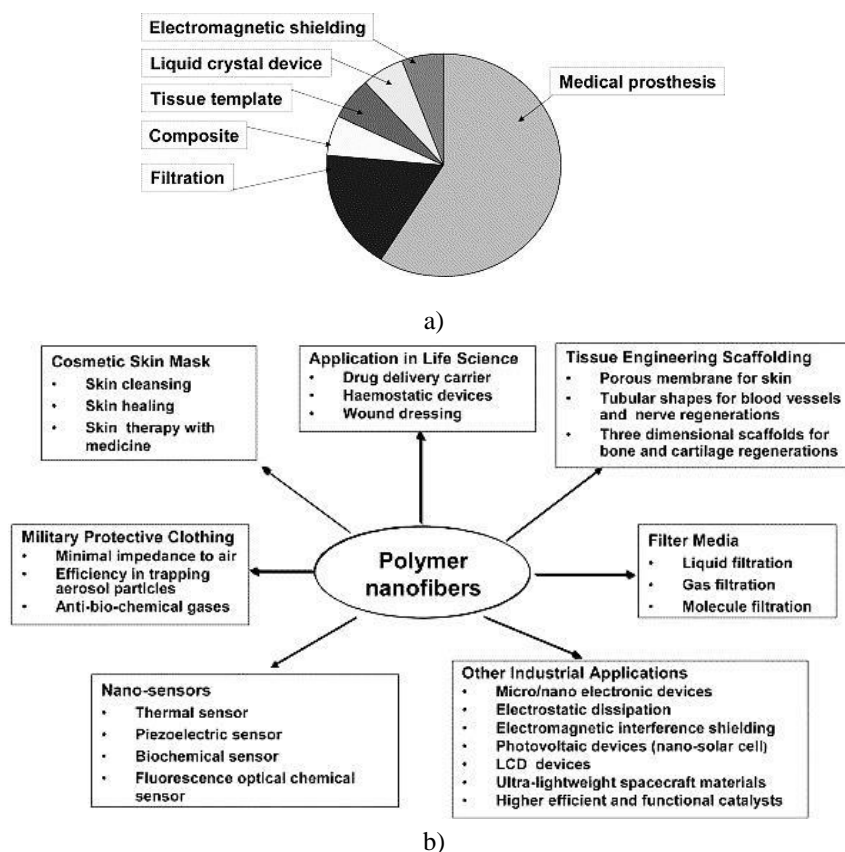


**Fig. 2-4** Electrospun nanofibers and mats application fields: a) targeted by US patents; b) potential applications of electrospun polymer nanofibers [83].

Fig. 2-4 shows the electrospinning applications in various fields.

### 2.3.2 Nanoparticle technology

#### 2.3.2.1 Nanoparticle's advantages and its applications

As the dimensions of a solid particle decrease to the scale of a nanometer (one millionth of a millimeter), the fundamental physical properties, such as the melting point, latent heat of fusion  $\Delta H_m$ , and surface area (shown in Fig. 2-5) [90-92], can change drastically. In addition, as particles get smaller than the wavelength of visible light, they not only become transparent but also emit a special light by plasma absorption. They show completely different electromagnetic or physicochemical properties from their bulk materials.

The definition of nanoparticles differs depending on the materials and applications concerned. In the narrowest sense, they are regarded as particles smaller than 10–20 nm, where the physical properties of the solid materials themselves drastically change. On the other hand, particles in the range from 1 nm to 1  $\mu\text{m}$  may also be called nanoparticles [93, 94]. Nanoparticles normally are made from chemical reactions or ball milling [95].

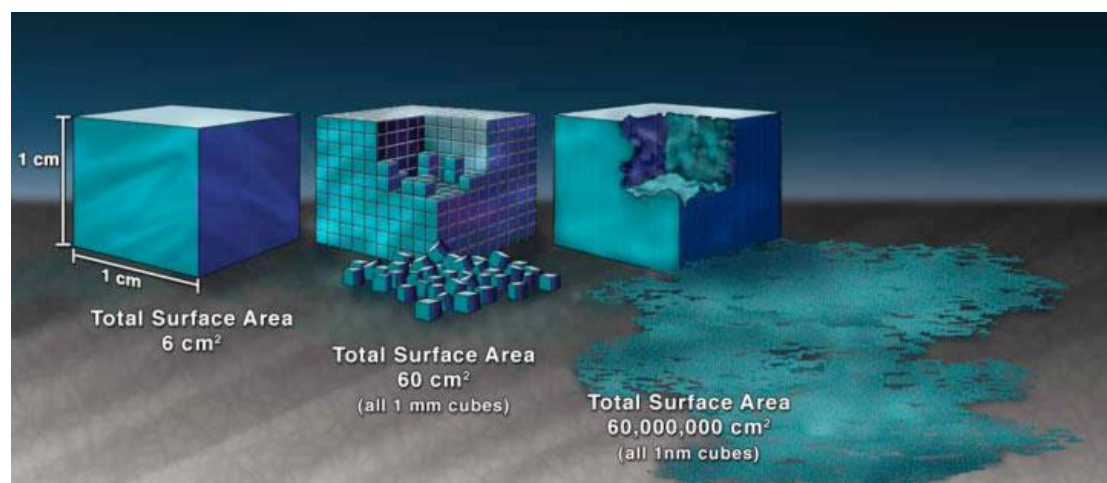


**Fig. 2-5** Illustration demonstrating the effect of the increased surface area provided by nanostructured materials [92].

In industry, nanoparticles are already being used in the manufacture of scratchproof eyeglasses, crack-resistant paints, anti-graffiti coatings for walls, transparent sunscreens, stain-repellent fabrics, self-cleaning windows and ceramic coatings for

solar cells. Nanoparticles as fillers in tires can improve adhesion to the road, reducing the stopping distance in wet conditions. The stiffness of the car body can be improved by use of nanoparticle-strengthened steels [76].

#### 2.3.2.2 Incorporation of nanoparticles with photocatalysis theory

Nowadays, researchers in different areas are still paying so much attention on application of nanoparticles. In [96], the photocatalytic properties were studied for phenol photodegradation and for acetic acid oxidation under UV and visible irradiation with Ag nanoparticles and CuO nanoclusters (large silver cores decorated with small clusters of CuO) synthesized on TiO<sub>2</sub> (P25) which indicates that surface modification with nanoparticles plays a role in charge-carrier separation, increasing the activity under UV-light. In Textile area, TiO<sub>2</sub> nanoparticles were used for self-cleaning fabrics. [97] As studied in [98], TiO<sub>2</sub> nanoparticles were grafted with the acrylate copolymer which obtained high ultraviolet absorption, high transparency and excellent photo-oxidative stability as protective agent for ancient ivory or any other bone relics. TiO<sub>2</sub> nanoparticle is even one of the most fascinating materials for stimulating germination and growth of various seeds [99].

In wastewater cleaning area, nanoparticles have been widely studied, and the function mostly realized due to the outstanding adsorption properties and the photocatalytic properties. Photocatalytic oxidation processes have been widely considered as powerful methods to remove non-biodegradable organic pollutants in water [100]. The photocatalytic processes have the potential to mineralize complicated organics and reduce toxicity without the generation of sludge and by-products and TiO<sub>2</sub> is the most common and practical material as the environmental photocatalyst [101-103].

Photocatalysis with TiO<sub>2</sub> nanoparticles has been studied for the degradation of wastewater pollutants. This process has several advantages including complete mineralization of organic pollutants like aliphatics, aromatics, polymers, dyes, surfactants, pesticides and herbicides to CO<sub>2</sub>, water and mineral acids, no waste solids to dispose of and mild temperature and pressure conditions. Photocatalysis with TiO<sub>2</sub> nanoparticles uses two kinds of reaction systems, namely suspension and immobilized systems [104-113].

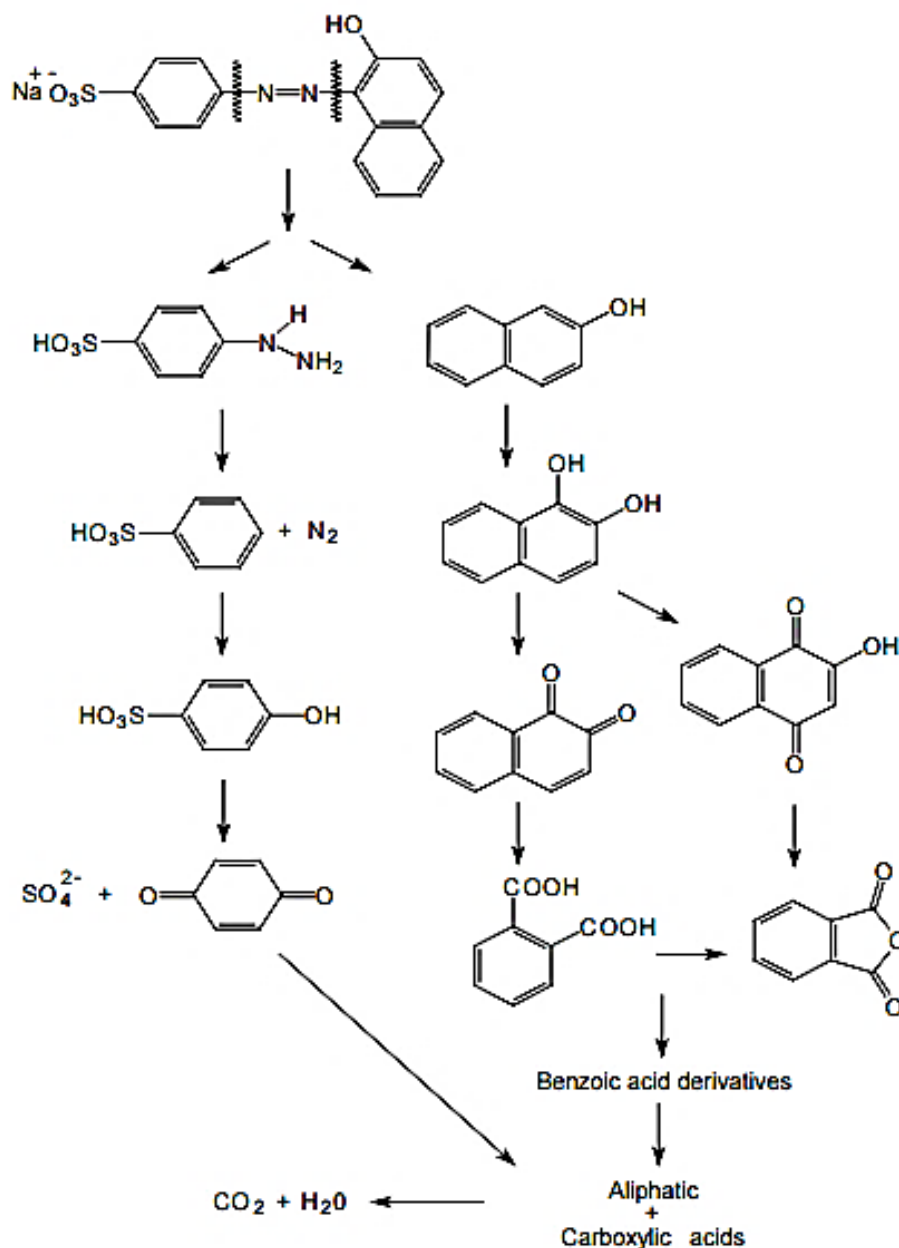


**Fig. 2-6** Major photocatalytic pathways of C.I. Acid Orange 7, a representative azo dye for phenyl-azonaphthol chemical group, based on the identification of by-products from previous reported degradation studies [104, 114, 115].

C.I. Acid orange 7 (AO7) is the most studied compound among the azo dyes as far as its photocatalytic degradation under several experimental conditions. The degradation pathways and the formation of by-products is also fully described [114, 116-118] which shows in Fig. 2-6. Thus, AO7 can be used as a model compound for oxidative degradation studies of azo dyes [119].

### 2.3.3 Surface modification for nanofibrous membrane

In the membrane technology field, the limiting factor or disadvantage of membrane technology is fouling [120-123]. Fouling refers to the accumulation of undesired materials on the membrane surface, which causes an increase in expenditure in the industry due to shorter membrane life span, more maintenance works required, low efficiency in the separation performances, and higher pumping energy consumption. Thus, research has continued since the discovery of some of the methods used in overcoming fouling problems, and membrane modification by incorporating nanoparticles in polymeric membranes is one of them [85].

Many functionalized composite nanofibers were produced directly by electrospinning polymer solutions containing nanoparticles of different types in order to improve the performances of the membranes, such as the permeability, selectivity, strength, and hydrophilicity. The incorporation of metal nanoparticles in polymer matrices has allowed the development of materials with unique properties due to the nanoscale size and shape of the dispersed nanoparticles [124]. For example, nanoparticle composite membranes exhibited good mechanical properties and high antibacterial activities [125]. polyethersulfone/aluminum oxide membranes exhibited lower flux decline, higher porosity, and pseudo steady-state permeability [126]. Taha [127] prepared porous carbon nanofibers modified by Ag nanoparticles using a one-pot/self-template synthesis strategy by combining electrospinning and carbonization methods, and the membrane exhibited excellent dye degradation and bacteria disinfection in batch experiments. The method of incorporating graphene oxide and chemically reduced graphene oxide nanosheets with polyamide 6 solutions was proved as a way for improve the steady viscosity, the thermal stability, and adsorption capacity of polyamide 6 nanofibers [128].

### 2.3.4 Nanophotocatalysis

Recently, nanostructured materials based on metal nanoparticles have been studied extensively for various applications because of their attractive physical, chemical, and catalytic properties. The nanocrystalline TiO<sub>2</sub> coatings that can chemically break down adsorbed organic contaminants in sunlight have received much attention due to their potential applications ranging from window glass and cement to textiles [123,

129].

The detailed mechanism of the photocatalytic process has been discussed extensively in the literature [119, 130, 131] and the principle of photocatalytic degradation is well known since UV illumination onto a photocatalyst excites to produce an electron and hole pair with a high-energy state, which migrate to the particle surface and initiate various chemical redox reactions [132, 133].

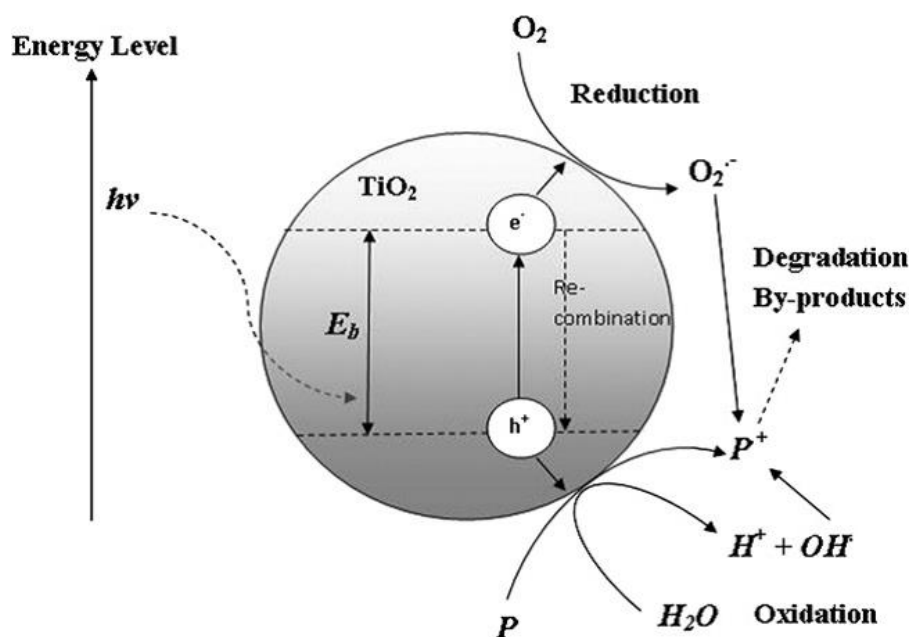


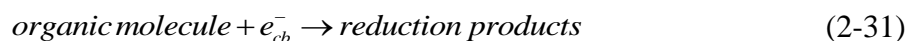
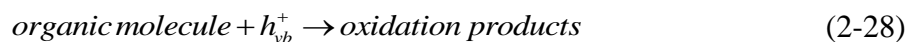
**Fig. 2-7** Photo-induced formation mechanism of electron-hole pair in a semiconductor  $\text{TiO}_2$  particle with the presence of water pollutant (P) [134].

Illumination of an aqueous  $\text{TiO}_2$  suspension with irradiation energy greater than the band gap energy ( $E_{bg}$ ) of the semiconductor ( $E_{bg}=3.2$  eV in the case of  $\text{TiO}_2$ ) generates valence band holes ( $h_{vb}^+$ ) and conduction band electrons ( $e_{cb}^-$ ):



The photogenerated valence band holes and conduction band electrons can either recombine to liberate heat, or make their separate ways to the surface of  $\text{TiO}_2$ , where they can react with species adsorbed on the catalyst surface according to Eqs. (2-26)-(2-31):





Hydroxyl radical  $HO^\bullet$ , along with perhydroxyl radical  $HO_2^\bullet$  can oxidize most of the organic compounds to mineral products, thus reducing the organic load of the wastewater (Eq. (2-32)):



Furthermore, in the present case an additional explanation can be given in terms of the specific surface area of the catalysts employed. It has been stated that in cases where the surface reaction rates of conduction band electrons  $e_{cb}^-$  and valence band holes  $h_{vb}^+$  with various substrates are faster than the electron–hole recombination, the photocatalytic activity increases with increasing specific surface area [119, 135, 136].



## CHAPTER 3. MATERIALS AND METHODS

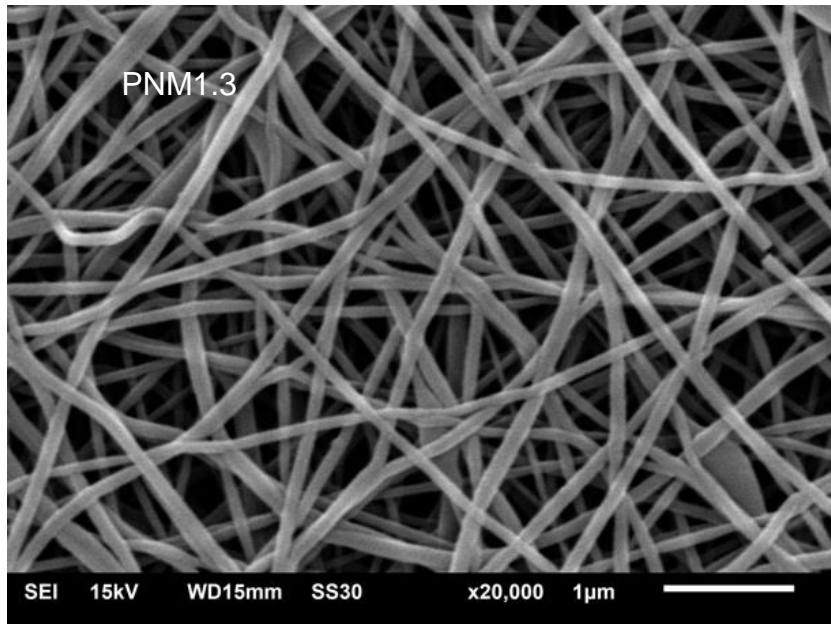
### 3.1 MATERIALS AND APPRATUS

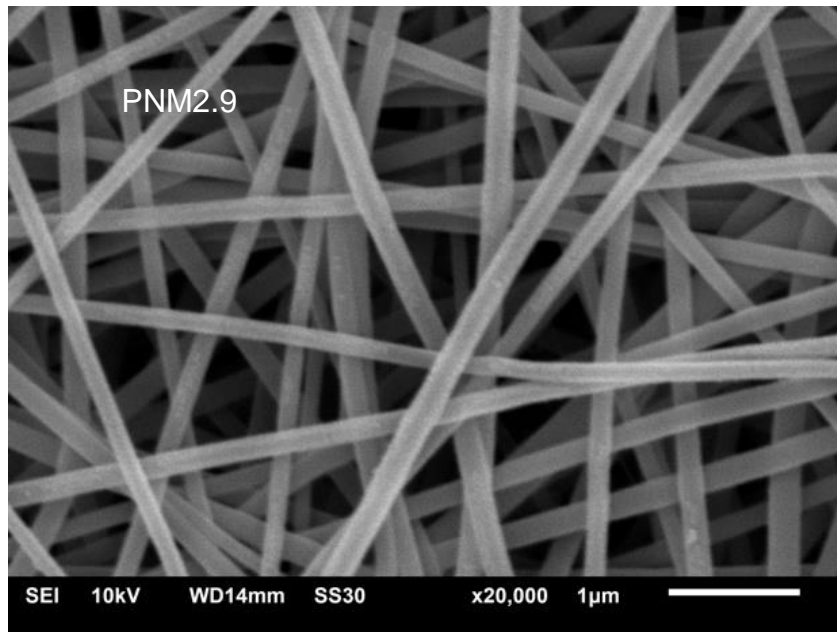
#### 3.1.1 Sorbent

##### 3.1.1.1 Polyamide 6 nanofibrous membrane (PNM)

PNM with areal density 1.3 and 2.9 g/m<sup>2</sup> purchased from ELMARCO s. r. o were mainly used as sorbents.

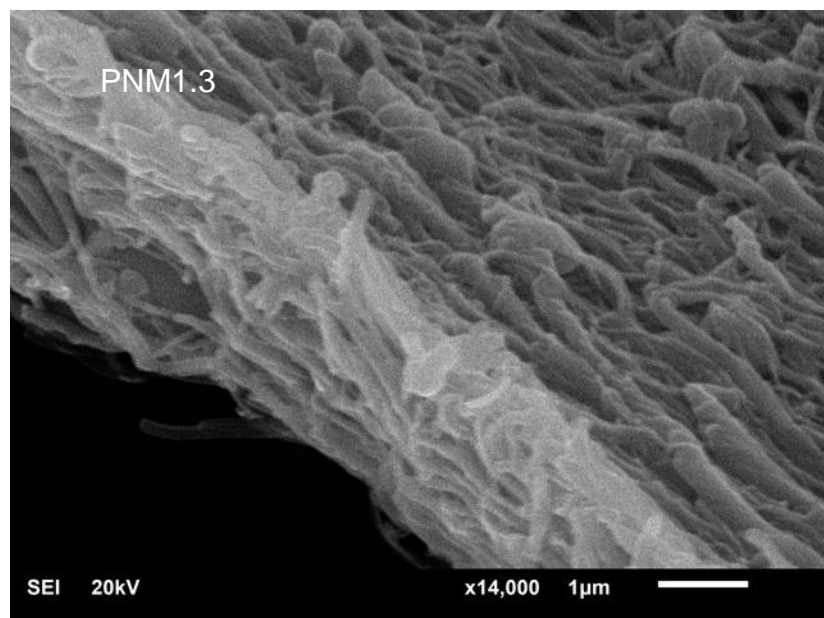
The morphologies of PNM1.3 and PNM2.9 were observed by Scanning Electron Microscopy (SEM) using a JEOL JSM-6510LV (Japan) with 10-20 kV of accelerating voltage. The electrospun samples were coated with Au/Pd before being mounted on SEM chamber. The fibers on the membranes were randomly selected to measure the individual fiber diameters by identifying two points at opposite ends of a fiber diameter for each sample 50 times. The samples were broken in liquid Nitrogen and the cross section images were taken by SEM. Thickness was measured for each sample 10 times.





**Fig. 3-1** SEM images of nanofibrous membranes surface.

From the surface images, we can obtain the diameter of the fibers in each membrane. 50 times of each were measured and the average value was calculated as  $113 \pm 16$  nm for PNM1.3 and  $187 \pm 25$  nm for PNM2.9.



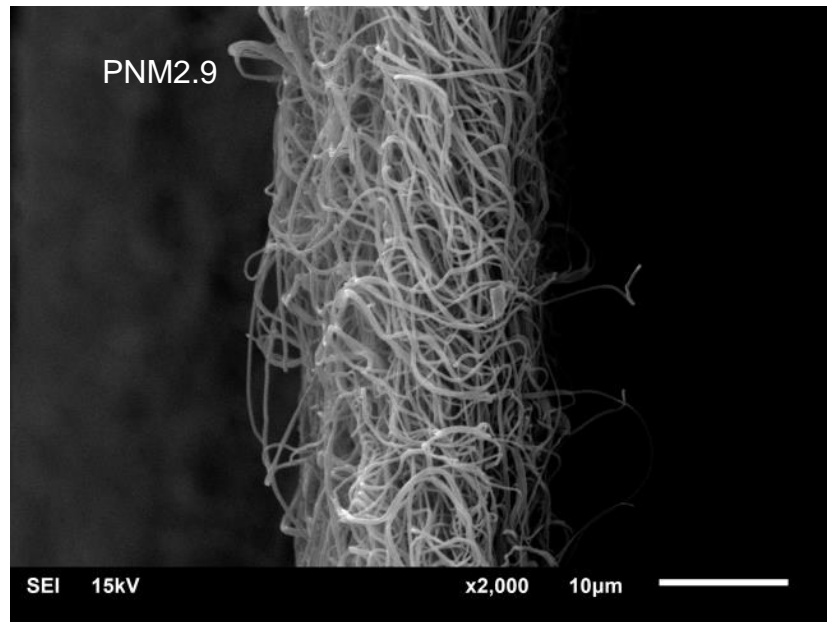
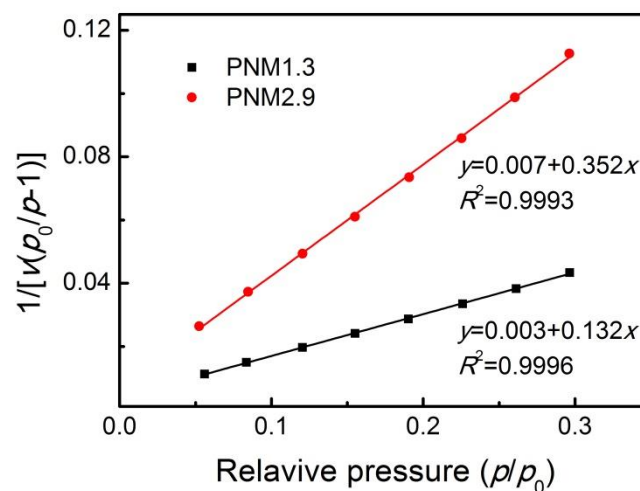


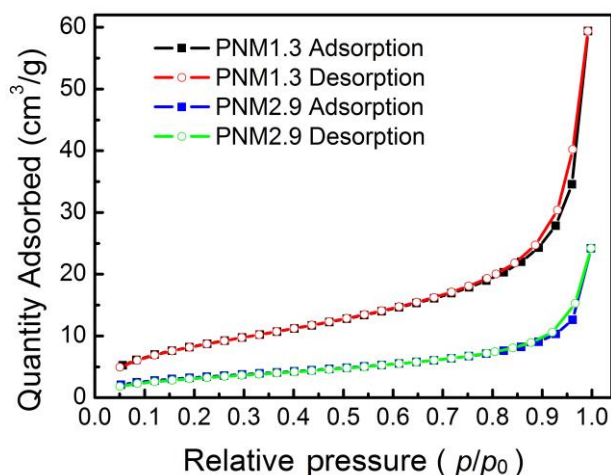
**Fig. 3-2** SEM images of nanofibrous membranes cross section.

As the images shown in Fig. 3-2, the thickness of the samples was measured 10 times for each and the results are  $1.85 \pm 0.21 \mu\text{m}$  and  $15.98 \pm 1.83 \mu\text{m}$  respectively.

BET test was taken by Accelerated Surface Area and Porosimetry System, ASAP 2020, U.S.A. Nitrogen gas was used as the sorbed material to measure the adsorption property of samples. Specific surface area and the properties of the pores were calculated according to the reported method [57, 59, 60]. According to equations described in 2.2.5.1, BET plots of two samples were plotted in Fig. 3-3. Pore volume and pore size of two samples were obtained, shown in Table 3-1.



a)



b)

**Fig. 3-3** BET testing result of polyamide 6 nanofibrous membranes. a) BET plots of two membranes; b) Quantity adsorbed of Nitrogen versus relative pressure applied during BET test.

**Table 3-1** Testing results from BET test on two nanofibrous membranes.

Sample code	Weight per unit area g/m <sup>2</sup>	Diameter of nanofibers nm	BET surface area m <sup>2</sup> /g	Pore volume* cm <sup>3</sup> /g	Pore Size nm
PNM1.3	1.26	113±16	32.00	0.09	11.48
PNM2.9	2.90	187±25	12.13	0.04	12.34

Note: \*Pore volume of pores less than 1086.0122 nm diameter at P/Po = 0.998239998.

Table 3-1 shows the BET surface area of PNM1.3 is 32.00 m<sup>2</sup>/g, which is nearly three times larger than the surface area of PNM2.9. It indicates a much better gas sorption properties of thinner fibers. The specific surface area and the pore size both affected the fouling of membrane during the dynamic sorption processes.

Fourier transform infrared spectroscopy (FTIR) and Differential scanning calorimetry (DSC) tests were performed respectively by Bruker Tensor 27 (Germany) and PerkinElmer Diamond DSC (U. S. A.) with temperature increasing rate 10 °C/min.

PNM1.3 and PNM2.9 were analyzed by FTIR. The reflectance peaks in Fig. 3-4 show similar chemical groups motions in two samples. The glass transition temperature ( $T_g$ ) of two samples are respectively 53.59 and 59.46 °C with similar melting temperature ( $T_m$ ) around 222 °C.

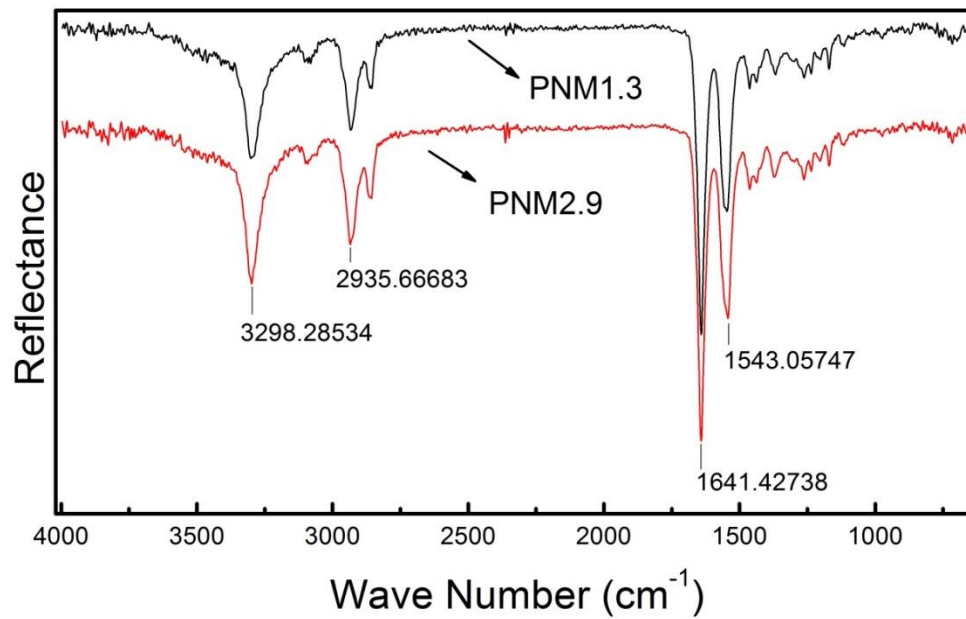


**Fig. 3-4** FTIR spectrum of polyamide nanofibrous membranes.

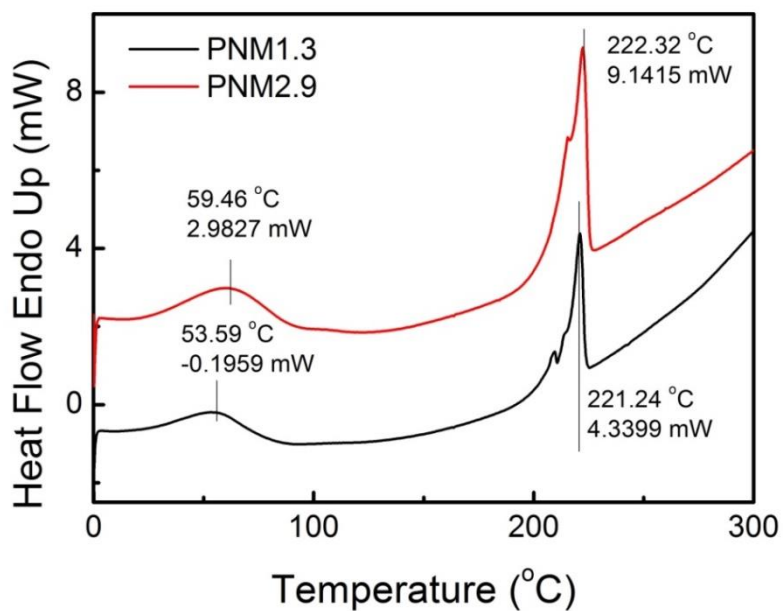


**Fig. 3-5** Heat flow endo result from DSC test.

### 3.1.1.2 Other fiber mats

Electrospun polyamide 6 nanofibrous membranes with areal density of 0.5 g/m<sup>2</sup>

purchased from ELMARCO s. r. o and spunbond nonwoven fabrics (SB) with areal density of 20, 40, 50, 70, and 100 g/m<sup>2</sup> provided by Asahi KASEI fibers corporation, woven fabric from TUL, and Polyacrylonitrile (PAN) from ELMARCO s. r. o were used.

**Table 3-2** Description of samples with different areal densities used in this experiment.

Sample abbreviation	Description	Areal density	Fiber diameter	Thickness
		g/m <sup>2</sup>	nm	μm
PNM0.5	polyamide 6	0.5	138±25	
PNM1.3	nanofibrous	1.3	113±16	1.85±0.21
PNM2.9	membrane	2.9	187±25	15.98±1.83
SB20	polyamide 6 Sponbond nonwoven membrane	20	1470±70	190±10
SB40		40	1600±60	320±10
SB50		50	1530±70	350±10
SB70		70	1550±60	430±20
SB100		100	1520±120	530±10
W175		woven fabric	175	
Polyacrylonitrile				
PAN0.4	nanofibrous membrane	0.4	242±53	

The fiber diameter of fibers and thickness of samples are shown in Table 3-2 and the diameter of fibers were each measured 50 times from SEM images.

The chemical structure of polyamide 6 and Polyacrylonitrile are shown in Fig. 3-6.

Fig. 3-7 shows the SEM images of samples used as sorbents.

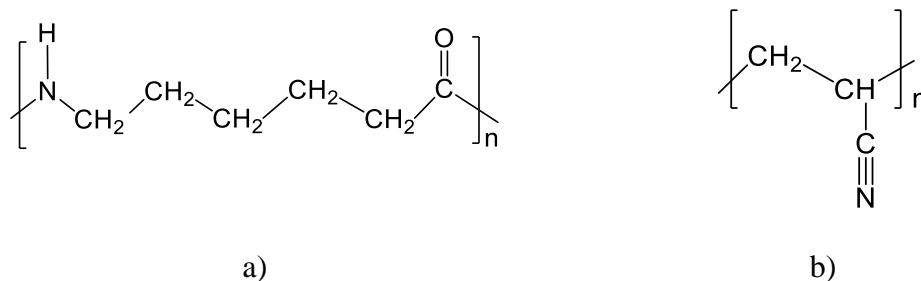
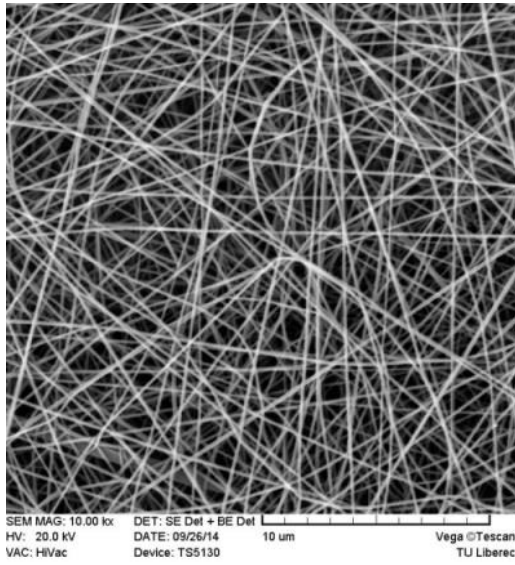
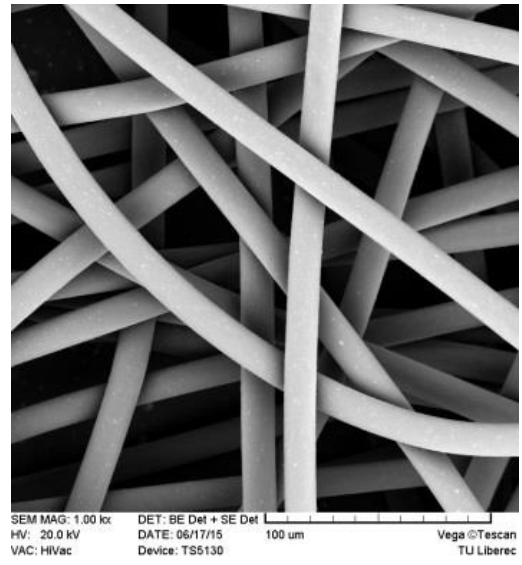


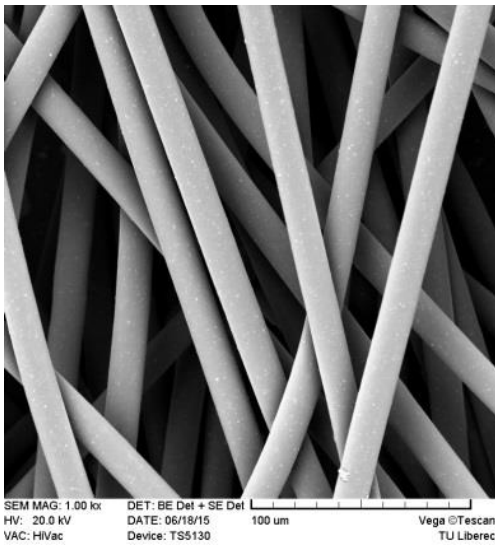
**Fig. 3-6** Chemical structures of polyamide 6 (a) and polyacrylonitrile (b).



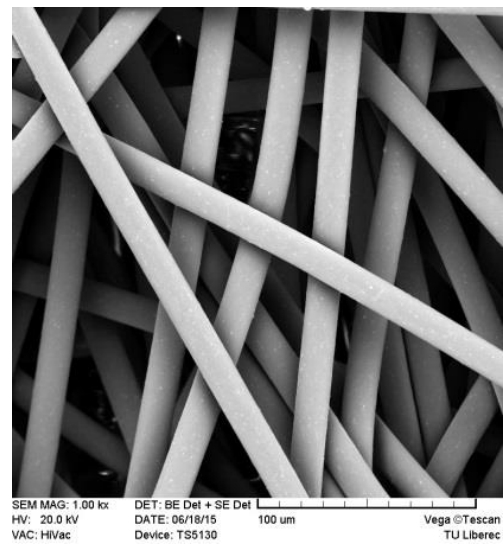
a)



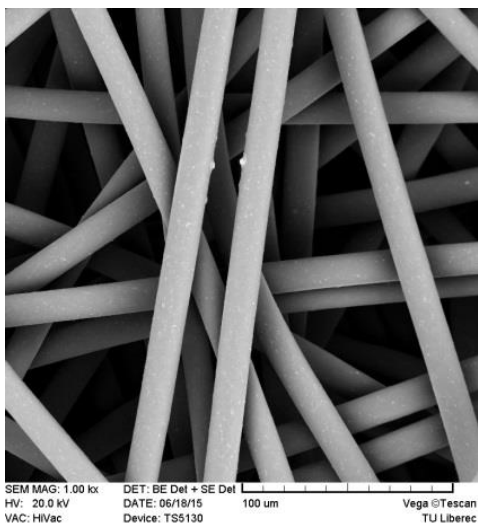
b)



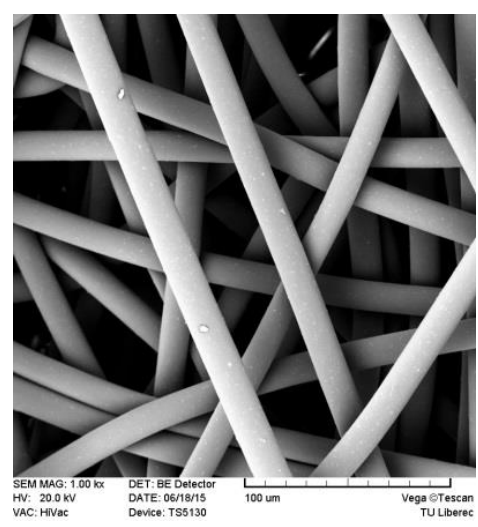
c)



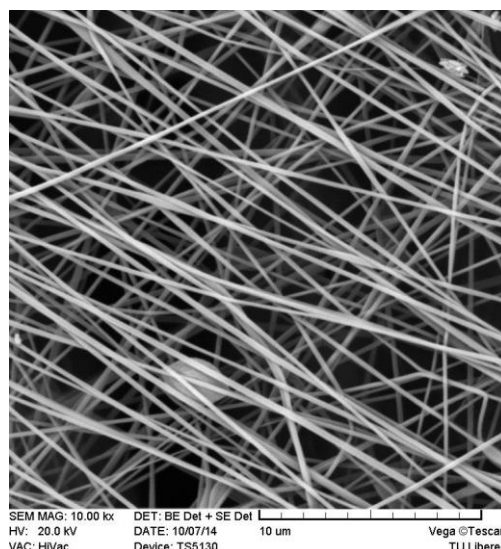
d)



e)



f)



g)

**Fig. 3-7** SEM images of filters: a) PNM with areal density of  $0.5 \text{ g/m}^2$ , b-f) SB with areal density of 20, 40, 50, 70, and  $100 \text{ g/m}^2$ ; g) PAN with areal density of  $0.4 \text{ g/m}^2$ .

Polyamide 6 woven fabric was used as a comparison for PNM and the porosity was 48.8%.

### 3.1.2 Sorbed material

#### 3.1.2.1 Hormone

The hormone we used was  $17 \beta$ -estradiol with 99.7% purity purchased from SIGMA with scientific data shown below:

**Table 3-3** Physical and chemical characteristics of  $17 \beta$ -estradiol.

Abbr.	CAS No.	Molecular weight (g/mol)	Molecular formula	Molecular structure	Maximum UV-Vis absorbance wavelength (nm)
ED	50-28-2	272.39	$\text{C}_{18}\text{H}_{24}\text{O}_2$		280

#### 3.1.2.2 Dyestuff

C. I. Acid Blue 41 (AB41), C.I Acid Yellow 11 (AY11), C.I Acid Yellow 36 (AY36) ,C.I Acid Red 73 (AR73), and C. I. Acid Orange 7 with purity over 85%



purchased from Sigma-Aldrich were used as sorbed materials and simulated pollutant in nanophotocatalysis experiment. The structures and scientific data of dyes are shown as follows:

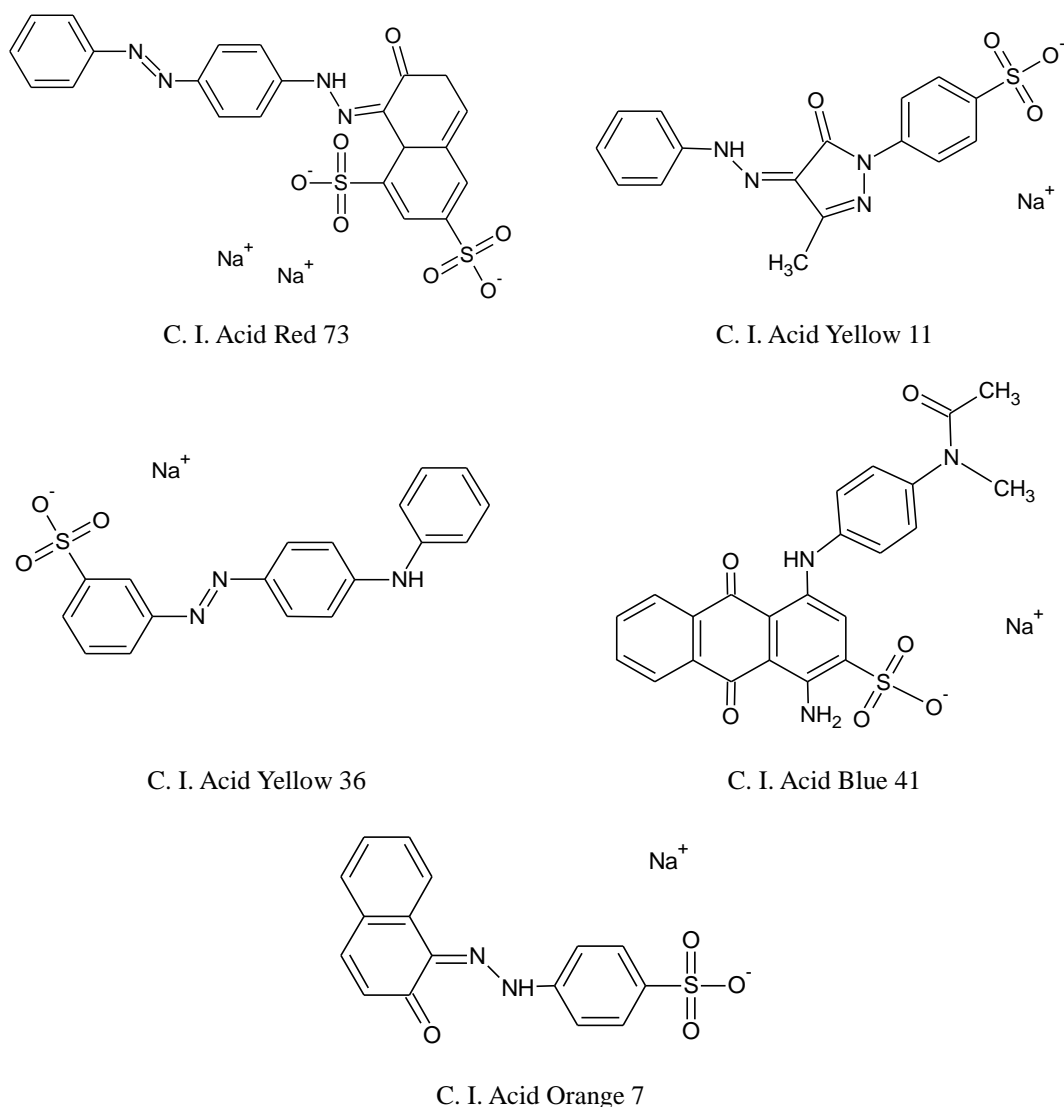


**Fig. 3-8** The molecular structures of selected dyestuffs.

The light absorbance spectrums of AY11, AY36, AR73, and AB41 were tested by Thermo Scientific Helios Epsilon UV-Visible Spectrophotometer. The 1 cm×1 cm cuvettes were used to test the concentration of the acid dye solution during all the experiments. The wavelength of peak absorbance was marked in Fig. 3-9 which shows the maximum UV-Vis absorbance wavelength used for testing dye solutions later were 392, 440, 509, and 598 nm for AY11, AY 36, AR73, and AB41 respectively.

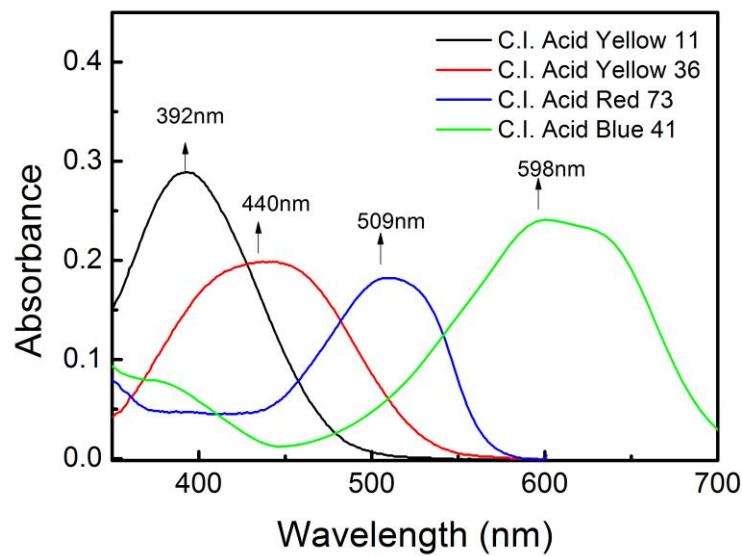


**Fig. 3-9** Light absorbance spectrum in wavelength of AY11, AY36, AR73, and AB41.

The dye solutions with different concentrations (0.005, 0.01, 0.02, 0.03, and 0.05 g/L) were prepared and tested in chosen wavelength for each dye. Firstly, 1 g/L dye solutions were prepared, then the prepared solution was diluted with distill water into the particular concentrations as mentioned above. The light absorbances of different concentrations were plotted in following figure and the linear fitting functions were given.

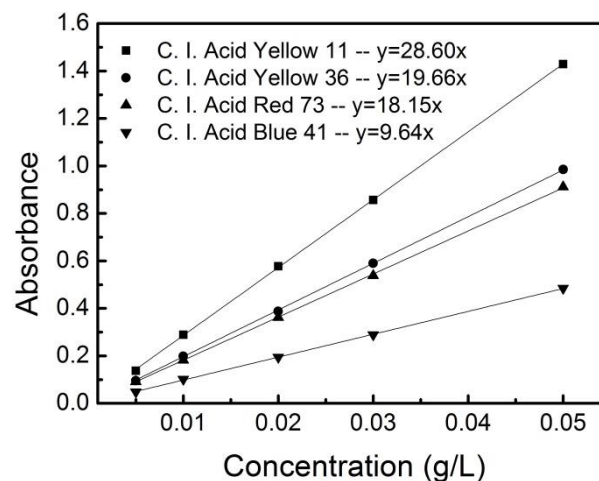


**Fig. 3-10** Light absorbance of different dye solution concentrations and the function of linear fitting for each dye.

The absorbances with different concentrations were plotted in above figure with over 0.9998  $R^2$  linear fitting.

**Table 3-4** Physical and chemical characteristics of selected dyestuffs.

Abbreviation	CAS No.	Molecular weight (g/mol)	Molecular formula	Maximum UV-Vis absorbance wavelength (nm)
AY11	6359-82-6	380.4	$C_{16}H_{13}N_4O_4SNa$	392
AY36	587-98-4	375.4	$C_{18}H_{14}N_3O_3SNa$	440
AR73	5413-75-2	556.5	$C_{22}H_{14}N_4O_7S_2Na_2$	509
AB41	2666-17-3	487.5	$C_{23}H_{18}N_3NaO_6S$	598
AO7	633-96-5	350.3	$C_{16}H_{11}N_2NaO_4S$	483

As a kind of water-soluble anionic dye, acid dyes have good affinity for polyamide fibers.

### 3.1.3 Other materials

#### 3.1.3.1 Chemical reagents

Guaranteed Reagent Hydrochloric acid 35% (HCl) and Sodium Hydroxide (NaOH) purchased from Lach-Ner, s.r.o. have been used in the experiment for adjusting the pH of dye solution. The pH values were adjusted with 5w/w% HCl and 5w/w% NaOH. Distilled water was used as a model water matrix.

#### 3.1.3.2 Catalyst

TiO<sub>2</sub> (P25) Anatas: Rutile 70:30, with particles diameter of 21 nm, purchased from Degussa Ltd. was used as catalyst.

## 3.2 DYNAMIC SORPTION STUDY APPARATUS ASSEMBLING

In this work, several apparatus were assembled and proposed for dynamic sorption process and study.

### 3.2.1 Vacuum sorption apparatus

The first version apparatus is the normal filtration unit as shown in Fig. 3-11.

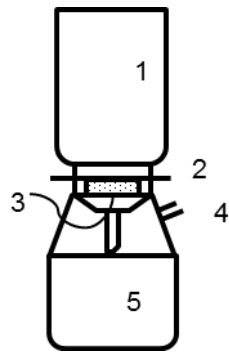
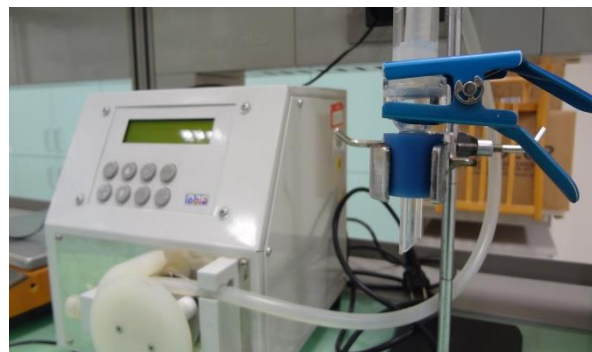
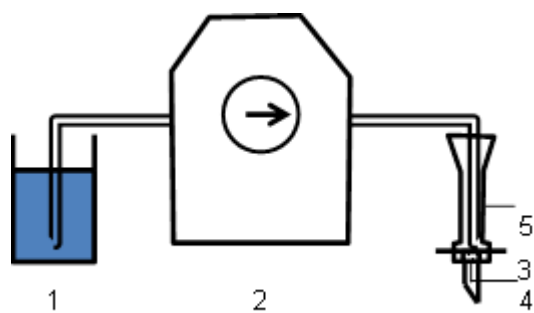


**Fig. 3-11** Vacuum sorption apparatus: 1-funnel; 2-sorbent; 3-sorbent supporting unit; 4-vacuum pressure port; 5-vacuum flask.

The dynamic sorption process was performed under vacuum pressure created by suction pump where the vacuum flask was used to collect the filtered sample. The diameter of the filter area was 38 mm.

### 3.2.2 Constant influent apparatus

This apparatus mainly included a pump whose flow rate can be adjusted from 0 to 60ml/min under the standard configuration. The membrane holder was used to support the sorbent. Two containers were used for containing original solution and treated solution, which went through sorbent. All the parts of this testing apparatus were connected with pipes to make a circuit (as shown in figure 3). The peristaltic pump provided the applied force/pressure/flow flux on sorbent, and the applied force/pressure/flow flux can be adjusted according to the flow rate of pump.



a)

b)

**Fig. 3-12** Constant influent apparatus: a) Structure of the apparatus: 1-beaker with influent, 2-peristaltic pump, 3-sorbent, 4-sorbent supporting unit, 5-funnel; b) Picture of the assembled apparatus.

The fatigue property of filter media in a long time duration can be observed due to the

continual testing circuit, and the performance of filter media can be observed in a long period. Besides, the performance of filter media can be studied in a fluctuating flow rate/pressure by adjusting the pump power.

### 3.2.3 On-line testing constant flow apparatus

On-line testing constant flow apparatus is shown in Fig. 3-13. This apparatus for achieving continual dynamic sorption process was prepared in order to investigate the dynamic sorption property of membrane more flexibly and efficiently.

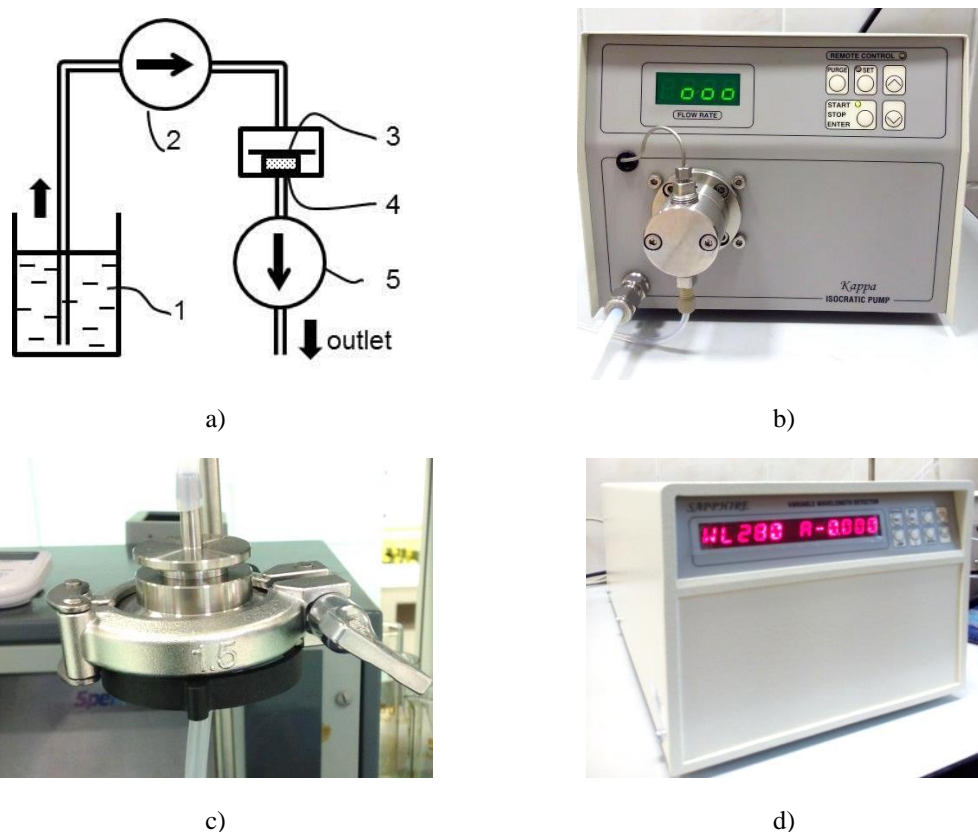


**Fig. 3-13** On-line testing constant flow apparatus: a) the sketch of testing apparatus: 1) container with original solution; 2) & b) isocratic pump; 3) sorbent; 4) & c) sanitary in-line stainless steel holder; 5) & d) UV-Vis variable wavelength detector.

This apparatus included:

1. Two containers which were used for influent and effluent
2. Isocratic pump (KAPPA 10 P, ECOM) with flow rate range 0.01-9.99 mL/min under the standard configuration
3. UV-Vis variable wavelength detector (SAPPHIRE 600, ECOM.) which is

available for routine analytical chromatography as well as for preparative chromatography in the range of 190 -600 nm and a noise level  $\pm 0.5 \times 10^{-5}$  AU

4. High pressure sanitary in-line stainless steel holder (KS 25 F 1/PK, ADVANTEC) used for supporting and fixing PNM between pipes without air leaking.

All the parts of this apparatus were connected with pipes to make a circuit. The diameter of the working area was 22 mm.

The on-line testing constant flow apparatus can meet the testing standard, and can provide more information in terms of flow flux, fatigue property and usage lifetime of fibrous membrane. Moreover, this apparatus improved the efficiency of testing.

### 3.2.4 Dynamic sorption photocatalysis apparatus

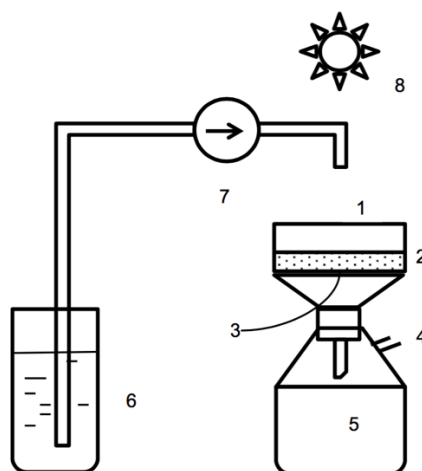


**Fig. 3-14** Apparatus for dynamic sorption process with UV lighting. 1-funnel; 2-sorbent; 3-sorbent supporting unit; 4-vacuum pressure port; 5-vacuum flask; 6-container with original solution; 7-peristaltic pump; 8-UV lighting system.

Dynamic sorption photocatalysis apparatus was a combination of vacuum sorption apparatus mentioned in 3.2.1, inlet supplying system, and UV lighting system. And some adjustments such as increasing of membrane working area and decreasing of inlet flow rate were selected for better sorption performance. The diameter of working area was 10 cm. Flow rate range was 0.05-40 mL/min which can be adjusted by peristaltic pump shown in Fig. 3-14 7). The UV lighting system was assembled with a lamp from Bandelin Co. D-69168 Wieslich, type N-36 K and frame for supporting. It gives radiation with wavelength 254 nm and performance  $4 \times 6$  W.

### 3.2.5 Crossflow dynamic sorption apparatus

As for the fouling problems occur, a crossflow unit has been set up for better performance of dynamic sorption. The PNM1.3 with working area  $0.10 \text{ m}^2$  (length: 112.7 cm, width: 8.8 cm) and a Polypropylene web were wrapped around a glass rod with diameter 5 mm and then inserted into a Polypropylene shell shown in Fig. 3-15 b). A vacuum pump provided the driving force and the flow rate was 25 mL/min.

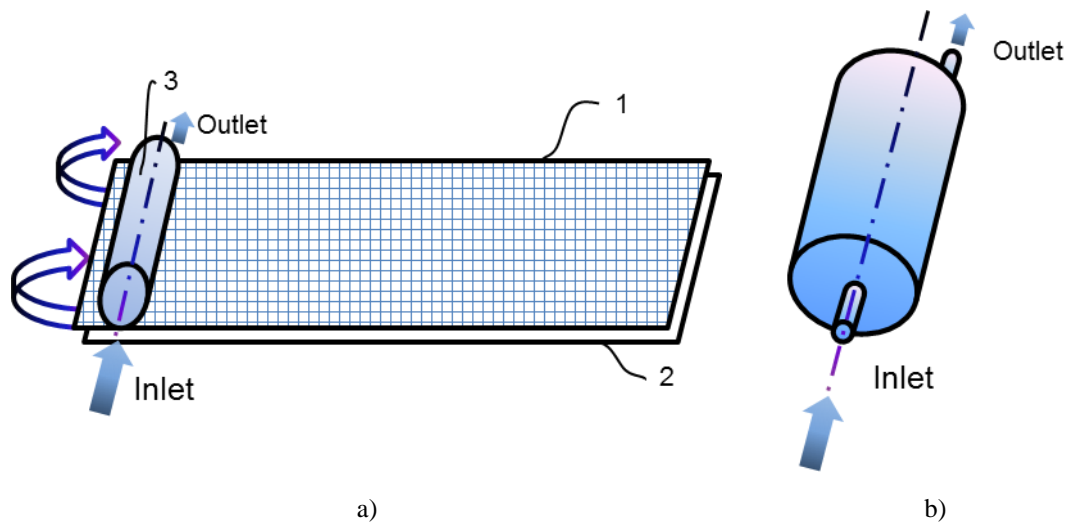


**Fig. 3-15** Crossflow dynamic sorption apparatus. a) Setting up method; b) Crossflow dynamic sorption unit; 1-Polypropylene web; 2-PNM1.3; 3-Glass rod.

Fig. 3-16 shows a filter after 500 mL 0.01 g/L AB41 filtrated.

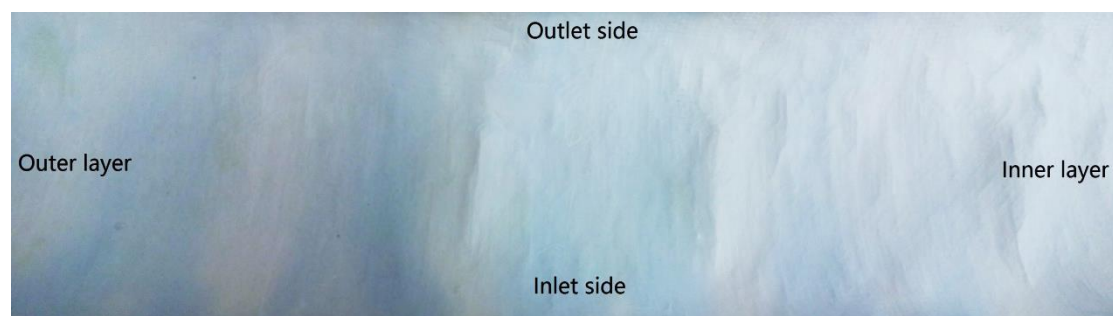


**Fig. 3-16** Spiral wound filter after using.

## 3.3 METHODS

### 3.3.1 Batch experimental methods

Sorption experiments were carried out in batch mode. Various parameters like bath

temperature, pH, solution concentration, dosage of sorbent, and fiber scale of sorbent were investigated. Sorption kinetic experiment was performed with a water bath shaker and thermodynamic parameters were calculated.

Experiment under three different bath temperatures ( $30\pm 1$ ,  $40\pm 1$ , and  $50\pm 1^\circ\text{C}$ ) were carried out with PNM1.3 dosage 0.4 g/L (0.02 g/50 mL) using Magnetic stirring Bitrum® mm7 with speed 120 rpm. The initial concentration of Acid Blue 41 was 0.01 g/L, and the concentration was tested at time 0, 5, 10, 15, 20, 30, 45, 60, 80, 100, and 120 minutes by Helios Epsilon UV-Visible Spectrophotometer (Thermo SCIENTIFIC).

Batch adsorption experiments with different pH were conducted using PNM1.3 and PNM2.9 dose 0.4 g/L (0.02 g/50 mL). The initial AB41 concentration was 0.01 g/L, and the contact time was 10 days. Distilled water was used as a model water matrix. Six pH values were used (2.1, 3.7, 4.4, 5.9, 7.5, and 8.7) to evaluate the effect of pH value on sorption. The pH values were adjusted with 5w/w% HCl and 5w/w% NaOH and measured by Eutech Instruments pH510 pH/mV/ °C meter, Chromservis, Czech Republic. The solution temperature were measured at the mean time as  $23.0\pm 0.6^\circ\text{C}$ .

Four different AB41 concentrations (0.005, 0.01, 0.02, and 0.03 g/L) were used. The dosage of PNM1.3 was 0.12 g/L (0.0024 g/20 mL). The contact time was 30 min, and the absorbance of dye solution was checked at time 0, 1, 2, 4, 6, 10, and 30 minutes by Spectrometer, Spekol 11, ZP100027.

PNM1.3 were conducted in distilled water at  $\text{pH } 5.9\pm 0.1$  with dosage ranging from 0.02 to 1 g/L (from 1 to 50 mg in 50 mL dye solution), the initial AB41 concentration was 0.01 g/L, and the contact time was 10 days. The experiments were performed at a room temperature as  $20\pm 1^\circ\text{C}$ . At time  $t=0$  and equilibrium, the dye concentrations of the solutions were measured by Helios Epsilon UV-Visible Spectrophotometer. These data were used to calculate dye exhaustion, and the adsorption capacity,  $C_s$ , of the adsorbent. Finally,  $C_s$  was plotted against equilibrium concentration,  $C_L$ . Data was fitted with Freundlich and Langmuir equilibrium isotherms. Polyamide 6 woven fabric W175 was measured the same way as PNM1.3 and dye exhaustion was calculated accordingly.

Batch adsorption experiments with PNM1.3 and PNM2.9 for kinetics study were



conducted using a same dose 200 mg/L (20 mg PNM in 100 mL dye solution). Three acid dyes (Acid Yellow 11, Acid Yellow 36, and Acid Red 73) were used as sorbed material and the initial dye concentration was 0.01 g/L, and the contact time was 24 hours. Distilled water was used as a model water matrix. To evaluate the effect of temperature on sorption, three water bath temperature values (30, 40, and 50 °C) were used. The solution temperature was measured during the experiments with an error of 1 °C. The rotation was provided by a water bath shaker with a rotation rate at  $90 \pm 5$  rpm. UV-2550 UV-Visible Spectrophotometer was used to detect the concentration changes within 24 hours and the data from first 120 minutes was fitted with kinetic models Elovich and Pseudo-Second Order.

Thermodynamic parameters of sorption of AB41 onto PNM1.3 were calculated according to the isotherm and kinetic experiments and the equations mentioned in 2.2.7.

### 3.3.2 Dynamic sorption experimental methods

The general comparison of dynamic sorption efficiency was conducted with vacuum sorption apparatus described in 3.2.1. 50 mL Hormone 17  $\beta$ -estradiol solution with concentration 0.005 g/L was filtrated by PNM1.3 and PNM2.9. The solution concentrations before and after filtration were evaluated by High Performance Liquid Chromatography. Hormone exhaustion and hormone removal capacity were calculated and compared.

Polyamide 6 fiber assembles with different fiber scale nanofibrous membrane (PNM) with areal density 0.5, 1.3, and 2.9 g/m<sup>2</sup>, Spun Bond nonwoven mats (SB) with areal density 20, 40, 50, 70, and 100 g/m<sup>2</sup>, and woven fabric (W) with areal density 175 g/m<sup>2</sup>) were used as filters for 1 L AB41 (0.01 g/L) removing. Solution concentrations before and after 5, 10, 30, 50, 100, 200, 300, ..., 900, 1000 mL dye solution filtrated were tested by Spectrometer, Spekol 11, ZP100027. Dye removal capacity with the filtrated volume change was calculated and plotted for comparison. The morphology images were taken by Dino-elite digital microscope.

Polyacrylonitrile (PAN) with areal density 0.4 g/m<sup>2</sup> was evaluated same as the process mentioned above.

The dynamic sorption was performed with the constant influent apparatus described

in 3.2.2 with starting flux around 2500 L/(m<sup>2</sup> h). The concentration after separation were examined every 10 mL, meanwhile the time taken by every 10 mL was recorded. The accumulated mass of dyestuff filtrated by PNM and the flux during the separation process were calculated.

The capacity of one layer and two layers PNM1.3 under three different feeding concentrations of acid dye solution AB41 was evaluated with on-line testing constant flow apparatus described in 3.2.3. The flow rate of piston pump was kept at 3 mL/min. The concentration of effluent was examined on-line by UV-Vis variable wavelength detector, and the time interval between two tests was approximately 0.18 s. Morphology of samples were observed by scanning electron microscopy (SEM).

### 3.3.3 Surface modification methods

#### 3.3.3.1 Surface modification by steaming

The steam treatment was performed on PNM1.3 with diameter 35.7 mm in the Tuttnauer Autoclave-Steam Sterilizer with model no. 2540ML. The temperature can be set from 90 to 140 °C. Eight different temperatures (100, 105, 110, 115, 120, 125, 130, and 135 °C) were chosen for steaming experiment on PNM1.3 surface modification. After reaching to the setting temperature, PNM1.3 was kept in the Autoclave-Steam Sterilizer for 5 minutes and then cooled down and natural dried overnight.

The batch experiment for checking the sorption properties of PNM1.3 was performed after the steam treatment. 30 mL AB41 with concentration 0.01 g/L was prepared for each sample, and absorbance of AB41 dye solution was investigated and calculated before and after 24 hours experiment.

FTIR was used for investigating the change in PNM's molecular chain after steam modification on its surface.

#### 3.3.3.2 Nanophotocatalysis for PNM self-cleaning

TiO<sub>2</sub> nanoparticles were evenly deposited onto PNM1.3 by vacuum sorption apparatus mentioned in 3.2.1. Ascorbic acid (AA) 0.2 mL with concentration 100 g/L was used as the catalyst as well. The light source was used a lamp from Bandelin Co. D-69168 Wieslich, type N-36 K. It gives radiation with wavelength 254 nm and

performance  $4 \times 6$  W.

The initial concentration  $\text{TiO}_2$  solution was 10 mg/L, and then the prepared solution was diluted with distill water into 50 mL with different amount as 0, 1, 2, 5, and 10 mL. Thermo Scientific Helios Epsilon UV-Visible Spectrophotometer was used for measurement of the absorbance of  $\text{TiO}_2$  solutions at 400 nm wavelength before and after filtration. After filtration and nature drying, the  $\text{TiO}_2$  nanoparticles were deposited onto PNM1.3. Samples after depositing were named in the following table:

**Table 3-5** Sample code of  $\text{TiO}_2$  nanoparticles deposited onto PNM1.3.

Amount of $\text{TiO}_2$ solutions mL	$\text{TiO}_2$ concentration on PNM mg/m <sup>2</sup>	Sample code	
		With AA	Without AA
0	0	AA1	BB1
1	9	AA2	BB2
2	18	AA3	BB3
5	44	AA4	BB4
10	88	AA5	BB5

After depositing, 10  $\mu\text{L}$  of AO7 solution with a concentration of 1 g/L was dropped onto the samples, and the color histogram of samples was analyzed 5 times for each at different exposed time under UV by software program Image J with 50000 pixels.

### 3.3.3.3 Dynamic sorption process with nanophotocatalysis

Apparatus described in 3.2.4 was used for deposition of  $\text{TiO}_2$  nanoparticles and dynamic sorption experiment of Acid Orange 7 on polyamide 6 nanofibrous membrane with areal density 2.5 g/m<sup>2</sup>.

**Table 3-6** Sample code of dynamic sorption experiment with  $\text{TiO}_2$  nanophotocatalysis.

Sample code	Amount of $\text{TiO}_2$ solutions	UV lighting time	Flow rate
	mL	min	mL/min
Control	0	0	17
UV	0	65	17
NPsUV	100	65	17
NPsIUUV	100	200	8.3

100 mL  $\text{TiO}_2$  NPs solution with concentration 0.01 g/L was filled into the funnel

while the vacuum pump working. AO7 solution was prepared with concentration 0.002 g/L, and 10 times 50 mL AO7 solution were pumped for one experiment. 17 and 8.3 mL/min of flow rate were used for the experiment, which has been described in detail in Table 3-6.

The absorbance of influent and effluents after each 50 mL AO7 solution inserted were detected with Spectrometer, Spekol 11, ZP 100027. The dye removal amount and sorption capacity were calculated and compared.

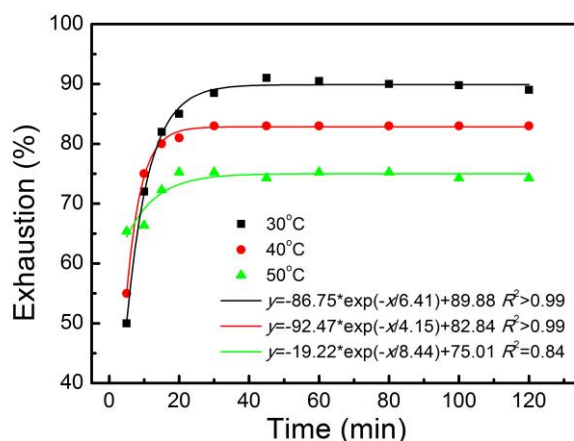
## CHAPTER 4. RESULT AND DISCUSSION

### 4.1 ANALYSIS OF DYE SORPTION ONTO POLYAMIDE 6 NANOFIBROUS MEMBRANE

#### 4.1.1 Factors influencing sorption of dyes by polyamide 6

##### 4.1.1.1 Temperature

Three different temperatures respectively  $30\pm 1$ ,  $40\pm 1$ , and  $50\pm 1$ °C were used for comparing the dye removal rate according to time of PNM1.3 under stirring condition. The comparing result is shown in Fig. 4-1 as follows:



Temperature °C	Reduced Chi-Square	Residual Sum of Squares	Degree of Freedom
30	0.63	4.42	7
40	0.25	1.73	7
50	2.21	15.45	7

**Fig. 4-1** PNM1.3 exhaustion of dye AB41 under different temperatures.

As shown in Fig. 4-1, solution temperature shows huge effect on both initial and equilibrium stage of exhaustion. The data at the beginning of experiment (5 min) indicate a rapid dye uptake before 5 minutes while the temperature was high cause 65.4% of dye has already been cleaned other than 50 and 55% under the temperature of 30 and 40°C. However, the equilibrium dye removal rate shows better dye sorption of low temperature due to less desorption of dyes from the membranes under lower temperatures.

The result was fitted with exponential equation, and statistics parameters such as

residual sum of squares, degree of freedom, and reduced Chi-square were given in the table below the figure. the residual sum of squares is the sum of the squares of residuals (deviations predicted from actual empirical values of data). It is a measure of the discrepancy between the data and an estimation model which indicates a tight fit of the model to the data for small value. The number of degrees of freedom is the number of values in the final calculation of a statistic that are free to vary. The reduced chi-square is obtained by dividing the residual sum of squares by the degrees of freedom which gave more obvious comparison for goodness of data fitting. As for Fig. 4-1, the results under 30 and 40°C showed better fitting with exponential equation.

#### 4.1.1.2 Initial pH of dye solution

The effect of initial pH on the equilibrium uptake capacity of AB41 by PNM at pH 2.1-8.7 and  $23.0 \pm 0.6$  °C is shown in Fig. 4-2. The sorption of AB41 by PNM was significantly influenced by pH in the chosen range. Two PNMs with different areal densities, 1.3 and 2.9 g/m<sup>2</sup> were chosen to compare the effect of areal density of sorbent on uptake capacity. Similar trends were observed for these two PNMs with different areal densities. The uptake capacity was significantly reduced as the solution became alkaline, while the minimum value was in pH 7.5. The sorption was at the maximum in acidic medium. In the natural state of pH 5.9 without pH adjustment, the sorption of AB41 was relatively high so that we chose to not adjust the pH in the future experiments in order to exclude unexpected pH adjustment error.

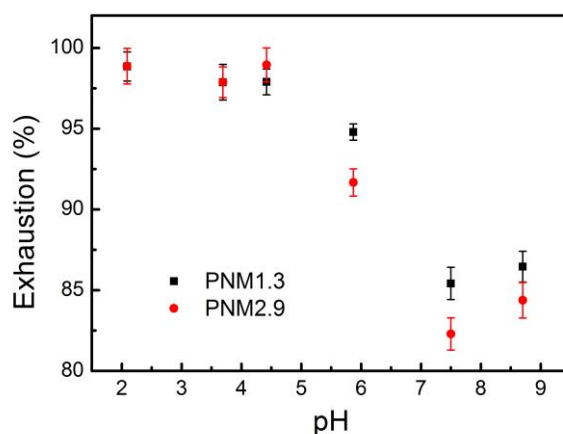
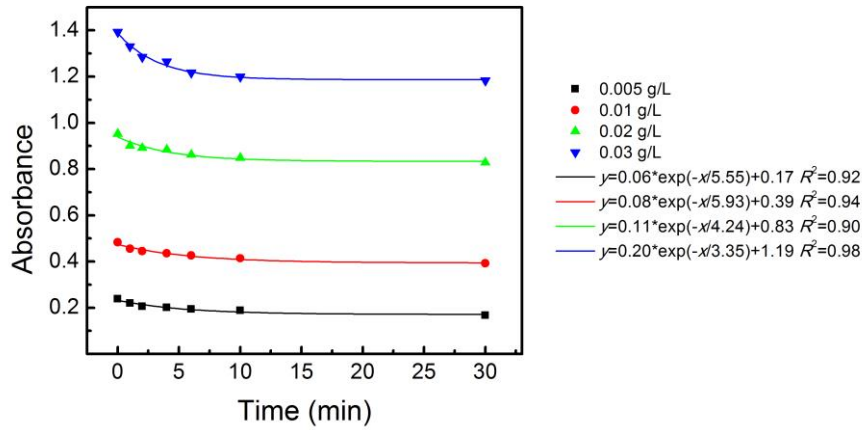


**Fig. 4-2** The effect of initial pH on the sorption capacity of dye AB41 by PNM1.3 and PNM2.9

Comparing the two PNMs with different areal densities, the sorption capacities of

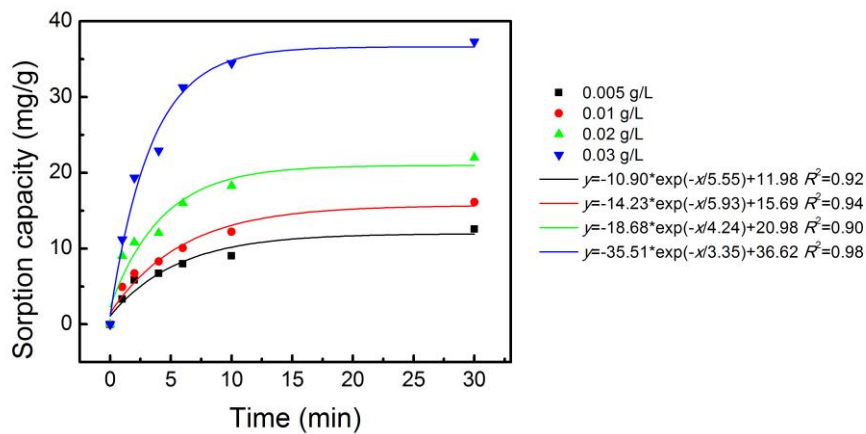
AB41 were similar in acidic medium but differed in alkaline medium, which PNM1.3 showed better sorption of AB41 than PNM2.9.

#### 4.1.1.3 Initial concentration of dye solution



Concentration g/L	Reduced Chi-Square	Residual Sum of Squares	Degree of Freedom
0.005	4.29E-5	1.72E-4	4
0.01	5.08E-5	2.03E-4	4
0.02	1.62E-4	6.48E-4	4
0.03	1.34E-4	5.36E-4	4

a)



Concentration g/L	Reduced Chi-Square	Residual Sum of Squares	Degree of Freedom
0.005	1.35	5.42	4
0.01	1.60	6.42	4
0.02	5.11	20.43	4
0.03	4.23	16.91	4

b)

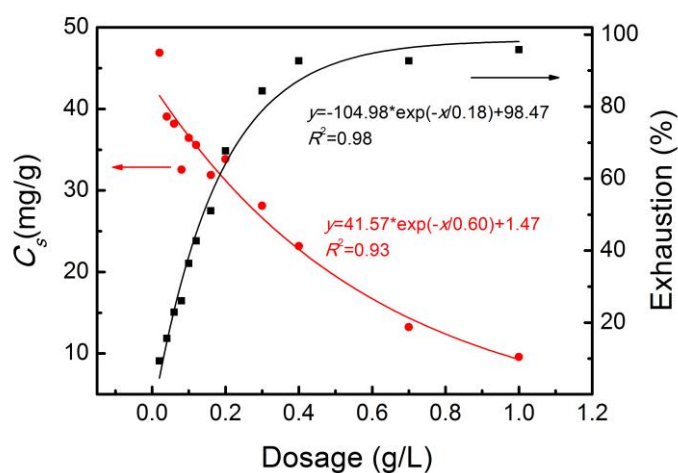
**Fig. 4-3** Absorbance and dye removal capacity change of dye solution by PNM sorption according to time.

The experiments were carried out with PNM1.3 dosage of 0.0024 g/20 mL solution. The natural solution pH was used without any adjustment. Fig. 4-3 b) shows the effects of time and AB41 initial concentration on the removal of AB41 by PNM1.3.

The plots show that the sorption of AB41 increases with an increase in time and initial concentrations. The high sorption rate at the initial stage was due to the sorption of AB41 by the exterior surface of PNM1.3. When the initial concentration increased, the mass transfer driving force became larger, hence resulting in higher AB41 sorption.

#### 4.1.1.4 Dosage of sorbed material

Twelve different dosages range from 0.02 to 0.1 g/L of PNM1.3 in 50 mL AB41 dye solution with concentration 0.01 g/L have been considered before the main experiment, and Fig. 4-4 shows the result as follows.



Code	Reduced Chi-Square	Residual Sum of Squares	Degree of Freedom
Exhaustion %	19.17	172.53	9
$C_S$ mg/g	7.78	69.99	9

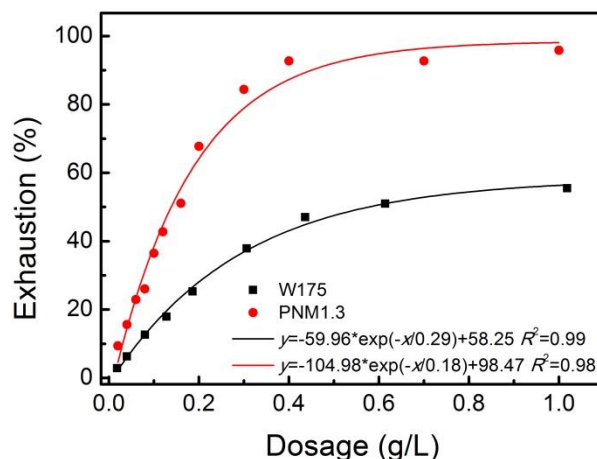
**Fig. 4-4** Effect of dosage of PNM1.3 on sorption capacity  $C_S$  and exhaustion of AB41.

The result shows the dosage of PNM1.3 around 0.2 g/L is sufficient for dye AB41 removal and meanwhile the capacity has been used effectively. However, in order to get better sorption effect, dosage 0.4 g/L of PNM1.3 has been considered as the best dosage to continue our main experiment.



#### 4.1.1.5 Fiber scale of sorbent

The sorption of dye AB41 on different fiber scale of sorbent respectively nanoscale (PNM1.3) and conventional scale (W175) have been compared in this part. Experimental data comparison was given in Fig. 4-5.



Sample	Reduced Chi-Square	Residual Sum of Squares	Degree of Freedom
W175	2.00	11.98	6
PNM1.3	19.17	172.53	9

**Fig. 4-5** Batch experimental data comparison between sorbents Woven and PNM1.3.

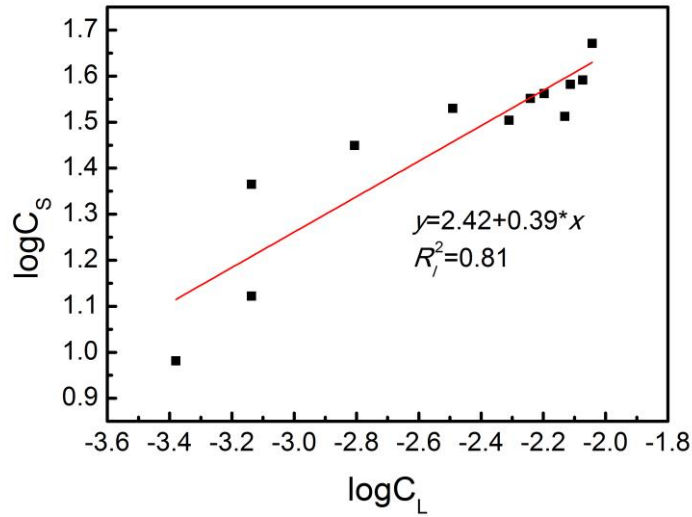
As shown in Fig. 4-5, different dosage of sorbent was considered for sorbent W175 and PNM1.3. Mostly the exhaustion of dye solution AB41 on W175 sample got half of the value of dye exhaustion on PNM1.3. The exhaustion of dye solution AB41 on PNM1.3 is increasing from 0 to 95.8% while increasing of sorbent dosage from 0.0 to 1.0 g/L. the exhaustion of dye solution AB41 on W175 shows the similar trend according to the change of dosage but it can reach maximum 55.5% in the range of 0.0 to 1.0 g/L. There is a sudden increase of exhaustion on W175 when the dosage of sorbent increased from 0.6 to 1.0 g/L.

#### 4.1.2 Equilibrium modeling

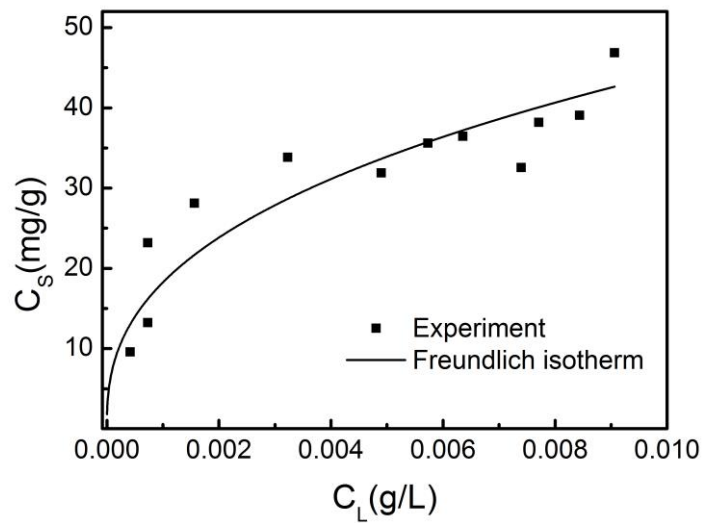
By sorption isotherms fitting after batch experiments, the correlation of sorption properties from aqueous solution with specific surface area would be discovered and discussed. Constants and coefficient of determinations of fitted Freundlich, and Langmuir isotherms were compared for PNM1.3 and PNM2.9. Sorption properties

between these two samples were discussed as well.

The linear fitting of Freundlich isotherm for PNM1.3 was shown in Fig. 4-6 (a) with a relatively low squared correlation coefficient 0.81.



a)



b)

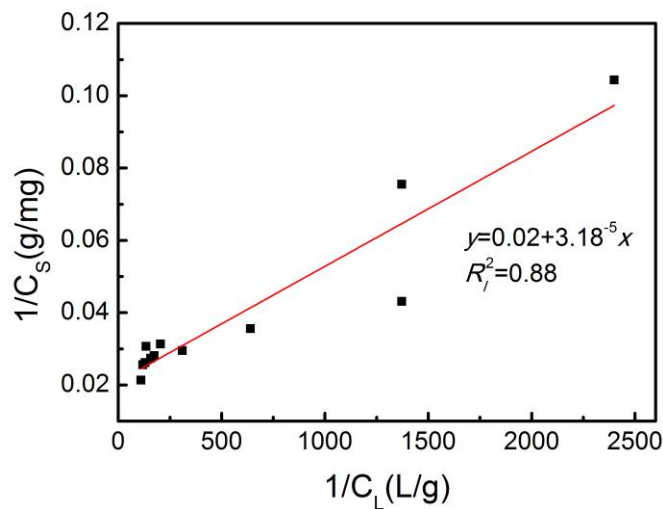
**Fig. 4-6.** Freundlich isotherm model applied on batch experiment results of PNM1.3: a) Freundlich isotherm linear fitting; b) The experimental data compared with Freundlich isotherm model.

By linear fitting, the constants  $K_f$  and  $1/n$  can be found through the slope and intercept values, with which the Eq. (2-8) could be changed into Eq. (4-1) below:

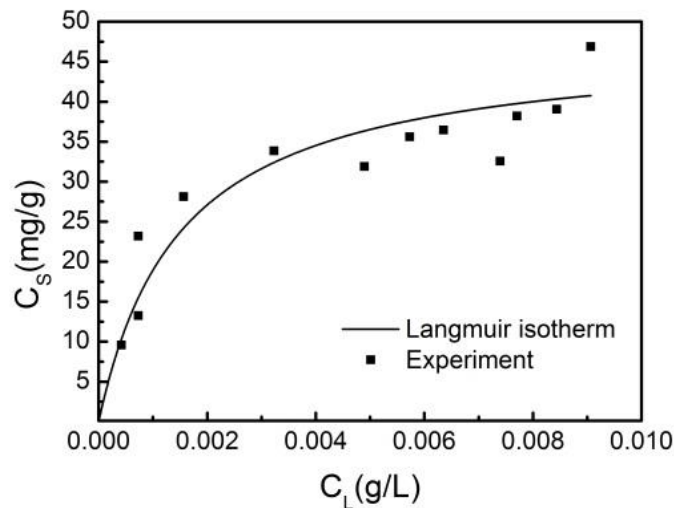
$$C_S = 260.86C_L^{0.39} \quad (4-1)$$

Fig. 4-6 (b) showed the Freundlich isotherm drawn according to Eq. (4-1) comparing with the original experimental data.

Instead of Freundlich, the Langmuir isotherm linear fitting for PNM1.3 was applied and showed in Fig. 4-7 (a) with a squared correlation coefficient comparatively high. The Langmuir equation is applicable to homogeneous sorption, where the sorption of each sorbed material molecule onto the surface is equal to sorption activation energy. [137]



a)



b)

**Fig. 4-7** Langmuir isotherm model applied on batch experiment results of PNM1.3: a) Langmuir isotherm linear fitting; b) The experimental data compared with Langmuir isotherm model.

Table 5-1 showed the constants and correlation coefficients according to the results

from both Freundlich and Langmuir isotherms fitting the experimental data.

**Table 4-1** Equilibrium isotherm constants at room temperature.

Sample no.	$K_f$ (mg/g)(L/g) <sup>n</sup>	$1/n$	$R_f^2$ (Freundlich)	$R^2$	$K_L$ L/mg	$q_0$ mg/g	$R_l^2$ (Langmuir)	$R^2$
PNM1.3	260.86	0.39	0.81	0.83	661.37	47.55	0.88	0.84

The constant  $q_0$  stands for the maximum amount of dye that can be adsorbed in mg/g. The constant  $n > 1$ , and the shape of the Freundlich isotherm for solid surfaces may be interpreted in terms of the latter's energetic heterogeneity, i.e., the highly energetic sites are covered first, etc., as bulk concentration of solute is increased.

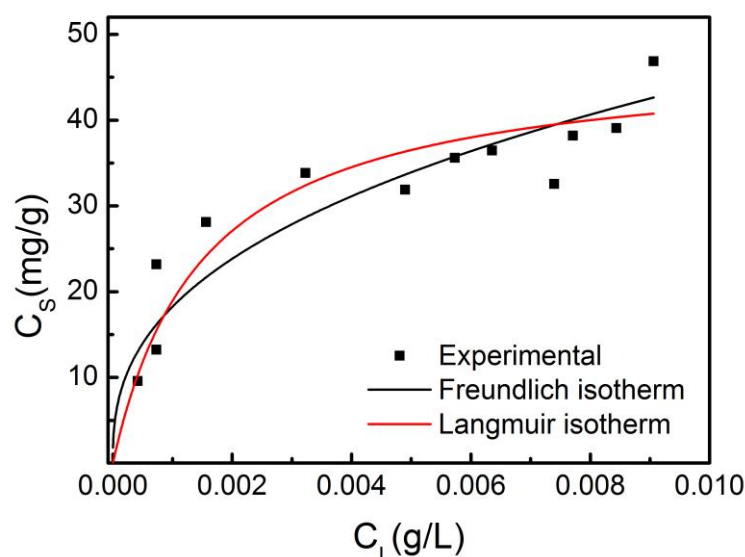


**Fig. 4-8** Comparison among Experimental data and two isotherm models.

Comparing the isotherms for PNM1.3 in Fig. 4-8, Freundlich isotherm showed steeper increasing trend than Langmuir isotherm. The coefficient of determination  $R^2$  showed that Langmuir isotherm fitted the experimental data better. The Langmuir isotherm is often associated physically with adsorption onto an energetically uniform surface without lateral adsorbate interactions. The plateau is thought to correspond to a densely-packed adsorbate monolayer after whose formation there is no further adsorption. The mutual cooperation and cancellation of a variety of effects can lead to Langmuir-type sorption. [63]

For better comparing these two isotherms, the  $R^2$  was calculated according to

Eq.(2-12)-(2-14) and the result were shown in Table 5-1. Both  $R_l^2$  and  $R^2$  showed the Langmuir isotherm fitted the experimental data better.

#### 4.1.3 Kinetic modeling

Sorption systems have been investigated to assess the applicability of PNM as a suitable sorbent for the removal of acid dyes in dye wastewater. An equilibrium analysis is one of the most important fundamental pieces of information required for evaluating the affinity or capacity of a sorbent. However, an ideal sorbent for wastewater pollution control must not only have a large sorption capacity, but also the sorption rate must be fast. Therefore, the sorption rate is the other important factor for the selection of the sorbent and sorption kinetics which must be taken into account.

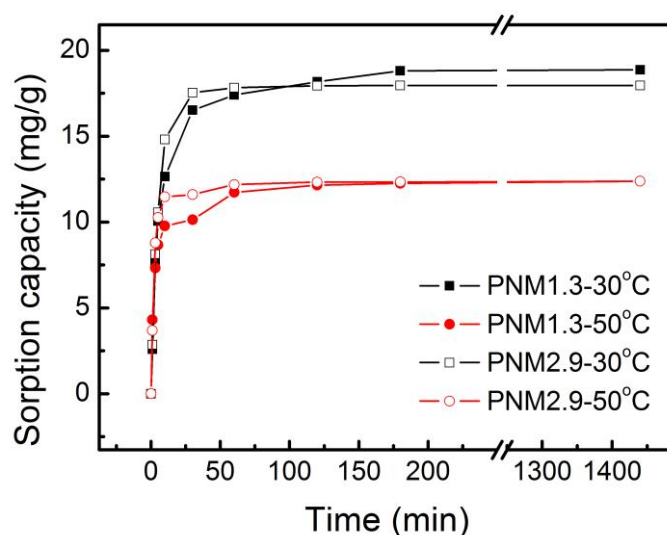


Fig. 4-9 Sorption capacity change of AY36 on different membranes under 30 and 50 °C.

In this part, two kinetic models have been applied to the sorption of acid dyes on PNM. The kinetic models are the Elovich equation and the pseudo-second order equation. The sorption kinetics describes the solute uptake rate and evidently, this rate controls the residence time of adsorbate uptake at the solid-solution interface.

Fig. 4-9 shows the sorption capacity results of AY36 on PNM1.3 and PNM2.9 under 30 and 50 °C. Several phenomenons can be draw from this figure. The rate of removal of dyestuff by sorption was rapid initially and then slowed gradually until it attained an equilibrium beyond which there was significant increase in the rate of removal. At

around 120 min, the dye removal values are achieved at 12, and 18 mg/g for sorption of dyestuff AY36. The maximum sorption of dyestuff onto PNM was observed at 120 minutes and it is thus fixed as the equilibrium time; 2. For this material of membrane, the sorption amounts on unit weight of different dyestuff are different that they removed more AY36 than AR73; 3. In same dyestuff solution, different membranes performed similar that ended at same dye removal value after 24 hours sorption and had similar trend at the initial stage of the sorption processes; 4, Higher  $h$  value can be found under a higher temperature which indicates a faster initial sorption rate when heat applied to the system.

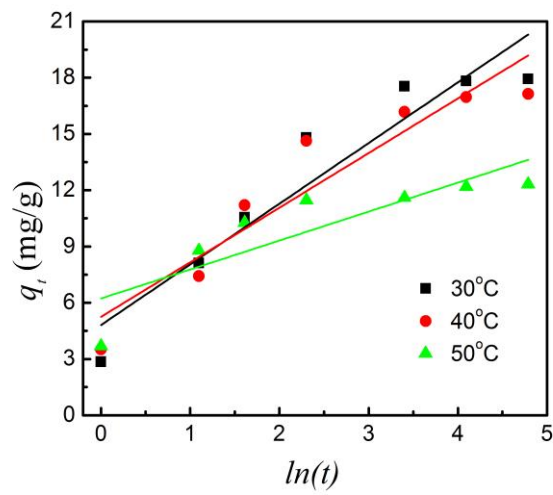
#### 4.1.3.1 Comparison of dye removal on temperature

PNM2.9 was investigated under different temperatures on removing AY36. The linear form of Elovich equation is given in 2.2.6.1. Kinetic model Pseudo-Second Order Equation was tested to determine the reaction order of the sorption process. Under different bath temperature, the samples were behaving different efficiency on dye removing. The linear fitting and fitting with Elovich and Pseudo-Second Order Equations were plotted in Fig. 4-10 and the result was showing in Table 4-2.

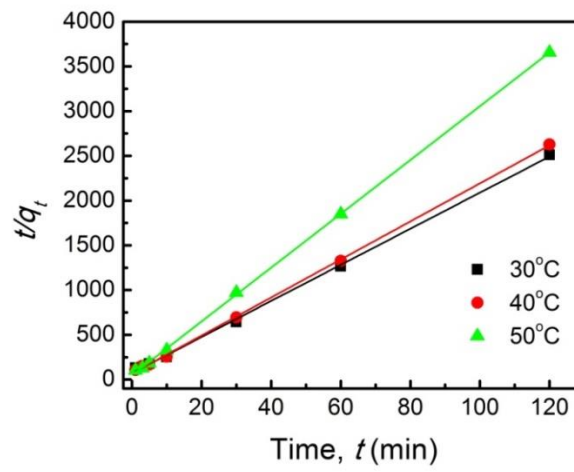
**Table 4-2** Result comparison about bath temperature of linear Elovich and Pseudo-second order equation fitting.

Temp.	Elovich				Pseudo-Second Order				
	$R_l^2$	$R^2$	$b$ g/mg	$a$ mg/ (g min)	$R_l^2$	$R^2$	$q_e$ mmol /g	$k_2$ g/ (mmol min)	$h$ mmol/ (g min) $\times 10^{-3}$
30	0.89	0.66	3.24	1.36	0.99	0.99	0.050	5.72	14.06
40	0.87	0.70	2.91	2.08	0.99	0.99	0.047	6.80	15.04
50	0.70	0.75	1.54	36.54	0.99	0.98	0.033	19.47	21.51

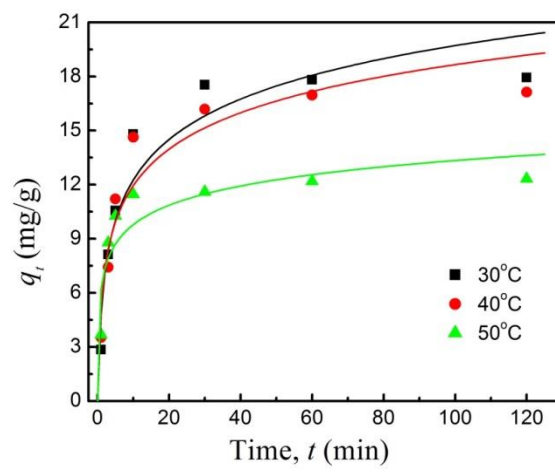
It showed with correlation coefficient  $R_l^2$  that Pseudo-Second Order equation fitted the experimental data better in the case of acid dye removed by PNM. From constant  $a$  and  $h$  we can found that the highest temperature brought fastest sorption process.



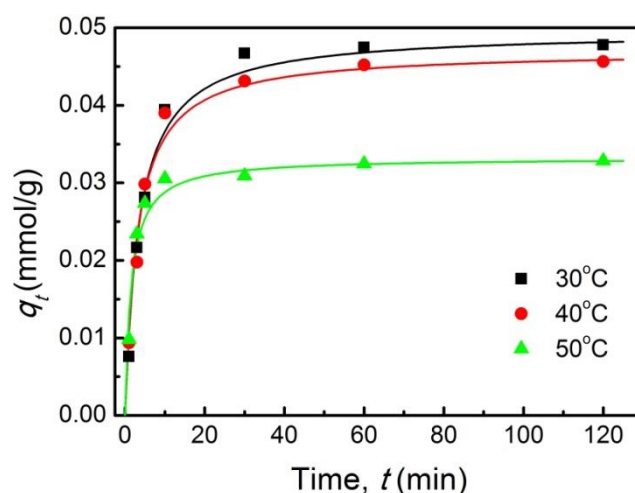
a)



b)



c)



d)

**Fig. 4-10** Elovich and Pseudo-Second Order equation fitting for comparison under different bath temperature: a) linear fitting of Elovich equation; b) linear fitting of Pseudo-Second Order equation; c) Elovich equation curve and experimental data; d) Pseudo-Second Order equation curve and experimental data.

The dye removal capacity was shown in Fig. 4-10 and with the constant  $q_e$  in Table 4-2 that as bath temperature increased, the dye removal capacity decreased from 0.050 to 0.033 mmol/g.

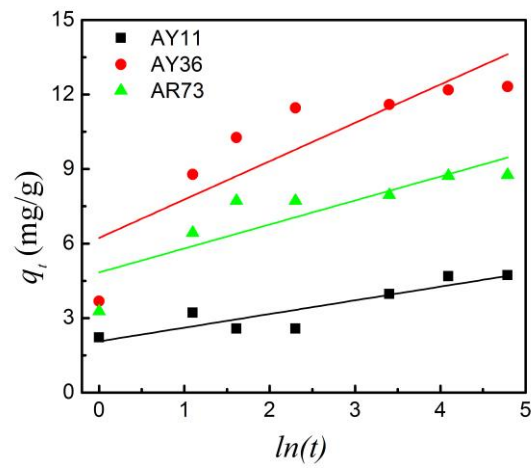
#### 4.1.3.2 Comparison of dye removal on different dyes

Fig. 4-11 shows the linear plots of Elovich and Pseudo-Second Order equation for the sorption of AY11, AY36, and AR73 onto PNM2.9 under bath temperature 50 °C. Similar results were obtained for other bath temperatures and PNM1.3. And the Table 4-3

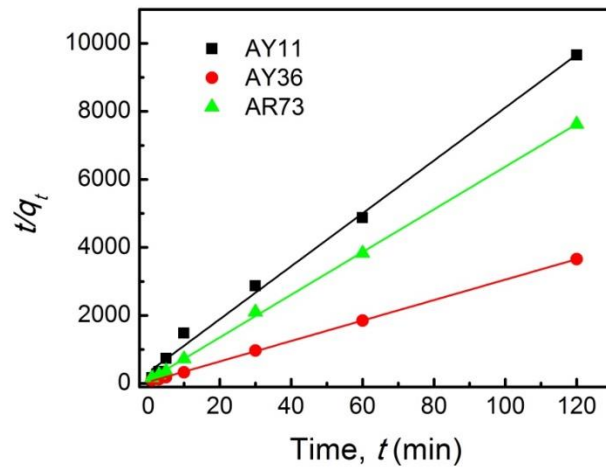
**Table 4-3** Result of linear Elovich equation and Pseudo-second order equation fitting on PNM2.9 under 50 °C.

Dye	Elovech				Pseudo-Second Order				
	$R_l^2$	$R^2$	$b$	$a$	$R_l^2$	$R^2$	$q_e$	$k_2$	$h$
			g/mg	mg/(g min)			mmol/g	g/(mmol min)	mmol/(g min) $\times 10^{-3}$
AY11	0.78	0.91	0.55	76.94	0.99	0.88	0.013	18.16	3.00
AY36	0.70	0.75	1.54	36.54	0.99	0.98	0.033	19.47	21.51
AR73	0.70	0.89	0.97	154.55	0.99	0.99	0.016	40.12	10.18

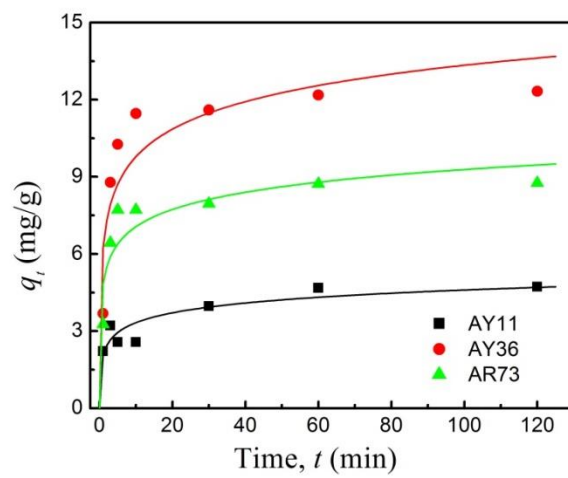




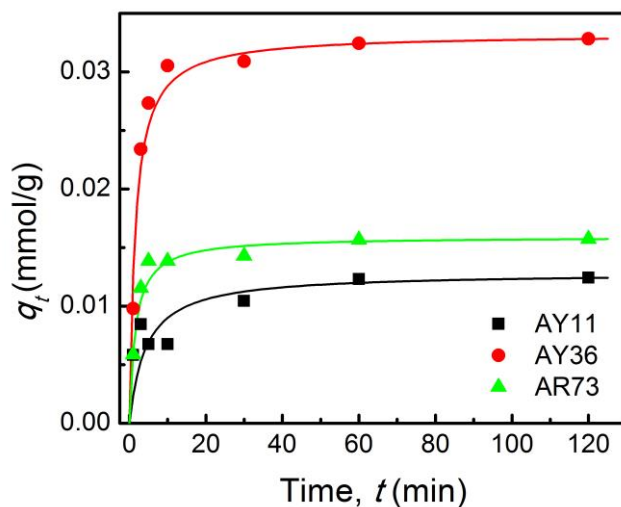
a)



b)



c)



d)

**Fig. 4-11** Elovich and Pseudo-Second Order equation fitting for comparison different dyestuff: a) linear fitting of Elovich equation; b) linear fitting of Pseudo-Second Order equation; c) Elovich equation curve and experimental data; d) Pseudo-Second Order equation curve and experimental data.

#### 4.1.4 Thermodynamic considerations

In any adsorption process, both energy and entropy considerations must be taken into account in order to determine what process will occur spontaneously. Values of thermodynamic parameters are the actual indicators for practical application of a process. The amount of AB41 adsorbed onto PNM1.3 at equilibrium and at different temperatures (30, 40, 50 °C) has been examined to obtain thermodynamic parameters for the adsorption system. According to the Arrhenius type relationship equation [138], a linear plot of  $\ln k_2$  vs  $1/T$  for the adsorption of AB41 onto PNM1.3 was constructed in Fig. 4-12.

The result obtained is 79.45 kJ/mol (shown in Table 4-4) for the adsorption of AB41 onto PNM1.3, indicating that the adsorption has a high activation energy and more orients and corresponds to a chemisorption.

The plot of  $\ln K_C$  as a function of  $1/T$  (Fig. 4-13) gives effectively a linear relationship with determination coefficients of 0.95.  $\Delta H^\circ$  and  $\Delta S^\circ$  were calculated from the slope and the intercept of Van't Hoff plots of  $\ln K_C$  vs  $1/T$ . The results were given in Table 4-4.

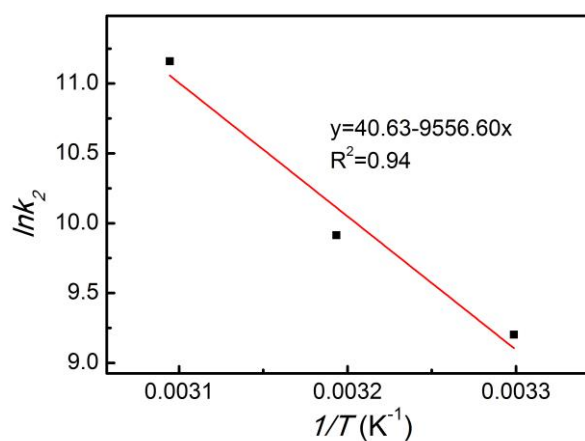


**Fig. 4-12** Arrhenius plot for the adsorption of AB41 onto PNM1.3.

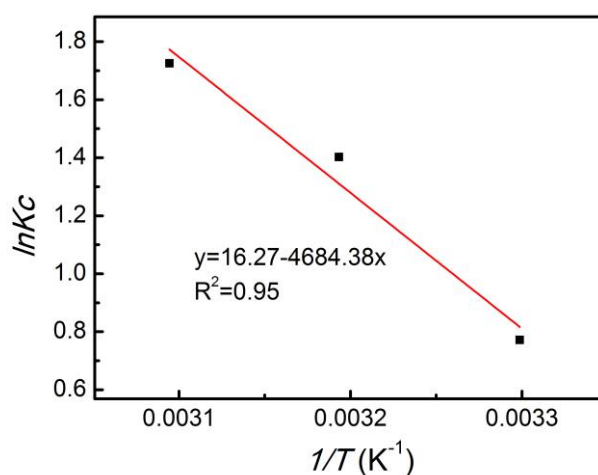


**Fig. 4-13** Van't Hoff plots for determination of thermodynamic parameters for the adsorption of AB41 onto PNM1.3.

The values of adsorption thermodynamic parameters are listed in Table 4-4 .

**Table 4-4** Thermodynamic parameters of AB41 dye adsorption on PNM1.3.

Temperature °C	$E_a$ kJ/mol	$\Delta G^\circ$ kJ/mol	$\Delta H^\circ$ kJ/mol	$\Delta S^\circ$ J/(mol K)
30	79.45	-1.945	38.95	135.26
40		-3.655		
50		-4.64		

The negative value of the change of free energy ( $\Delta G^\circ$ ) confirms the feasibility of the adsorption process and also indicates spontaneous adsorption of AB41 onto PNM1.3

in the temperature range studied and the adsorption process is entropy-driven [74]. On the other hand, the value of the standard enthalpy change ( $\Delta H^\circ$ ) is positive, indicating that the sorption is endothermic. The positive value of standard entropy change ( $\Delta S^\circ$ ) (135.26 J/mol K) suggests the increased randomness and degree of freedom at the solid-solution interface during the adsorption of AB41 onto PNM1.3.[137, 139-141]

## 4.2 ANALYSIS OF DYNAMIC SORPTION

### 4.2.1 General comparison on dynamic sorption efficiency

Different areal densities of polyamide 6 membranes and different materials of membrane with similar areal density were compared as follows.

#### 4.2.1.1 Comparison of different areal densities

##### i Hormone 17- $\beta$ Estradiol dynamic sorption on PNM1.3 and PNM2.9

Dynamic sorption of Estradiol on PNM1.3 and PNM2.9 were performed on vacuum sorption apparatus. The detected results from High Performance Liquid Chromatography (HPLC) are shown below:

**Table 4-5** 17- $\beta$  Estradiol dynamic sorption result by PNM with different areal densities.

Sample no.	BET surface area	ED exhaustion	ED sorption capacity	
	m <sup>2</sup> /g	%	mg/g	mmol/g
PNM1.3	32.00	34	7.53	0.028
PNM2.9	12.13	29	2.87	0.011

As for the BET surface area, PNM1.3 has 2.64 times more than PNM2.9. In addition, as for the hormone sorption capacity, PNM1.3 shows 2.55 times better than PNM2.9. This result indicates an effective Estradiol removing by means of filtration by polyamide 6 nanofibrous membranes and the removal amount is affected by their surface area.

##### ii Dye AB41 removal by polyamide 6 fiber assemblies with different areal densities

Mainly three groups of polyamide 6 fiber assemble were tested and compared in this experiment: nanofibrous membrane (PNM) with areal density 0.5, 1.3, and 2.9 g/m<sup>2</sup>, Spun Bond nonwoven mats (SB) with areal density 20, 40, 50, 70, and 100 g/m<sup>2</sup>, and woven fabric (W) with areal density 175 g/m<sup>2</sup>.

The morphology of filters after dynamic sorption process is shown in Fig. 4. Small colored particles aggregated together are seen on PNMs and SBs showed uniform colored surfaces. As the areal density of SB filters increased, the image shows smaller pores between fibers.

Fig. 4-14 shows the comparison of dye removal properties among fiber mats with different areal density.

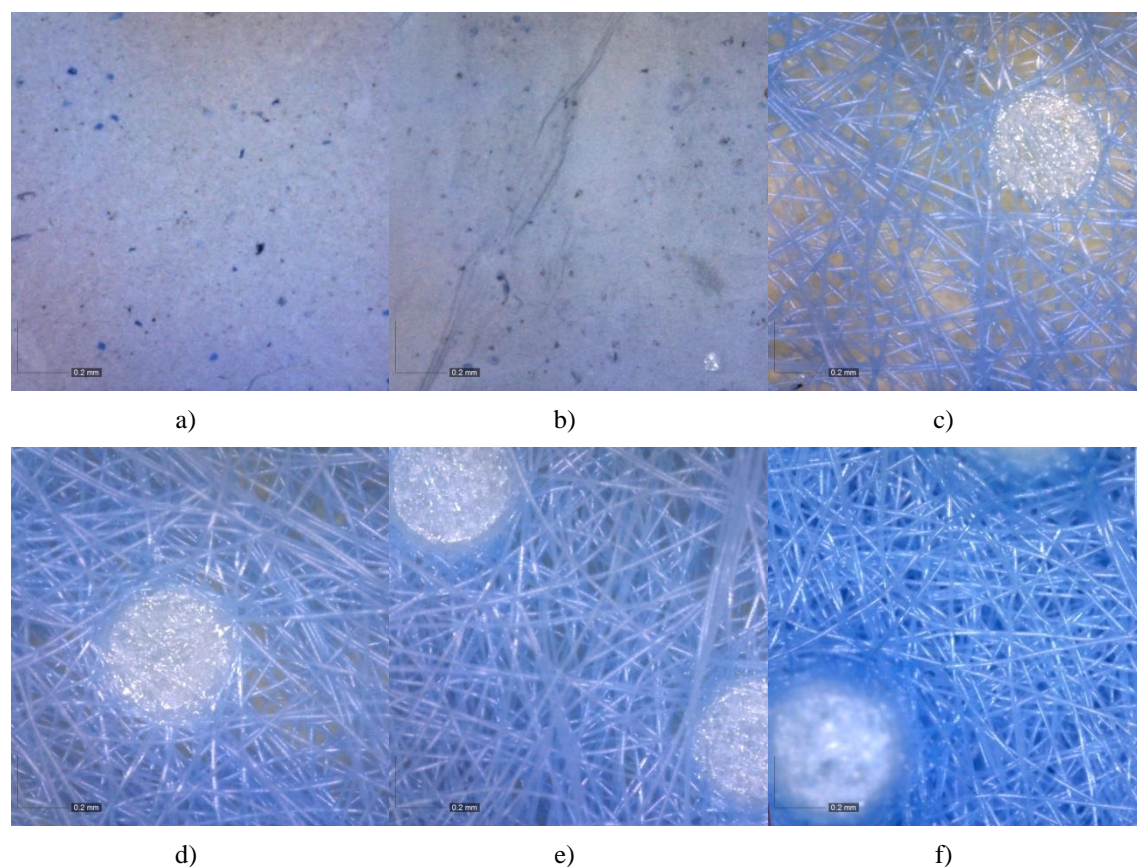
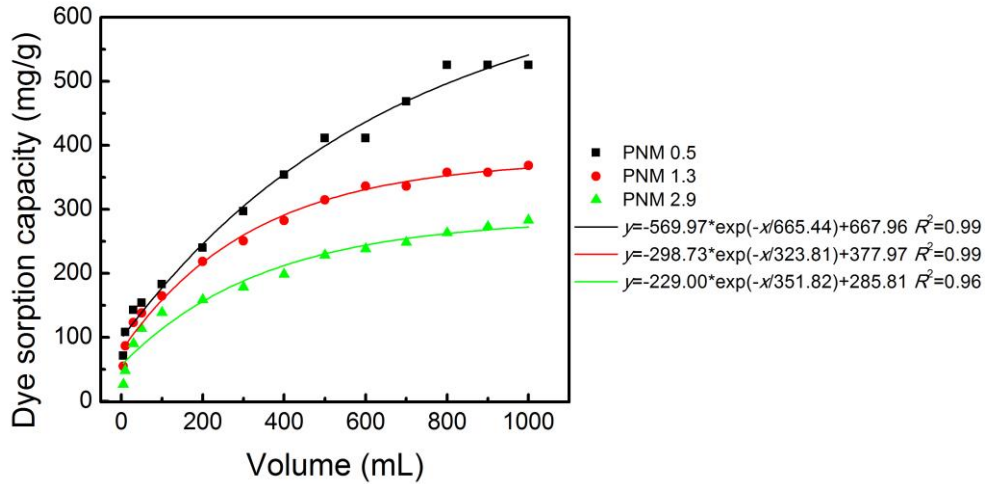


**Fig. 4-14** Morphology of fiber mats after 1 L dye solution sorption: a) PNM1.3; b) PNM2.9; c) SB20; d) SB40; e) SB50; f) SB100.

As shown in Fig. 4-15 a) & d), the dye sorption capacity of fibers is decreasing while the areal density is increasing and the fiber diameter is to some extent increasing which is mostly due to the larger specific surface area of smaller diameter fibrous mat. The slope of the curves shown in Fig. 4-15 d) which indicates the dye removal efficiency decreased while the areal density increasing. That means in Nano scale, the smaller the fiber diameter of the fibrous membrane is, the better sorption properties it performs.

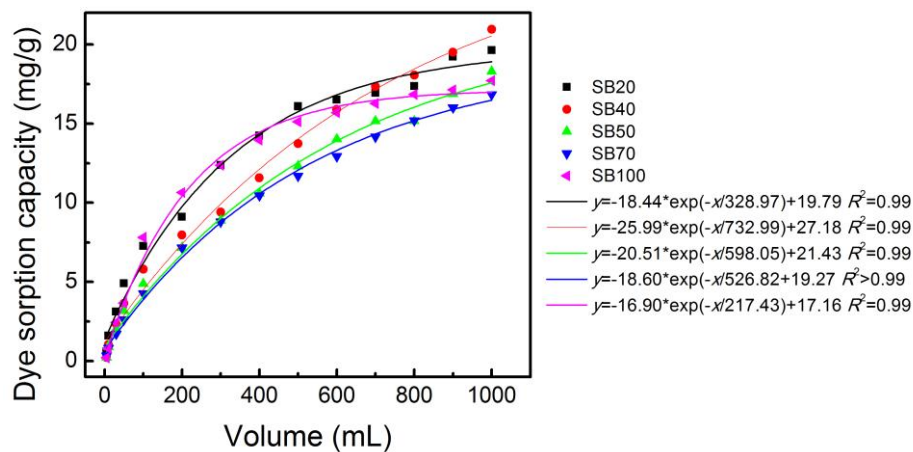
Similar trend of dye sorption capacity is shown in Fig. 4-15 b) as the areal densities of

the conventional nonwoven fabrics differing. Only SB20 and SB100 show bigger slope of the curves within the first 500 mL sorption. It is due to the smaller fiber diameter for SB20 and smaller pore size caused by bigger thickness for SB100.



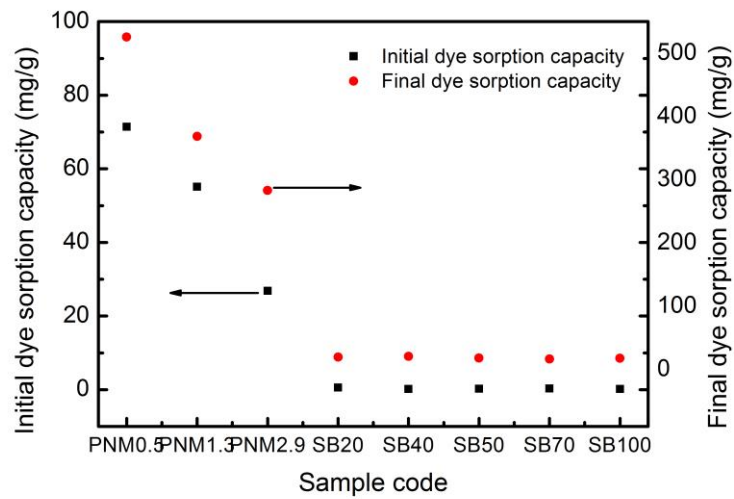
Sample	Reduced Chi-Square	Residual Sum of Squares	Degree of Freedom
PNM0.5	325.96	3585.51	11
PNM1.3	155.79	1713.70	11
PNM2.9	309.33	3402.67	11

a)

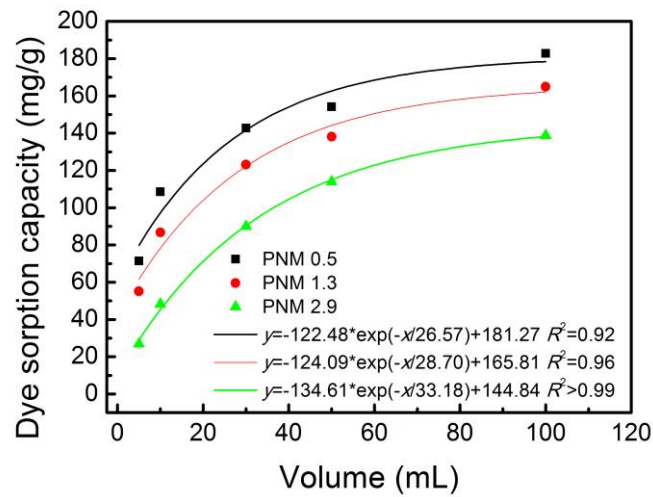


Sample	Reduced Chi-Square	Residual Sum of Squares	Degree of Freedom
SB20	0.54	5.89	11
SB40	0.47	5.18	11
SB50	0.33	3.59	11
SB70	0.13	1.39	11
SB100	0.32	3.52	11

b)



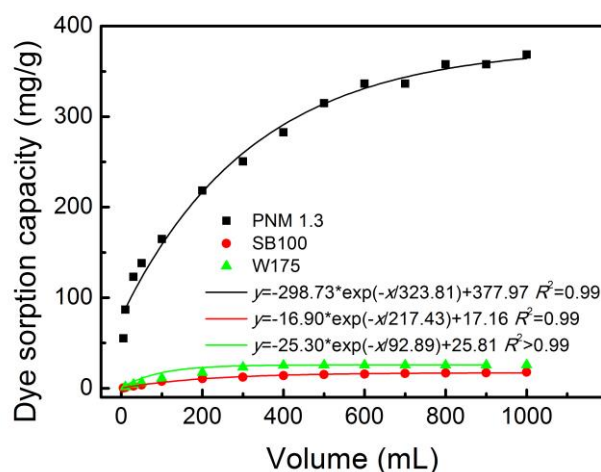
c)



d)

Sample	Reduced Chi-Square	Residual Sum of Squares	Degree of Freedom
PNM0.5	144.68	289.36	2
PNM1.3	79.07	158.15	2
PNM2.9	7.71	15.41	2

**Fig. 4-15** Dye sorption capacity of PNM and SB fiber mats: (a) PNM with areal density 0.5, 1.3, and 2.9 g/m<sup>2</sup>, (b) SB with areal density 20, 40, 50, 70, and 100 g/m<sup>2</sup>; (c) Comparison of dye sorption capacity at 5 mL and 1 L sorption among all fiber mats; (d) The curve between dye sorption capacity and volume of PNMs at the initial stage.



Sample	Reduced Chi-Square	Residual Sum of Squares	Degree of Freedom
PNM1.3	155.79	1713.70	11
SB100	0.32	3.52	11
W175	0.39	3.86	10

**Fig. 4-16** Dye sorption capacity of mats with different areal densities.

When comparing PNM and conventional SB nonwoven together as shown in Fig. 4-15 c), both initial and final dye sorption capacity show a significant difference which indicates a huge potential dye removing application of nano scale fibers other than conventional scale textile nonwovens.

The general comparison with these three groups was shown in above figure, and the large difference between nano scale fibers and conventional scale fibers can be easily observed.

#### 4.2.1.2 Comparison of different materials

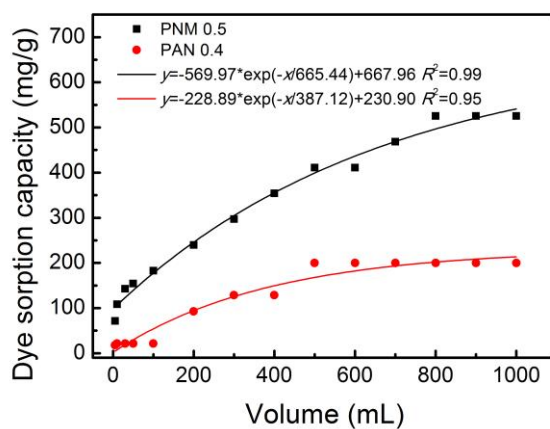
Result comparison between polyamide 6 and polyacrylonitrile with similar areal density was shown in Fig. 4-17.

Nearly triple times of dye sorption capacity of PNM0.5 than PAN0.4 was shown in the above figure which indicated a better dynamic sorption capacity and efficiency of polyamide 6 than Polyacrylonitrile for acid dye AB41.

Polyurethane (PU) and Polyvinylidene difluoride (PVDF) have been tested as well, and even though under the vacuum pressure, the membranes were not able to be wetted. The experiment was realized with an opposite way of vacuum to check if air



can penetrate, and the result shows even air cannot go through the PU or PVDF nanofibrous membranes.



Sample	Reduced Chi-Square	Residual Sum of Squares	Degree of Freedom
PNM0.5	325.96	3585.51	11
PAN0.4	325.58	3581.35	11

**Fig. 4-17** Dye sorption capacity of polyamide 6 and polyacrylonitrile.

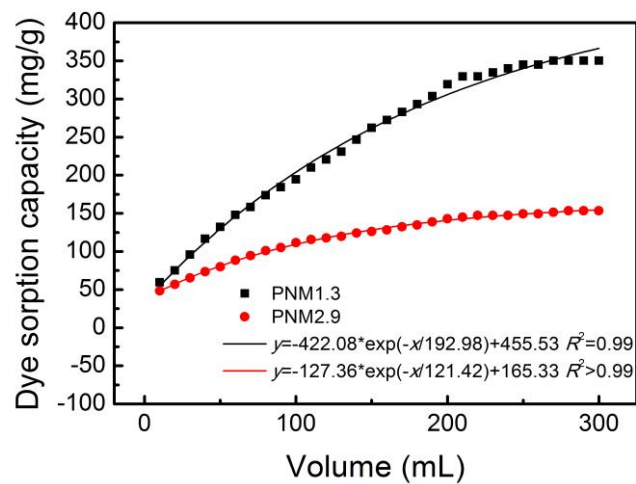
#### 4.2.2 Factors influencing dye sorption capacity and fouling of PNM

Assembled constant influent and on-line testing constant flow apparatus were applied to study the dynamic sorption property of the polyamide 6 nanofibrous membrane.

##### 4.2.2.1 Areal density of membrane

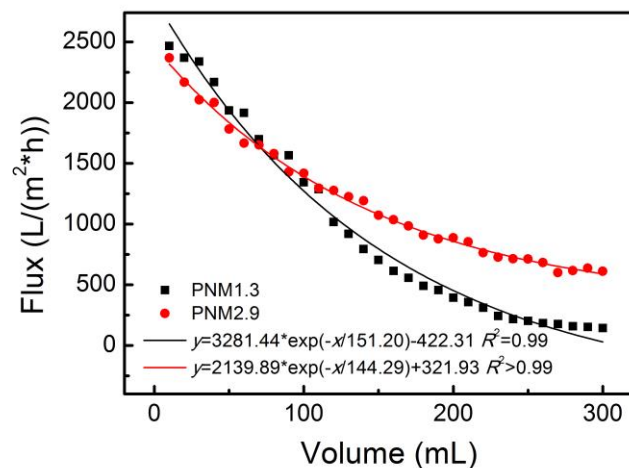
The concentration of every 10 mL effluent was detected, and the flux change was recorded.

Fig. 4-18 shows the effect of specific surface area on the dynamic sorption property and the fouling phenomenon. With the 0.03 g/L concentration, the dynamic sorption was performed on two membranes with different specific surface area. The accumulated mass of dye absorbed by membranes according to the effluent volume has been plotted as shown in the Fig. 4-18 a) which shows a dramatic difference between two processes. Both dye sorption capacity was increasing along with the dynamic sorption process, and got the equilibrium after around 200 mL simulated wastewater adsorbed. 319 and 143 mg/g are the maximum amount of dye removed by PNM1.3 and PNM2.9. The flux reduced and the values of flux for PNM1.3 was similar as PNM2.9 then reduced more after 100 mL dye solution adsorbed (as shown in Fig. 4-18 b).



Sample	Reduced Chi-Square	Residual Sum of Squares	Degree of Freedom
PNM1.3	57.54	1553.67	27
PNM2.9	2.15	58.00	27

a)



Sample	Reduced Chi-Square	Residual Sum of Squares	Degree of Freedom
PNM1.3	7860.96	212245.99	27
PNM2.9	1206.27	32569.38	27

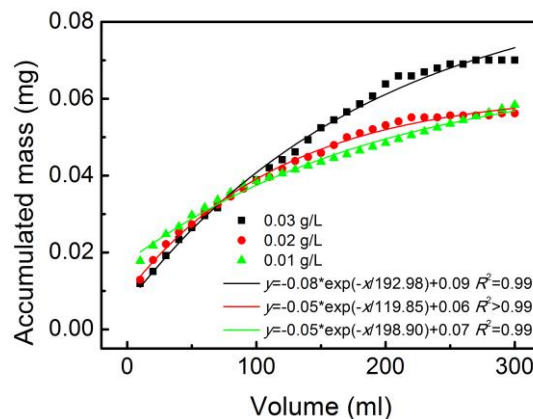
b)

**Fig. 4-18** Accumulated mass per mass of fibrous membrane and flux changing during the dynamic sorption process with dye solution concentration 0.03 g/L: a) adsorption capacity of membranes versus volume; b) flux versus volume.

Higher specific surface area creates more surface area of fibers for adsorbing dyestuff, which caused much higher adsorbed mass of dye. Due to the quick increasing of the dye sorption, the flux reduced more at the beginning of the process.

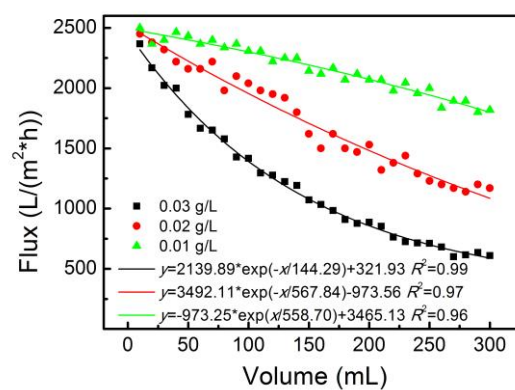
## 4.2.2.2 Influent concentration

According to the result showed in Fig. 4-19, the accumulated masses removed by the membrane were around 0.06 mg after 300 mL dye solution sorption with lower concentration and nearly 0.08 mg with 0.03 g/L concentration. 94% reduction of flux with dye solution concentration 0.03 g/L was detected while 47% and 14% reduction were found with 0.02 and 0.01 g/L concentration.



Sample	Reduced Chi-Square	Residual Sum of Squares	Degree of Freedom
0.03 g/L	2.30E-6	6.21E-5	27
0.02 g/L	8.00E-7	2.16E-5	27
0.01 g/L	1.02E-6	2.76E-5	27

a)



Sample	Reduced Chi-Square	Residual Sum of Squares	Degree of Freedom
0.03 g/L	1206.27	32569.38	27
0.02 g/L	5804.91	156732.67	27
0.01 g/L	1710.64	46187.31	27

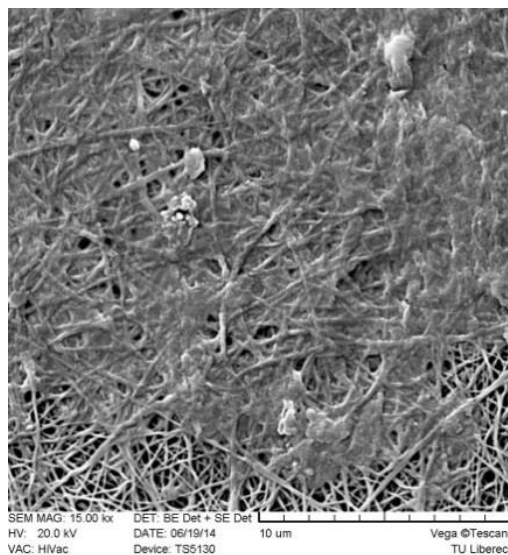
b)

**Fig. 4-19** Accumulated mass and flux changing during the dynamic sorption process by membrane with PNM1.3: a) accumulated mass versus volume; b) flux versus volume.

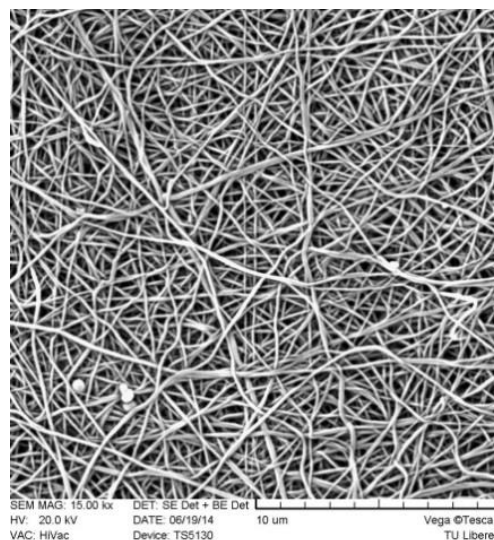
The accumulated mass adsorbed by the fibrous membrane increased slightly with the concentration increasing while a dramatic flux reduction showed especially for the highest concentration of the simulated wastewater.

#### 4.2.2.3 Sorbent quantity

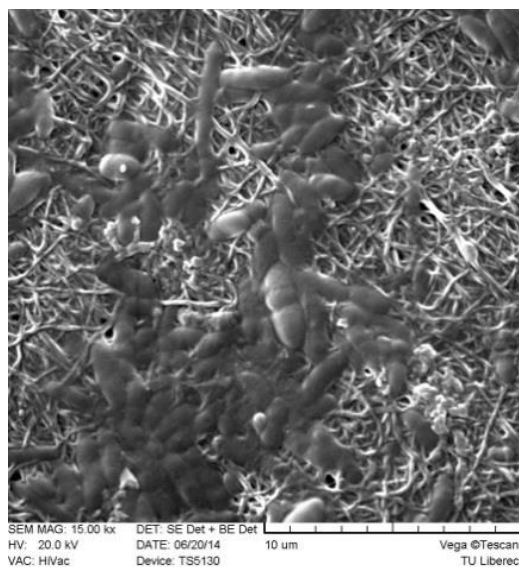
The capacity of one layer and two layers PNM1.3 under three different feeding concentrations of acid dye solution AB41 was evaluated.



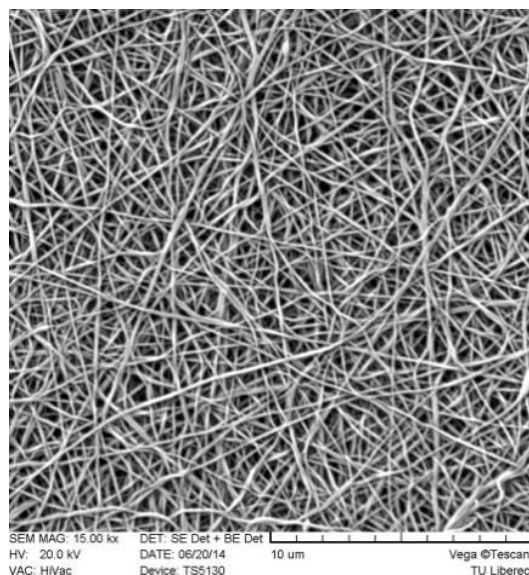
a)



b)



c)



d)

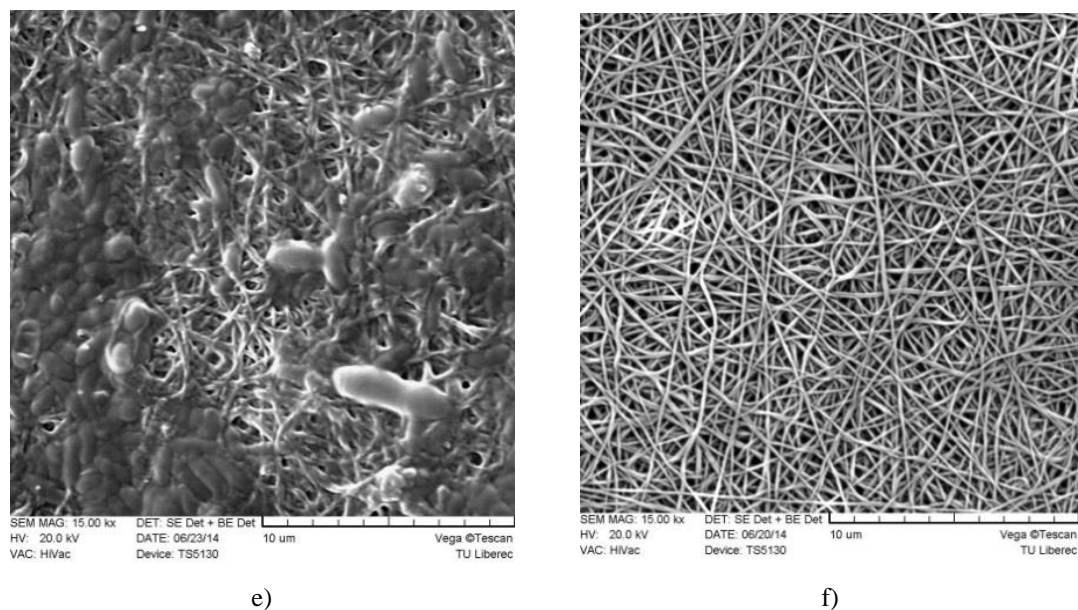
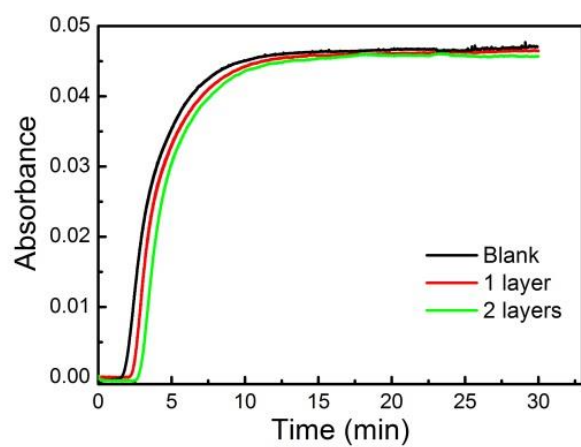


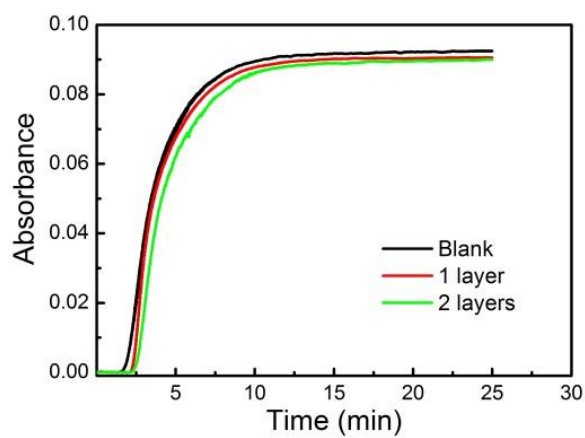
**Fig. 4-20** SEM images of PNM1.3 after dynamic sorption process: a, c, & e) first layer membrane after dynamic sorption process with concentration of 0.01, 0.02, and 0.03 g/L respectively; b, d, & f) second layer membrane after dynamic sorption process with concentration of 0.01, 0.02, and 0.03 g/L respectively.

Some continuous films formed on the surface of the first layer PNM1.3 showed in Fig. 4-20 a, c, & e) as the first layer membrane adsorbed the dyestuff and meanwhile blocked larger particles from the dyestuff and bacteria. The coverage of the films increased as the increase of concentration of dye solution, which indicated a larger amount of dyestuff blocked by PNM1.3 under the higher concentration acid dye solution. The second layer PNM1.3 still showed clean surfaces after dynamic sorption (Fig. 4-20 b, d, & f), which indicated that PNM1.3 had a very good effectiveness on blocking larger dyestuff particles.

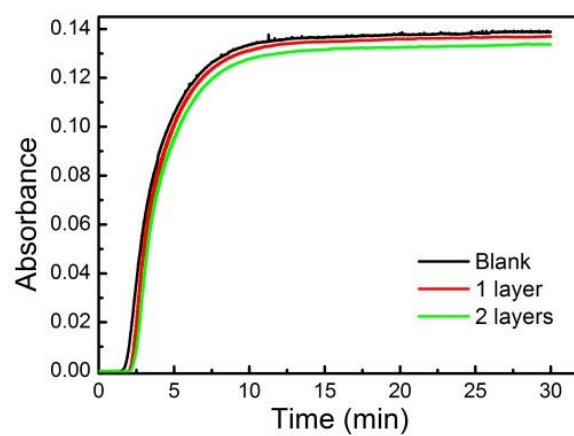
In order to investigate the dye dynamic sorption efficiency of PNM, the absorbance of effluents with and without PNM1.3 sorption was recorded. The absorbance curves of effluents regarding to time are given in Fig. 4-21.



a)



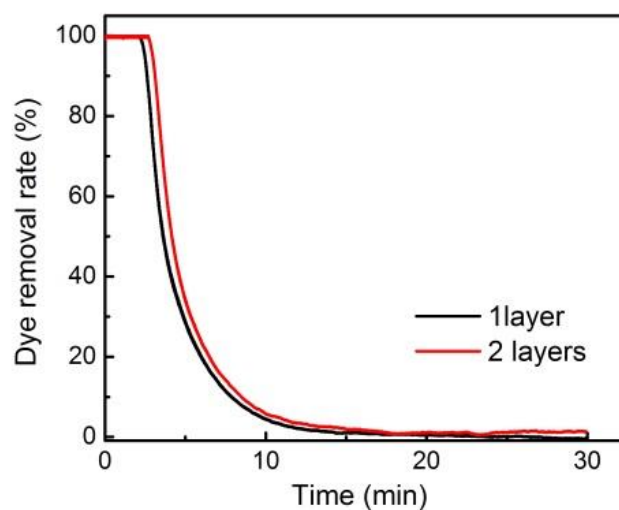
b)



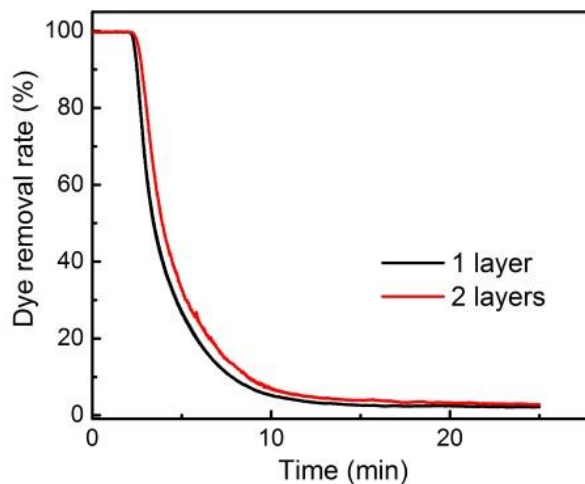
c)

**Fig. 4-21** Absorbance curves of effluents regarding to time with different feeding dye solution concentrations: a) 0.01 g/L; b) 0.02 g/L; c) 0.03 g/L.

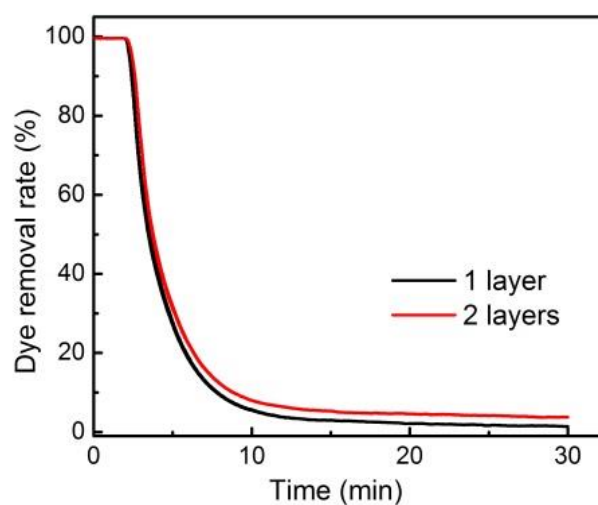
The absorbance curve can generally be divided into three zones. The first zone is from the very beginning to about 2 min, where the absorbance of solutions was very small which indicated the PNM1.3 adsorbed and blocked most of the dyestuff. In other words, the PNM1.3 had the highest dye removal rate. The second zone is from 2 minutes to about 10 min, where the absorbance of effluents was keeping increasing, which indicated the adsorption/blocking capacity of PNM was decreasing continuously. After around 10 min, the absorbance curves came to the third zone where the absorbance was almost the same and close to the absorbance of feed solution concentration, which indicated the adsorption amount of PNM came to the saturation.



a)



b)



c)

**Fig. 4-22** Dye removal rate by PNM1.3 regarding to time with different feeding dye concentrations: a) 0.01 g/L; b) 0.02 g/L; c) 0.03 g/L.

Besides, the trend of absorbance curves of two layers PNM1.3 had a delay comparing with one layer, which indicated that the second layer PNM1.3 also played a role in absorbing dyestuff.

In order to compare the maximum dye removal capacity by PNM1.3, the accumulated mass of dye adsorbed/blocked should be in saturation state. As Fig. 4-21 showed, the absorbance of dye solutions are almost the same with feeding dye solution after 10 minutes. Therefore, the saturated value was chosen at 13 minutes. The dye removal capacity of PNM under difference feed dye solution concentrations are given in Table 4-6.

**Table 4-6** Dye removal values comparison while the dynamic sorption process reaches 13 minutes.

Solution concentration g/L	Dye removal capacity (mg/g)	
	1 layer	2 layers
0.01	53.9±4.3	80.5±6.2
0.02	84.9±3.7	127.9±6.7
0.03	81.7±3.4	132.4±9.0

The dye removal capacity of PNM1.3 had an increase when the feeding dye solution concentration increased, but the difference of dye removal capacity of PNM1.3 was very small when the feeding dye solution concentrations were 0.02 and 0.03 g/L.

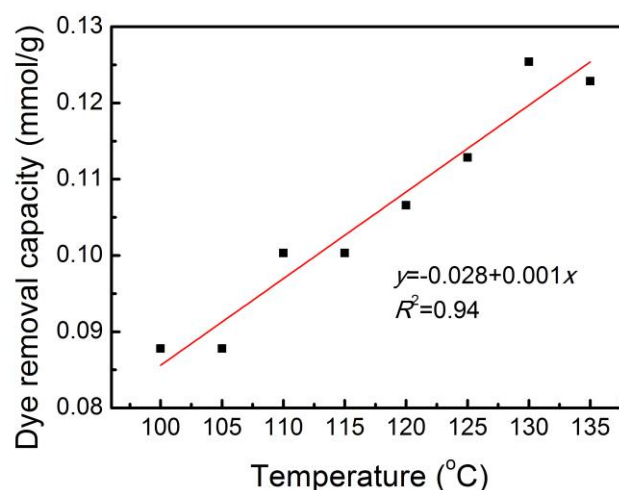


Moreover, two layers PNM1.3 had better dye removal capacity than one layer. This could be due to the adsorption capacity of PNM on acid dye.

### 4.3 SURFACE MODIFICATION ON POLYAMIDE 6 NANOFIBROUS MEMBRANE

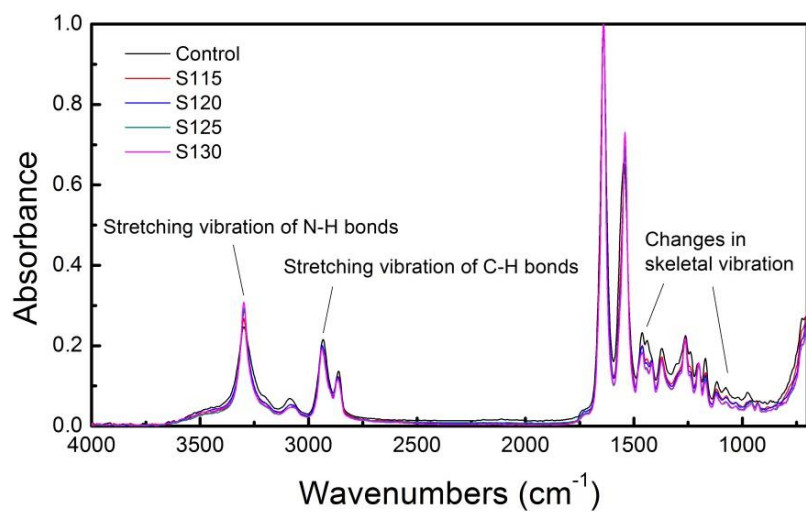
#### 4.3.1 Steam treatment

Fig. 4-23 showed dye removal capacity with different steam treating temperature on PNM1.3. The data can be fitted in one line, which indicates a linear increasing of dye removal capacity with increasing of steam temperature in this temperature range from 100 to 135 °C. The control sample was tested in the same method and the dye removal capacity of it was 0.11 mmol/g, which indicated a dye removal improving only when high temperature (higher than 120 °C) steam was applied onto PNM.

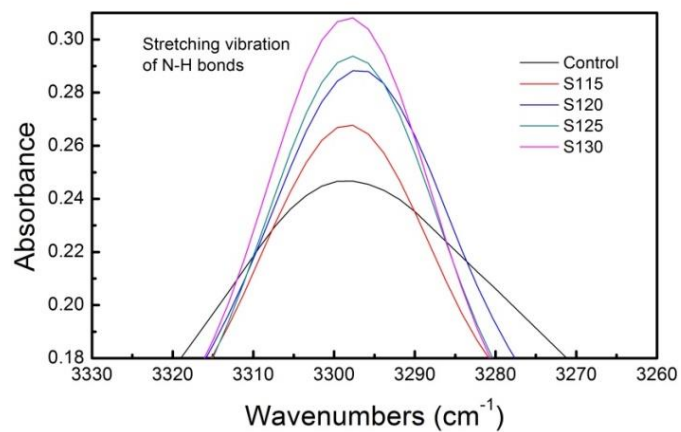


**Fig. 4-23** Dye removal capacity changes according to steaming temperature.

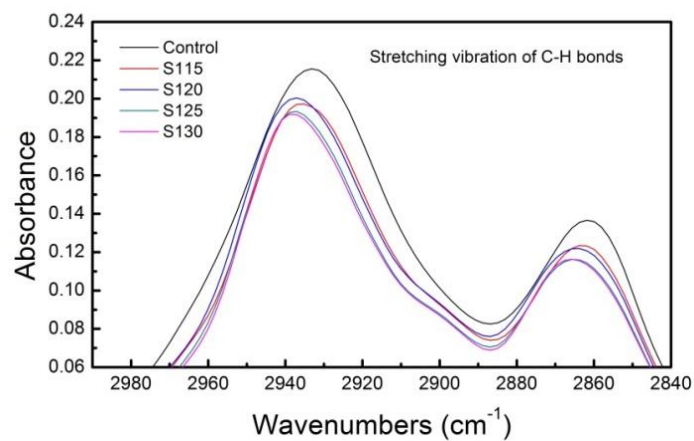
The FTIR has been tested and shown in Fig. 4-24. It was shown in Fig. 4-24 b) and c) that as the steam temperature increased, the absorbance peak which indicates stretching vibration of N-H bonds moved higher, and the absorbance peak which stands for stretching vibration of C-H bonds moved lower. It could mean shortening of the hydrocarbon chains with the phenomenon of increasing the intensity of stretching vibration of N-H bonds in comparison with decreasing the intensity of stretching vibration of C-H bonds. It was also found the decreasing changes in skeletal vibrations, which cannot be clearly assigned to specific bonds.



a)



b)



c)

**Fig. 4-24** FTIR spectra

The steam treatment has shifted the visible spectrum of PNM to lower absorbance evenly over the entire measuring range. Such displacement occurring indicates a change in surface morphology such as formation of cavities and overall surface roughening.

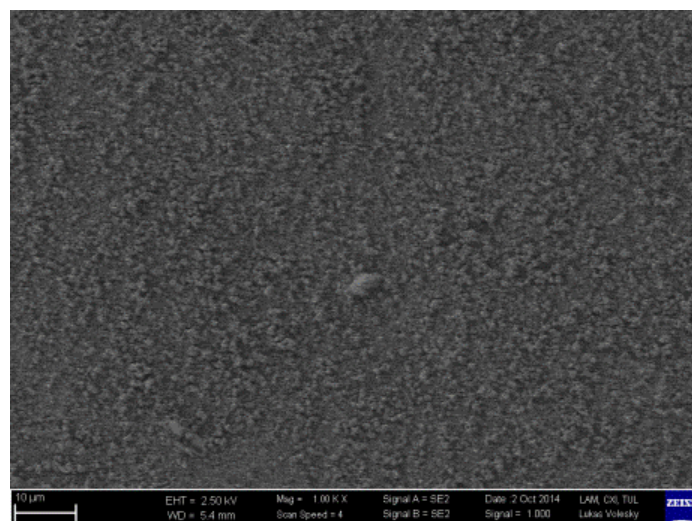
For conventional polyamide 6 fibers, the dye uptake and the diffusion coefficient are generally increased by the steam setting. This tendency increases with the temperature of the steam setting. Tsuruta [142] believed that the change of dyeability on steam setting is not attributable to a decrease in the orientation of crystallites but is caused by loosening of the molecular packing in the amorphous region as a result of inclusion of water.

#### 4.3.2 Nanophotocatalysis to implement self-cleaning of PNM

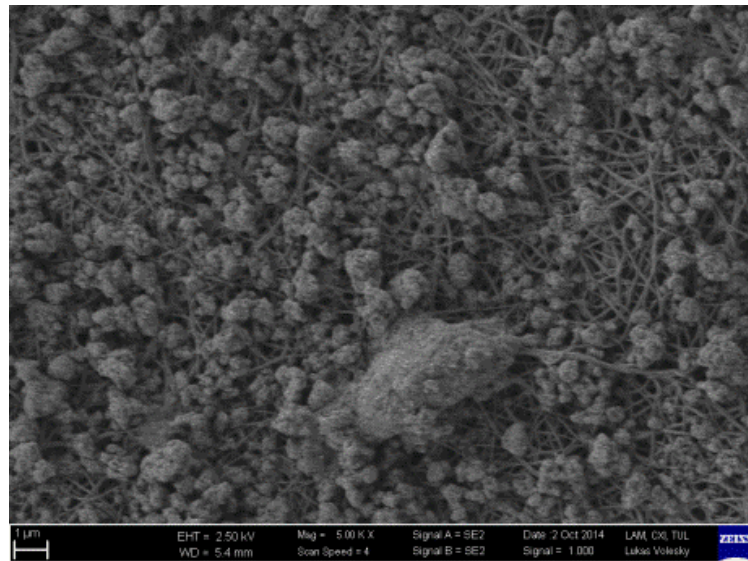
TiO<sub>2</sub> nanoparticles were evenly deposited as shown in Fig. 4-25. Besides, the TiO<sub>2</sub> nanoparticles were trapped into or attached onto PNM due to the size of pores and TiO<sub>2</sub> nanoparticles. The absorbance of TiO<sub>2</sub> solution with concentration of 10 mg/L before and after filtration was 1.211 and 0.001. According to Eq. (4-2), more than 99.9% TiO<sub>2</sub> nanoparticles were deposited onto PNM.

$$\text{Particle removal rate (\%)} = \left( 1 - \frac{A_{\text{after}}}{A_{\text{before}}} \right) * 100\% \quad (4-2)$$

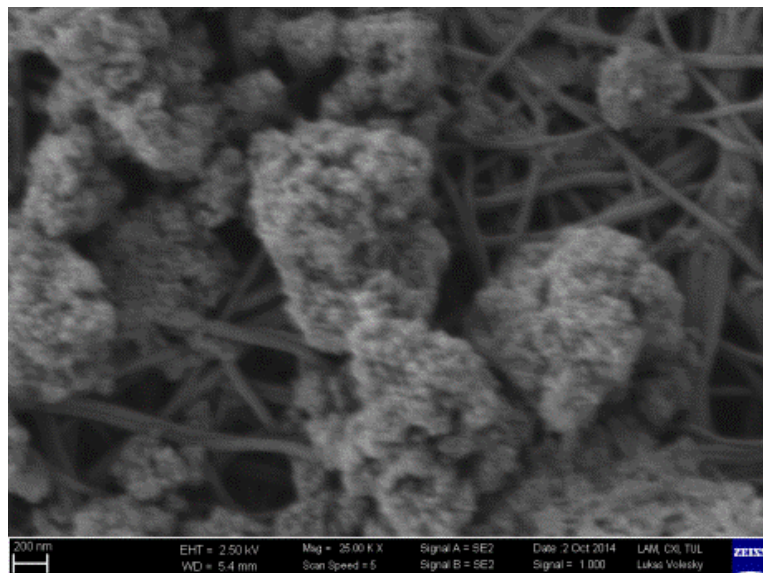
The TiO<sub>2</sub> concentration of PNM was 0, 9, 18, 44, and 88 mg/m<sup>2</sup> accordingly.



a)



b)
















































c)

**Fig. 4-25** Surface morphology of PNM coated by  $\text{TiO}_2$  nanoparticles ( $1000\times$ ,  $10000\times$ ,  $25000\times$ ).














































Table 4-7 & Table 4-8 show the scanning images of all samples before and after UV treatment with different treating time.

It was obvious that after UV light treating, dye AO7 stains on the samples fade as the  $\text{TiO}_2$  concentration on PNM and the treating time increased.

**Table 4-7** Scanning images of UV treated samples with different treating time-AA group.

no.	UV treating time (min)								
	0	30	60	90	120	180	240	300	400
AA1									
AA2									
AA3									
AA4									
AA5									

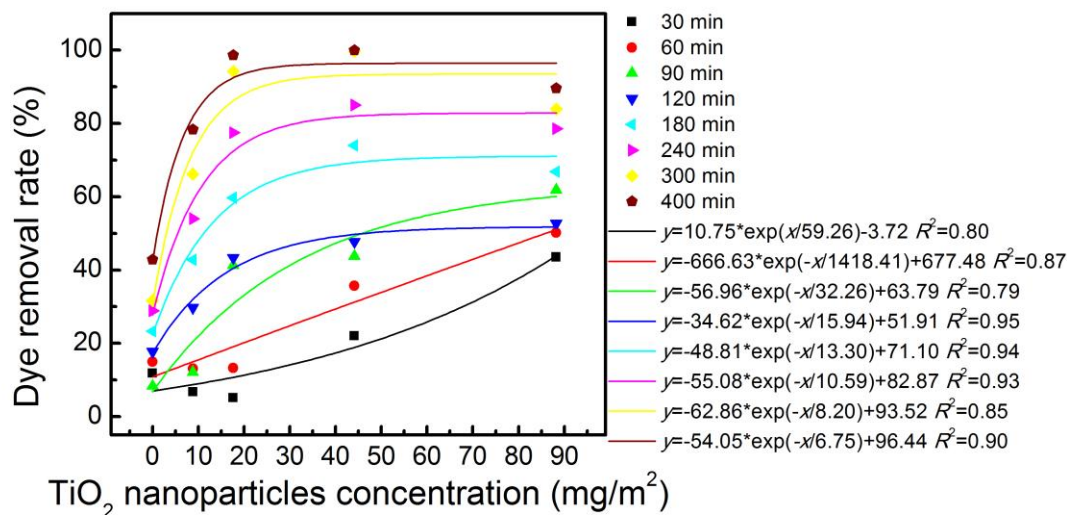
**Table 4-8** Scanning images of UV treated samples with different treating time-BB group.

no.	UV treating time (min)								
	0	30	60	90	120	180	240	300	400
BB1									
BB2									
BB3									
BB4									
BB5									

#### 4.3.2.1 Effect of TiO<sub>2</sub> concentration on PNM

Comparing with the control sample, the samples with TiO<sub>2</sub> deposition showed a much better self-cleaning properties as the intensity value increased rapidly from around 170 to around 220 with the increasing of UV treating time. For the sample with TiO<sub>2</sub> concentration 44 mg/m<sup>2</sup>, the intensity of light showed a 100% similar

value between the stain area (intensity value equals to 225.0) and background (intensity value equals to 225.0) after 400 minutes UV treatment. This indicated a 100% dye removal rate with TiO<sub>2</sub> nanoparticles deposition method.



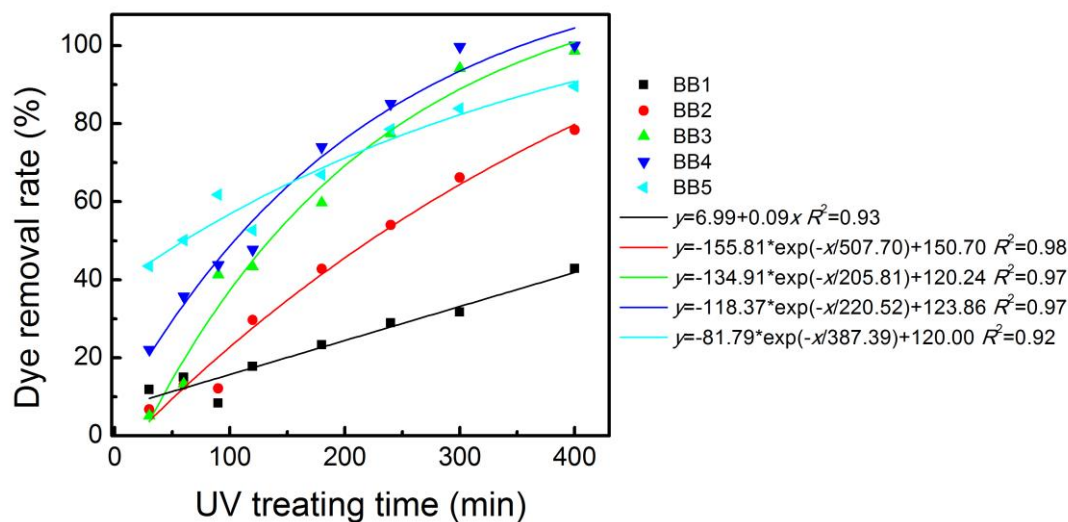
Sample	Reduced Chi-Square	Residual Sum of Squares	Degree of Freedom
30 min	34.58	69.16	2
60 min	37.38	74.77	2
90 min	106.77	213.54	2
120 min	9.29	18.58	2
180 min	26.44	52.88	2
240 min	38.97	77.95	2
300 min	116.54	233.07	2
400 min	55.00	109.99	2

**Fig. 4-26** Dye removal rate change according to TiO<sub>2</sub> nanoparticles concentration under different UV light treating time.

As shown in above figure, while long enough UV light providing (equal to or above 120 min), dye removal rate increased with the increasing of TiO<sub>2</sub> nanoparticles concentration. And the samples with TiO<sub>2</sub> nanoparticles concentration above 18 mg/m<sup>2</sup> was obtaining similar amount of dye removal rate which means higher concentration has no contribution to the dye removal rate and 18 mg/m<sup>2</sup> was a quite sufficient TiO<sub>2</sub> nanoparticles concentration for PNM surface self-cleaning modification by photocatalysis.

## 4.3.2.2 Effect of the UV treating time

Fig. 4-27 showed the dye removal rate with different TiO<sub>2</sub> nanoparticles concentrations at different UV treating time.



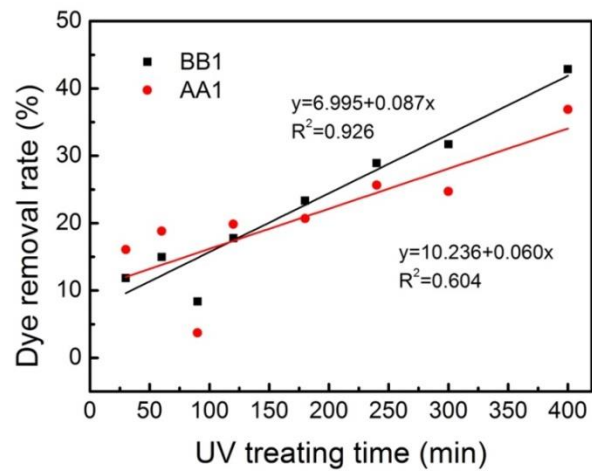
Sample	Reduced Chi-Square	Residual Sum of Squares	Degree of Freedom
BB1	--	59.17	6
BB2	17.11	59.17	5
BB3	32.38	85.56	5
BB4	26.00	161.89	5
BB5	22.47	130.00	5

**Fig. 4-27** Stain removal efficiency shown as dye removal rate at different point of UV light treating time.

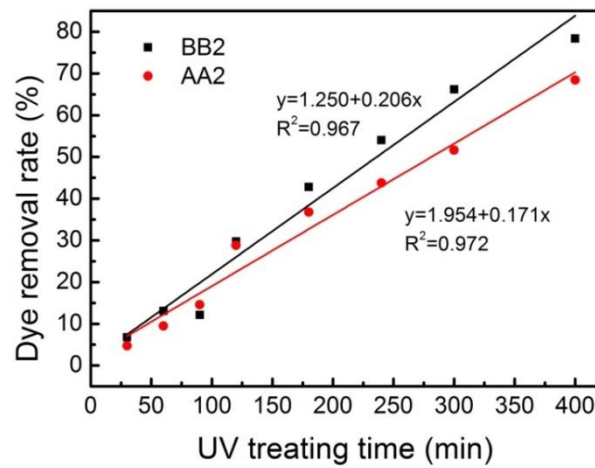
It shows linear trend between dye removal rate and UV light treating time. In Fig. 4-27, As the UV light treating time prolonging, the dye removal rate increases linearly for the low TiO<sub>2</sub> nanoparticles concentration at around 9 mg/m<sup>2</sup>. For higher TiO<sub>2</sub> nanoparticles concentrations, after 240 minutes UV light treatment, the dye removal rate can reach up to 100%, which was the maximum it can be. And the plot was no longer that much linear as the samples with lower TiO<sub>2</sub> nanoparticles concentration which shows in Fig. 4-28 that the linear fitting correlation coefficient  $R^2$  even drop below 0.9.

For sample BB1 and AA1, after long time UV light treatment, the dye removal rate increased from 10% to 40% without the present of TiO<sub>2</sub> nanoparticles, and at 90 minutes UV light treating, the dye removal rate showed a drop to lower than 10% ,

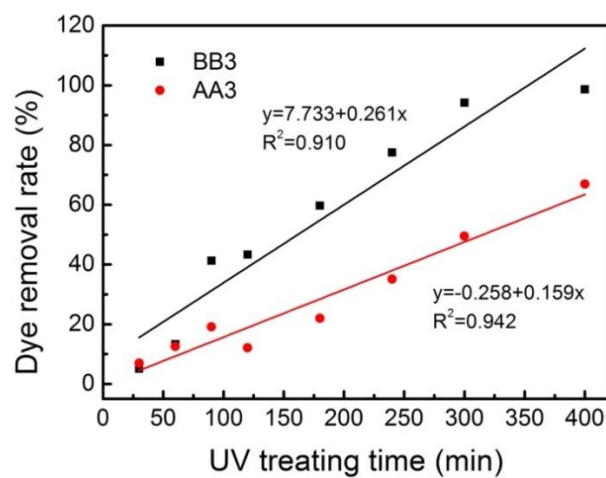
which was shown in Fig. 4-28 a).



a)

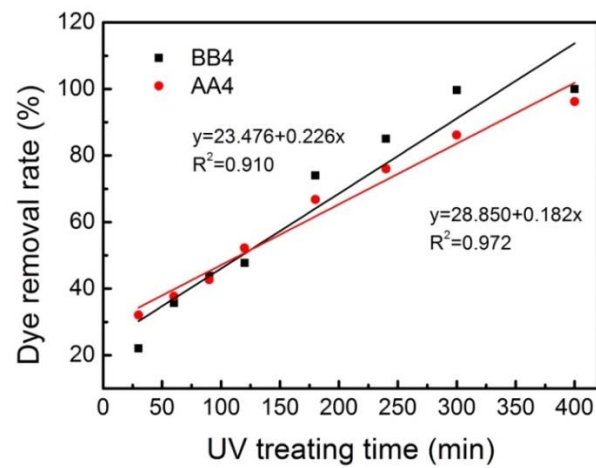


b)

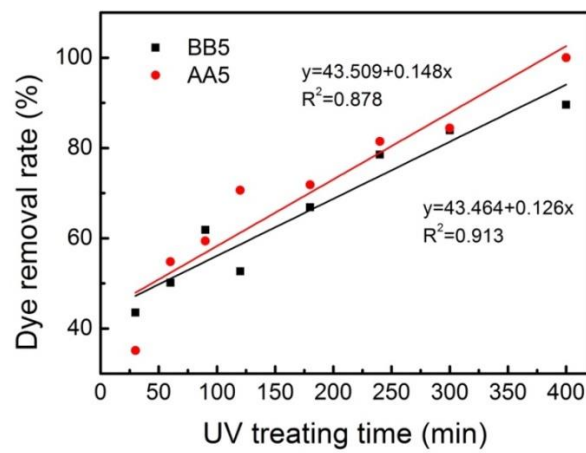


c)

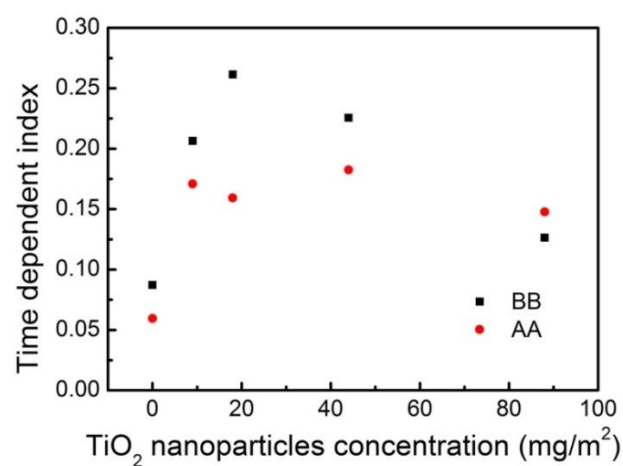




d)



e)



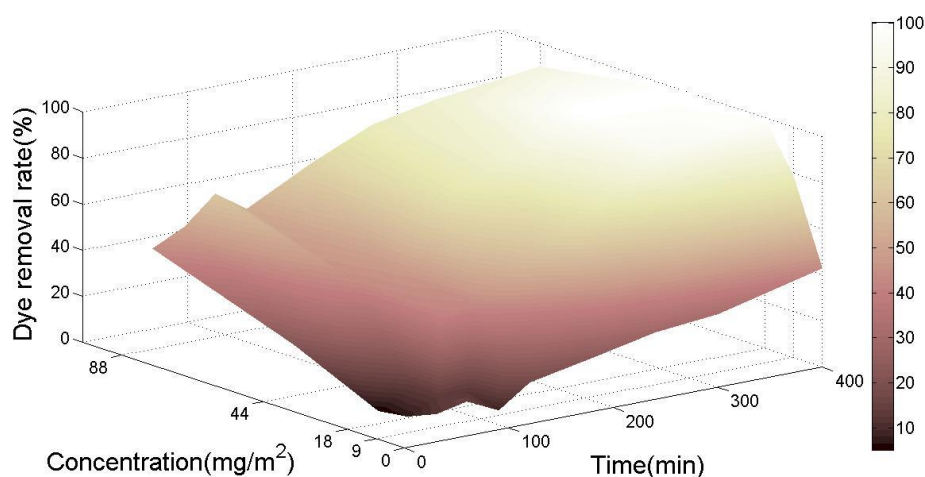
f)

**Fig. 4-28** Linear regressions for samples with different concentrations of  $\text{TiO}_2$  nanoparticles: a-e) 0, 9, 18, 44, and 88  $\text{mg/m}^2$ ; f) time dependent index result of all samples.

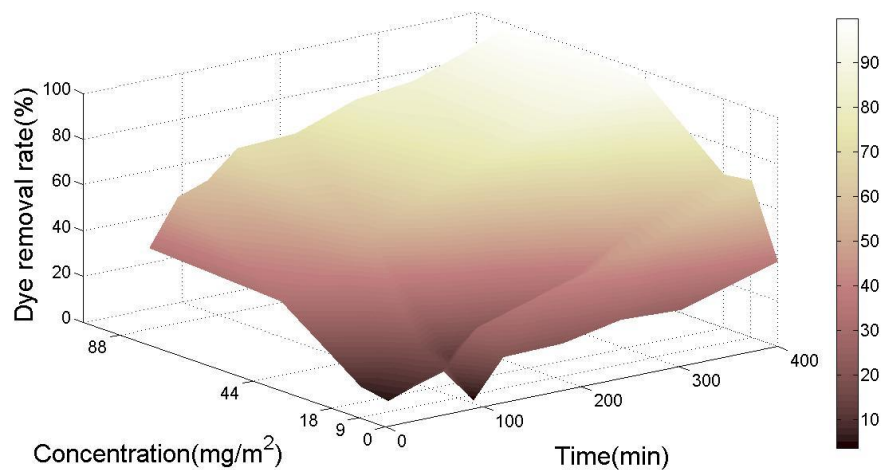
Results were clearly showing the slope difference between the samples with different concentrations of TiO<sub>2</sub> nanoparticles no matter with or without adding AA. The slope was around 0.07 for the control samples with deposition concentration 0 mg/m<sup>2</sup> and around 0.13 for the samples with deposition concentration 88 mg/m<sup>2</sup>. The slope actually shows the dependence of the changing of light intensity on the UV light treating time, which has been plotted in Fig. 4-28 f). As the TiO<sub>2</sub> nanoparticles concentration increasing to 18 mg/m<sup>2</sup>, the time dependent index (slope of the dye removal rate versus UV light treating time linear fitting) increased sharply from 0.081 to 0.261 for sample BB, which means the photocatalysis phenomenon is sensitive to the UV light treatment with comparatively low TiO<sub>2</sub> nanoparticles concentration. The time dependent index of sample BB5 dropped into 0.148 due to the high efficiency of photocatalysis with this high TiO<sub>2</sub> nanoparticles concentration that dye removal rate already reached to 60% after 90 minutes UV light treatment. Fig. 4-28 c) shown a sudden drop of dye removal rate of sample AA3 after 90 minutes UV light treatment and the slope of its linear fitting dropped as well.

#### 4.3.2.3 Role of the catalyst Ascorbic Acid

As both TiO<sub>2</sub> nanoparticles concentration and UV light treating time affect dye removal rate, 3D figures were conducted to compare the result of samples with or without Ascorbic Acid (AA).



a)



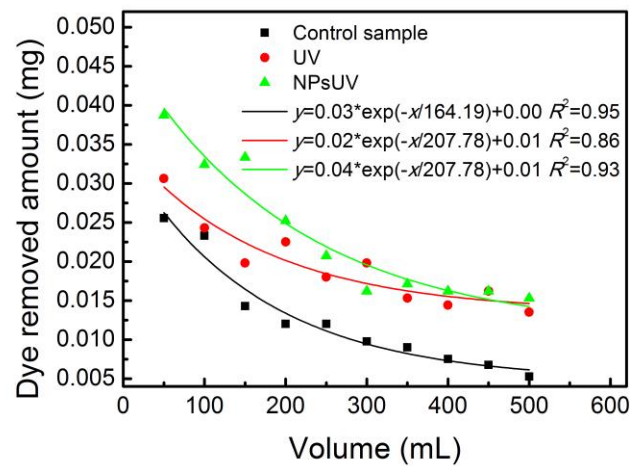
b)

**Fig. 4-29** 3D plot of dye removal rate versus  $\text{TiO}_2$  concentration and UV light treating time: a) samples deposited with different concentration of  $\text{TiO}_2$  nanoparticles; b) samples deposited with different concentration of  $\text{TiO}_2$  nanoparticles with the presence of ascorbic acid.

Fig. 4-28 a) showed the result of sample BB1 and AA1 which were without  $\text{TiO}_2$  nanoparticles deposition. It was shown that after 30 or 60 minutes UV light treatment, AA1 was having better stain cleaning effect than the control sample BB1 but lower dye removal rate when UV light treatment longer than 60 min. This indicates better oxidation with AA's presence under short time UV light treatment. However, with the deposition of  $\text{TiO}_2$  nanoparticles with all the concentrations other than  $88 \text{ mg/m}^2$ , AA showed a restrained effect on the dye removal of PNM. Fig. 4-29 showed a brighter surface on the left side of the data in b) than in a) which indicates a better performance of photocatalysis with highest  $\text{TiO}_2$  nanoparticles concentration with less time of UV light treatment. On the top area, Fig. 4-29 a) is brighter than b) which shows a better result after long time UV treating without AA's presence.

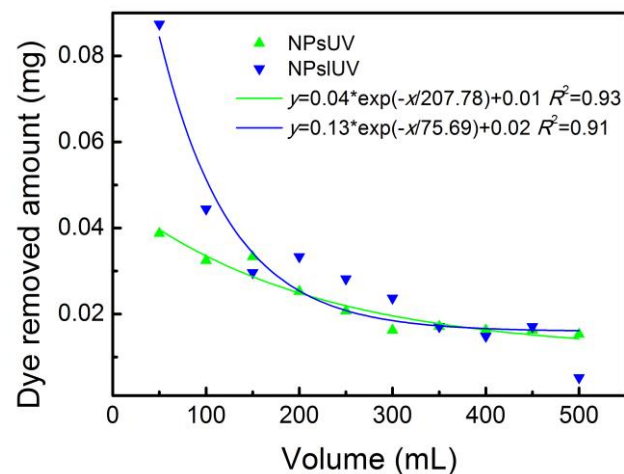
#### 4.3.3 Dynamic sorption process with nanophotocatalysis

The absorbance of influent and effluents after each 50 mL AO7 solution went through the dynamic sorption photocatalysis apparatus were detected. The dye removed amount, and dye sorption capacity were calculated and the results were shown in Fig. 4-31 and Fig. 4-31.



Sample	Reduced Chi-Square	Residual Sum of Squares	Degree of Freedom
Control sample	2.38E-6	1.67E-5	7
UV	3.83E-6	2.68E-5	7
NPsUV	5.57E-6	3.90E-5	7

a)



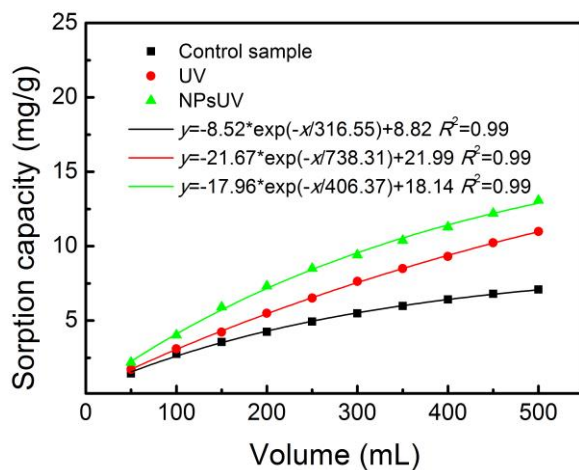
Sample	Reduced Chi-Square	Residual Sum of Squares	Degree of Freedom
NPsUV	5.57E-6	3.90E-5	7
NPsIUUV	4.93E-5	3.45E-4	7

b)

**Fig. 4-30** Dye removed amount comparison of different samples: a) comparison among control sample, UV, and NPsUV; b) samples with different UV treating time.

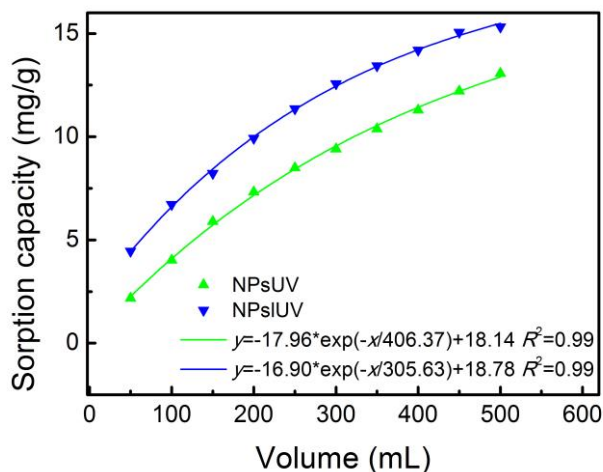
As shown in Fig. 4-31 a), the dye removed amount of three samples were compared. The figure shows that the dye removed amount decreased while more dye solution pumped through the PNM2.5, and it became stable after around 300 mL solution went

through for PNM2.5 samples with UV light treatment. It is obviously indicated that UV light treatment improved dye removed amount of AO7 on PNM2.5, and TiO<sub>2</sub> NPs photocatalysis improved the dye removed amount at the beginning of dynamic sorption process by 26.5%.



Sample	Reduced Chi-Square	Residual Sum of Squares	Degree of Freedom
Control sample	0.006	0.042	7
UV	0.003	0.022	7
NPsUV	0.025	0.176	7

a)



Sample	Reduced Chi-Square	Residual Sum of Squares	Degree of Freedom
NPsUV	0.025	0.176	7
NPsUV	0.019	0.132	7

b)

**Fig. 4-31** Sorption capacity comparison of different samples: a) comparison among control sample, UV, and NPsUV; b) samples with different UV treating time.

Fig. 4-31 b) shows that while prolonging the UV treating time, same trend was found and the initial dye removed amount improved over 125%. However, PNM2.5 was broken after around 300 mL solution processed due to too long time UV heating, which was shown in the figure as a sudden drop after the volume reached 300 mL and even worse drop appeared after the last 50 mL dye solution processed.

After calculation of accumulated dye removed amount, sorption capacity versus volume were plotted in Fig. 4-31. Fig. 4-31 a) showed that after 500 mL AO7 dye solution pumped through PNM2.5, TiO<sub>2</sub> NPs photocatalysis improved the sorption capacity of PNM2.5 from 7.09 to 13.07 mg/g. Moreover, Fig. 4-31 b) showed that comparing with the photocatalysis sample, after prolonging the UV treating time, value of dye sorption capacity reached up to 15.32 mg/g.

## CHAPTER 5. CONCLUSIONS

This thesis presented the sorption performance of polyamide 6 nanofibers assembly, and effect of surface modification of polyamide 6 nanofibers. The experimental results are:

### 1) Analysis of dye sorption onto polyamide 6 nanofibrous membrane

The factors such as temperature, solution pH value, solution concentration, dosage of sorbent, and fiber scale of sorbent were studied. Result revealed that temperature and solution concentration encouraged the exhaustion of acid dye on PNM and others have negative effect.

Dye sorption of PNM was fitted with Freundlich and Langmuir isotherms. Freundlich isotherm showed steeper increasing trend meanwhile the correlation coefficient  $R^2$  indicated a better fitting with Langmuir isotherm.

The sorption rate of three dyestuffs on PNM was analyzed with kinetic models. Experimental data was fitted with the linear forms of kinetic models under 30, 40, and 50 °C. 24 hours experiment was performed and 120 minutes was considered as the equilibrium time. The kinetic parameters showed the sorption rate of acid dyes on PNM a positive relationship with bath temperature, and Acid Yellow 36 showed best affinity with PNM. Pseudo-Second Order equation fitted experimental data better than Elovich equation with  $R^2$  over 0.99.

Thermodynamic parameters of acid dye sorption onto PNM were calculated. The Arrhenius activation energy ( $E_A$ ) was more than 40 kJ/mol which indicated a chemisorption oriented process. The negative value of the change of free energy ( $\Delta G^\circ$ ) confirmed a feasibility, spontaneous, and entropy-driven process in the temperature range 30-50 °C. The positive value of standard enthalpy change ( $\Delta H^\circ$ ) and standard entropy change ( $\Delta S^\circ$ ) revealed an endothermic sorption process and it increased the randomness and degree of freedom.

### 2) Analysis of dynamic sorption

A dynamic sorption process was carried out and the result showed that nanofibers have superior dye removal properties than conventional fibers. The hormone (17

$\beta$ -Estradiol) and dye removal capacity of nanofibers increased while the diameter decreased due to the specific surface area increasing. Among the Spun Bond nonwovens, SB20 and SB100 showed better initial dye removal efficiency due to smaller fiber diameter and smaller pore size respectively.

The factors such as areal density, influent solution concentration, and fibers quantity were considered for the dye removal rate of PNM. The dye sorption capacity of PNM showed a positive relation with fibers mat specific surface area and quantity. Meanwhile, high feeding concentration caused much severer fouling problem.

### 3) Surface modification on polyamide 6 nanofibrous membrane

The result of steam treatment showed that dye removal capacity could be improved as the temperature over 120 °C. The molecular and morphological change was observed after steam treatment.

TiO<sub>2</sub> nanoparticles deposition and UV light treatment was tested efficiently removing the dyestuff from PNM with TiO<sub>2</sub> nanoparticles concentration over 18 mg/m<sup>2</sup> and 90 minutes under UV light. Ascorbic Acid alone can help increasing the stain cleaning with short time UV light treatment, but not together with TiO<sub>2</sub> nanoparticles. TiO<sub>2</sub> nanoparticles concentration 18 mg/m<sup>2</sup> is recommended, and 80% dye removal rate would be guaranteed with over 240 minutes UV light treating.

TiO<sub>2</sub> nanoparticles photocatalysis was proved to be one method for improving the dynamic sorption capacity of Acid Orange 7 on PNM. The initial sorption amount can be improved by prolonging the UV light treating time, however, the material cannot withstand long time aging with UV light.



## REFERENCES

1. Bhowmick, A.K. and H. Stephens, *Handbook of Elastomers, Second Edition*. 2000: Taylor & Francis.
2. Martienssen, W. and H. Warlimont, *Springer Handbook of Condensed Matter and Materials Data*. 2006: Springer Berlin Heidelberg.
3. White, J.L., *Principles of Polymer Engineering Rheology*. 1990: Wiley.
4. Malaika, S.A., A. Golovoy, and C.A. Wilkie, *Chemistry and Technology of Polymer Additives*. 1999: Wiley.
5. Zhang, X. and U.o.I.a. Urbana-Champaign, *Thermodynamics of Polyamide Separation Membrane in Contact with Aqueous Solutions*. 2008: University of Illinois at Urbana-Champaign.
6. Lewin, M., *Handbook of Fiber Chemistry, Third Edition*. 2006: CRC Press.
7. Espinosa-Jimenez, M., et al., *Investigation of the Polyamide 6,6 dyeing process with Acid Blue 45 dye. Part I. Thermodynamics of Acid Blue 45 adsorption*. *Journal of Adhesion Science and Technology*, 2002. **16**(3): p. 285-301.
8. Olabisi, O. and K. Adewale, *Handbook of Thermoplastics*. 1997: Taylor & Francis.
9. Kricheldorf, H.R., *Polycondensation: History and New Results*. 2013: Springer Berlin Heidelberg.
10. Burton, G., *Chemical Storylines*. 2000: Pearson Education.
11. Burkinshaw, S.M. and A. Filarowski, *Physico-chemical Aspects of Textile Coloration*. 2016: Wiley.
12. Cook, J.G., *Handbook of Textile Fibres: Man-Made Fibres*. 1984: Elsevier Science.
13. Brydson, J.A., *Plastics Materials*. 1999: Butterworth-Heinemann.
14. Kê B., *Newer methods of polymer characterization*. 1964: Interscience Publishers.
15. Wei, W., et al., *Removal of Cd(II) from aqueous solution by Electrospun Nylon 6 Nanofibrous Nonwoven containing Attapulgate*. *Advanced Textile Materials*, Pts 1-3, 2011. **332-334**: p. 1295-1299.
16. Hota, G., B.R. Kumar, and W.J.N.S. Ramakrishna, *Fabrication and characterization of a boehmite nanoparticle impregnated electrospun fiber*

- membrane for removal of metal ions*. Journal of Materials Science, 2008. **43**(1): p. 212-217.
17. Basiri, F., et al., *Recycling of Direct Dyes Wastewater by Nylon-6 Nanofibrous Membrane*. Current Nanoscience, 2011. **7**(4): p. 633-639.
  18. De Vrieze, S., et al., *Filtration performance of electrospun polyamide nanofibres loaded with bactericides*. Textile Research Journal, 2012. **82**(1): p. 37-44.
  19. York, C.P.S.a.t.U.o. *Colorants*. 2013 18th March 2013; Available from: CIEC Promoting Science at the University of York.
  20. (IARC), W.H.O.I.A.F.R.O.C., *Some Aromatic Amines, Organic Dyes, and Related Exposures*, in *IARC Monographs on the Evaluation of Carcinogenic Risks to Humans 2010*, The International Agency for Research on Cancer: Lyon, France.
  21. Wiener, J., et al., *Sorption Process Using Polyamide Nanofibres to Remove Dye from Simulated Wastewater*. Nanocon 2012, 4th International Conference, 2012: p. 476-479.
  22. Ummartyotin, S. and C. Pechyen, *Role of ZnO on nylon 6 surface and the photocatalytic efficiency of methylene blue for wastewater treatment*. Colloid and Polymer Science, 2016: p. 1-8.
  23. Bagheri, H., et al., *Polypyrrole/polyamide electrospun-based sorbent for microextraction in packed syringe of organophosphorous pesticides from aquatic samples*. Journal of Separation Science, 2012. **35**(1): p. 114-120.
  24. Shi, L., et al., *Solution blowing nylon 6 nanofiber mats for air filtration*. Fibers and Polymers, 2013. **14**(9): p. 1485-1490.
  25. Kim, G.T., Y.C. Ahn, and J.K. Lee, *Characteristics of Nylon 6 nanofilter for removing ultra fine particles*. Korean Journal of Chemical Engineering, 2008. **25**(2): p. 368-372.
  26. Gao, Y., et al., *Electrospun Antibacterial Nanofibers: Production, Activity, and In Vivo Applications*. Journal of Applied Polymer Science, 2014. **131**(18).
  27. Dhineshbabu, N.R., et al., *Electrospun MgO/Nylon 6 Hybrid Nanofibers for Protective Clothing*. Nano-Micro Letters, 2014. **6**(1): p. 46-54.
  28. Dhineshbabu, N.R., P. Manivasakan, and V. Rajendran, *Hydrophobic and thermal behaviour of nylon 6 nanofibre web deposited on cotton fabric*

- through electrospinning*. *Micro & Nano Letters*, 2014. **9**(8): p. 519-522.
29. Randunu, K.M. and R.K. Marcus, *Initial Evaluation of Protein Throughput and Yield Characteristics on Nylon 6 Capillary-Channeled Polymer (C-CP) Fiber Stationary Phases by Frontal Analysis*. *Biotechnology Progress*, 2013. **29**(5): p. 1222-1229.
30. Stanelle, R.D. and R.K. Marcus, *Nylon-6 capillary-channeled polymer (C-CP) fibers as a hydrophobic interaction chromatography stationary phase for the separation of proteins*. *Analytical and Bioanalytical Chemistry*, 2009. **393**(1): p. 273-281.
31. Kugel, K., et al., *Microporous Poly(Caprolactam) Hollow Fibers for Therapeutic Affinity Adsorption*. *Journal of Membrane Science*, 1992. **74**(1-2): p. 115-129.
32. Klein, E., *Affinity membranes: a 10-year review*. *Journal of Membrane Science*, 2000. **179**(1-2): p. 1-27.
33. Zhang, H.T., et al., *Elaboration, characterization and study of a novel affinity membrane made from electrospun hybrid chitosan/nylon-6 nanofibers for papain purification*. *Journal of Materials Science*, 2010. **45**(9): p. 2296-2304.
34. Zhang, H.T., H.L. Nie, and L.M. Zhu, *Separation and purification of papain with Cibacron Blue F3GA carrying electrospun nylon/cellulose acetate nanofiber affinity membrane*. *Proceedings of 2009 International Conference on Advanced Fibers and Polymer Materials, Vols 1 and 2*, 2009: p. 567-570.
35. Leon-Santesteban, H., et al., *Pentachlorophenol sorption in nylon fiber and removal by immobilized *Rhizopus oryzae* ENHE*. *Journal of Hazardous Materials*, 2011. **190**(1-3): p. 707-712.
36. Worch, E., ed. *Adsorption Technology in Water Treatment: fundamentals, processes, and modeling*. 1st ed. 2012, Walter de Gruyter GmbH & Co. KG: Berlin/Boston.
37. Hutten, I., ed. *Handbook of Nonwoven Filter Media*. 2007, Elsevier Science & Technology Books
38. Slejko, F.L., ed. *adsorption technology*. 1st ed. 1985, Taylor & Francis: New York.
39. Suzuki, M., ed. *adsorption engineering*. 1st ed. 1990, Elsevier Science: Amsterdam.

40. Oscik, J., ed. *Adsorption*. 1st ed. 1982, Ellis Horwood: Warsaw.
41. Robinson, T., et al., *Remediation of dyes in textile effluent: a critical review on current treatment technologies with a proposed alternative*. *Bioresource Technology*, 2001. **77**(3): p. 247-255.
42. Wei, B., et al., *Adsorption Properties of Lac Dyes on Wool, Silk, and Nylon*. *Journal of Chemistry*, 2013.
43. Rowen, J.W. and R.L. Blaine, *Sorption of Nitrogen and Water Vapor on Textile Fibers*. *Industrial and Engineering Chemistry*, 1947. **39**(12): p. 1659-1663.
44. Zeng, H.Y., et al., *Lipase adsorption on woven nylon-6 membrane: Optimization, kinetic and thermodynamic analyses*. *Biocatalysis and Biotransformation*, 2014. **32**(3): p. 188-197.
45. Reuvers, N.J.W., H.P. Huinink, and O.C.G. Adan, *Plasticization lags behind water migration in nylon-6: An NMR imaging and relaxation study*. *Polymer*, 2015. **63**: p. 127-133.
46. Strnad, S., et al., *Surface properties of structural modified PA 6 fibers*. *Macromolecular Materials and Engineering*, 2002. **287**(4): p. 296-305.
47. Strnad, S., et al., *The influence of structural properties on the dye diffusion and dyeability of PA 6 fibres*. *Materials Research Innovations*, 2003. **7**(6): p. 358-365.
48. Avramova, N., *Effect of the structure on sorption and diffusion processes in polyamide 6, part 1: Activation energy and thermodynamic parameters of water Desorption in oriented and unoriented polyamide 6*. *Journal of Applied Polymer Science*, 2007. **106**(1): p. 122-129.
49. Reuvers, N., H. Huinink, and O. Adan, *Water Plasticizes Only a Small Part of the Amorphous Phase in Nylon-6*. *Macromolecular Rapid Communications*, 2013. **34**(11): p. 949-953.
50. Xia, Y.Y., et al., *Polyaniline (skin)/polyamide 6 (core) composite fiber: Preparation, characterization and application as a dye adsorbent*. *Synthetic Metals*, 2013. **175**: p. 163-169.
51. Wang, T.Y., et al., *A novel highly permeable positively charged nanofiltration membrane based on a nanoporous hyper-crosslinked polyamide barrier layer*. *Journal of Membrane Science*, 2013. **448**: p. 180-189.
52. Maryskova, M., et al., *Polyamide 6/chitosan nanofibers as support for the*

- immobilization of Trametes versicolor laccase for the elimination of endocrine disrupting chemicals*. Enzyme and Microbial Technology, 2016. **89**: p. 31-38.
53. Hekmati, A.H., et al., *Effect of nanofiber diameter on water absorption properties and pore size of polyamide-6 electrospun nanoweb*. Textile Research Journal, 2014. **84**(19): p. 2045-2055.
  54. Stachewicz, U. and A.H. Barber, *Enhanced Wetting Behavior at Electrospun Polyamide Nanofiber Surfaces*. Langmuir, 2011. **27**(6): p. 3024-3029.
  55. Shaw, D.J., *Introduction to Colloid and Surface Chemistry*. 1992: Butterworth-Heinemann.
  56. Williams, R., D.J. Shaw, and S. Biggs, *Introduction to colloid and surface chemistry*. 2007, Oxford: Butterworth-Heinemann.
  57. Stephen Brunauer, P.H.E., and Edward Teller, *Adsorption of gases in multi-molecular layers*. Journal of the American Chemical Society, 1938. **60**: p. 309-319.
  58. S. Brunauer, P.H.E., and E.Teller, *Adsorption of gases in multi-molecular layers*. Journal of the American Chemical Society, 1938. **60**: p. 309-319.
  59. Barrett, E.P., L.G. Joyner, and P.P. Halenda, *The Determination of Pore Volume and Area Distributions in Porous Substances .I. Computations from Nitrogen Isotherms*. Journal of the American Chemical Society, 1951. **73**(1): p. 373-380.
  60. Shull, C.G., *The Determination of Pore Size Distribution from Gas Adsorption Data*. Journal of the American Chemical Society, 1948. **70**(4): p. 1405-1410.
  61. Sing, K.S.W., *Adsorption methods for the characterization of porous materials*. Advances in Colloid and Interface Science, 1998. **76**: p. 3-11.
  62. Limousin, G., et al., *Sorption isotherms: A review on physical bases, modeling and measurement*. Applied Geochemistry, 2007. **22**(2): p. 249-275.
  63. P. K. Chatterjee, B.S.G., *Textile Science and Technology 13, Absorbent Technology*. first ed. 2002: Elsevier Science B. V.
  64. Ruthven, D.M., *Principles of Adsorption and Adsorption Processes*. 1984: John Wiley & Sons, Inc.
  65. HMF, F., *Over the adsorption in solution*. Z Phys Chem, 1906. **57**: p. 385-471.
  66. Wong, Y.C., et al., *Adsorption of acid dyes on chitosan - equilibrium isotherm analyses*. Process Biochemistry, 2004. **39**(6): p. 693-702.

67. Langmuir, I., *The adsorption of gases on plane surfaces of glass, mica and platinum*. J Am Chem Soc, 1918. **40**: p. 1361-403.
68. Low, M.J.D., *Kinetics of Chemisorption of Gases on Solids*. Chemical Reviews, 1960. **60**(3): p. 267-312.
69. Ho, Y.S. and G. McKay, *A comparison of chemisorption kinetic models applied to pollutant removal on various sorbents*. Process Safety and Environmental Protection, 1998. **76**(B4): p. 332-340.
70. Ho, Y.S., *Review of second-order models for adsorption systems*. Journal of Hazardous Materials, 2006. **136**(3): p. 681-689.
71. Sparks, D.L., ed. *Kinetics of reaction in pure and mixed systems, in Soil Physical Chemistry*. 1986, CRC Press: Boca Raton, Florida. 83-145.
72. Ho, Y.S. and G. McKay, *Pseudo-second order model for sorption processes*. Process Biochemistry, 1999. **34**(5): p. 451-465.
73. Nollet, H., et al., *Removal of PCBs from wastewater using fly ash*. Chemosphere, 2003. **53**(6): p. 655-665.
74. Jaycock, M.J. and G.D. Parfitt, *Chemistry of interfaces*. 1981: E. Horwood.
75. Gueu, S., et al., *Kinetics and thermodynamics study of lead adsorption on to activated carbons from coconut and seed hull of the palm tree*. International Journal of Environmental Science and Technology, 2007. **4**(1): p. 11-17.
76. (SCENIHR), S.C.O.E.A.N.I.H.R. *The appropriateness of existing methodologies to assess the potential risks associated with engineered and adventitious products of nanotechnologies* 2006; Available from: [http://ec.europa.eu/health/ph\\_risk/committees/04\\_scenihhr/docs/scenihhr\\_o\\_003b.pdf](http://ec.europa.eu/health/ph_risk/committees/04_scenihhr/docs/scenihhr_o_003b.pdf).
77. York, C.P.S.a.t.U.o. *Nanomaterials*. 2013 18th March 2013; Available from: <http://www.essentialchemicalindustry.org/materials-and-applications/nanomaterials.html>.
78. Lindsay, R.B. and D. Haar, *Men of Physics Lord Rayleigh—The Man and His Work: The Commonwealth and International Library: Selected Readings in Physics*. 2013: Elsevier Science.
79. J., Z., *The electrical discharge from liquid points, and a hydrostatic method of measuring the electric intensity at their surfaces*. Phys. Rev., 1914. **3**: p. 69-91.

80. A., F., *Process and apparatus for preparing artificial threads*. 1934: U.S.A.
81. Taylor, G., *Electrically Driven Jets*. Proceedings of the Royal Society of London Series a-Mathematical and Physical Sciences, 1969. **313**(1515): p. 453-&.
82. Bhardwaj, N. and S.C. Kundu, *Electrospinning: A fascinating fiber fabrication technique*. Biotechnology Advances, 2010. **28**(3): p. 325-347.
83. Huang, Z.M., et al., *A review on polymer nanofibers by electrospinning and their applications in nanocomposites*. Composites Science and Technology, 2003. **63**(15): p. 2223-2253.
84. Khenoussi, N., L. Schacher, and D.C. Adolphe, *Nanofiber Production: Study and Development of Electrospinning Device*. Experimental Techniques, 2012. **36**(2): p. 32-39.
85. Nidal Hilal, M.K., Chris J. Wright, ed. *Membrane Modification Technology and Applications*. 2012, Taylor & Francis Group, LLC.
86. Matulevicius, J., et al., *Design and Characterization of Electrospun Polyamide Nanofiber Media for Air Filtration Applications*. Journal of Nanomaterials, 2014.
87. Bagheri, H., S. Asgari, and H. Piri-Moghadam, *On-line Micro Solid-Phase Extraction of Clodinafop Propargyl from Water, Soil and Wheat Samples Using Electrospun Polyamide Nanofibers*. Chromatographia, 2014. **77**(9-10): p. 723-728.
88. Yin, G.B., et al., *The Electrospun Polyamide 6 Nanofiber Membranes Used as High Efficiency Filter Materials: Filtration Potential, Thermal Treatment, and Their Continuous Production*. Journal of Applied Polymer Science, 2013. **128**(2): p. 1061-1069.
89. Cao, Y., et al., *Determination of Phthalates Esters in Edible Oil by High Performance Liquid Chromatography with Solid-membrane Extraction Based on Electrospun Nylon 6 Nanofibrous Membrane*. Chinese Journal of Analytical Chemistry, 2013. **41**(12): p. 1837-1843.
90. Zhang, M., et al., *Size-dependent melting point depression of nanostructures: Nanocalorimetric measurements*. Physical Review B, 2000. **62**(15): p. 10548-10557.
91. Lai, S.L., et al., *Size-dependent melting properties of small tin particles:*

- Nanocalorimetric measurements*. Physical Review Letters, 1996. **77**(1): p. 99-102.
92. Initiative, N.N. *What's so special about nanoscale?* ; Available from: <http://www.nano.gov/nanotech-101/special>.
93. Hilal, N., M. Khayet, and C.J. Wright, *Membrane Modification: Technology and Applications*. 2016: CRC Press.
94. Hosokawa, M., et al., *Nanoparticle Technology Handbook*. 2007: Elsevier Science.
95. Elkhatib, E.A., A.M. Mahdy, and K.A. Salama, *Green synthesis of nanoparticles by milling residues of water treatment*. Environmental Chemistry Letters, 2015. **13**(3): p. 333-339.
96. Mendez-Medrano, M.G., et al., *Surface Modification of TiO<sub>2</sub> with Ag Nanoparticles and CuO Nanoclusters for Application in Photocatalysis*. Journal of Physical Chemistry C, 2016. **120**(9): p. 5143-5154.
97. Kubac, L., et al., *Photoactive Tio<sub>2</sub> and Its Application for Self-Cleaning Fabrics with Long-Term Stability*. Nanocon 2013, 5th International Conference, 2014: p. 351-356.
98. Li, W., et al., *Digital image colorimetry coupled with a multichannel membrane filtration-enrichment technique to detect low concentration dyes*. Analytical Methods, 2016. **8**(14): p. 2887-2894.
99. Mir, H., A.G. Ahangar, and N. Mir, *Superior performance of dye-sensitized versus conventional TiO<sub>2</sub> nanoparticles for promoting germination and early growth of Barley: From photovoltaic to biotechnological application*. Journal of Nano Research, 2016. **35**: p. 77-91.
100. Gupta, V.K., et al., *Adsorptive removal of dyes from aqueous solution onto carbon nanotubes: A review*. Advances in Colloid and Interface Science, 2013. **193**: p. 24-34.
101. EL-Mekkawi, D.M., et al., *Photocatalytic activity evaluation of TiO<sub>2</sub> nanoparticles based on COD analyses for water treatment applications: a standardization attempt*. International Journal of Environmental Science and Technology, 2016. **13**(4): p. 1077-1088.
102. Saharan, P., et al., *Ultra fast and effective treatment of dyes from water with the synergistic effect of Ni doped ZnO nanoparticles and ultrasonication*.



- Ultrasonics Sonochemistry, 2015. **22**: p. 317-325.
103. Chladova, A., J. Wiener, and M. Polakova, *Testing the Photocatalytic Activity of TiO<sub>2</sub> Nanoparticles with Potassium Permanganate Solution*. Nanocon 2011, 2011: p. 527-531.
  104. Vinodgopal, K., D.E. Wynkoop, and P.V. Kamat, *Environmental photochemistry on semiconductor surfaces: Photosensitized degradation of a textile azo dye, acid orange 7, on TiO<sub>2</sub> particles using visible light*. Environmental Science & Technology, 1996. **30**(5): p. 1660-1666.
  105. Linsebigler, A.L., G.Q. Lu, and J.T. Yates, *Photocatalysis on TiO<sub>2</sub> Surfaces - Principles, Mechanisms, and Selected Results*. Chemical Reviews, 1995. **95**(3): p. 735-758.
  106. Hashimoto, K., H. Irie, and A. Fujishima, *TiO<sub>2</sub> photocatalysis: A historical overview and future prospects*. Japanese Journal of Applied Physics Part 1-Regular Papers Brief Communications & Review Papers, 2005. **44**(12): p. 8269-8285.
  107. Nakata, K. and A. Fujishima, *TiO<sub>2</sub> photocatalysis: Design and applications*. Journal of Photochemistry and Photobiology C-Photochemistry Reviews, 2012. **13**(3): p. 169-189.
  108. Fujishima, A., X.T. Zhang, and D.A. Tryk, *TiO<sub>2</sub> photocatalysis and related surface phenomena*. Surface Science Reports, 2008. **63**(12): p. 515-582.
  109. Fujishima, A. and X.T. Zhang, *Titanium dioxide photocatalysis: present situation and future approaches*. Comptes Rendus Chimie, 2006. **9**(5-6): p. 750-760.
  110. Gupta, S. and M. Tripathi, *A review of TiO<sub>2</sub> nanoparticles*. Chinese Science Bulletin, 2011. **56**(16): p. 1639-1657.
  111. Ibhaddon, A.O. and P. Fitzpatrick, *Heterogeneous Photocatalysis: Recent Advances and Applications*. Catalysts, 2013. **3**(1): p. 189-218.
  112. Fox, M.A. and M.T. Dulay, *Heterogeneous Photocatalysis*. Chemical Reviews, 1993. **93**(1): p. 341-357.
  113. Mahmoodi, N.M. and M. Arami, *Degradation and toxicity reduction of textile wastewater using immobilized titania nanophotocatalysis*. Journal of Photochemistry and Photobiology B-Biology, 2009. **94**(1): p. 20-24.
  114. Styliidi, M., D.I. Kondarides, and X.E. Verykios, *Mechanistic and kinetic study*

- of solar-light induced photocatalytic degradation of Acid Orange 7 in aqueous TiO<sub>2</sub> suspensions*. International Journal of Photoenergy, 2003. **5**(2): p. 59-67.
115. Bandara, J., J.A. Mielczarski, and J. Kiwi, 2. *Photosensitized degradation of azo dyes on Fe, Ti, and Al oxides. Mechanism of charge transfer during the degradation*. Langmuir, 1999. **15**(22): p. 7680-7687.
116. Cheng, C., et al., *Mesoporous silica-based carbon dot/TiO<sub>2</sub> photocatalyst for efficient organic pollutant degradation*. Microporous and Mesoporous Materials, 2016. **226**: p. 79-87.
117. Sheidaei, B. and M.A. Behnajady, *Efficiency of a Photoreactor Packed with Immobilized Titanium Dioxide Nanoparticles in the Removal of Acid Orange 7*. Water Environment Research, 2016. **88**(5): p. 449-457.
118. Hajjaji, W., et al., *Aqueous Acid Orange 7 dye removal by clay and red mud mixes*. Applied Clay Science, 2016. **126**: p. 197-206.
119. Konstantinou, I.K. and T.A. Albanis, *TiO<sub>2</sub>-assisted photocatalytic degradation of azo dyes in aqueous solution: kinetic and mechanistic investigations - A review*. Applied Catalysis B-Environmental, 2004. **49**(1): p. 1-14.
120. Lee, S., et al., *Natural organic matter fouling due to foulant-membrane physicochemical interactions*. Desalination, 2007. **202**(1-3): p. 377-384.
121. Kim, D.S., J.S. Kang, and Y.M. Lee, *The influence of membrane surface properties on fouling in a membrane bioreactor for wastewater treatment*. Separation Science and Technology, 2004. **39**(4): p. 833-854.
122. Subramani, A. and E.M.V. Hoek, *Biofilm formation, cleaning, re-formation on polyamide composite membranes*. Desalination, 2010. **257**(1-3): p. 73-79.
123. Konstantinou, I.K. and T.A. Albanis, *Worldwide occurrence and effects of antifouling paint booster biocides in the aquatic environment: a review*. Environment International, 2004. **30**(2): p. 235-248.
124. Yun, J., et al., *Photocatalytic treatment of acidic waste water by electrospun composite nanofibers of pH-sensitive hydrogel and TiO<sub>2</sub>*. Materials Letters, 2010. **64**(22): p. 2431-2434.
125. Li, Y., K. Wu, and I. Zhitomirsky, *Electrodeposition of composite zinc oxide-chitosan films*. Colloids and Surfaces a-Physicochemical and Engineering Aspects, 2010. **356**(1-3): p. 63-70.
126. Maximous, N., et al., *Preparation, characterization and performance of*

- Al<sub>2</sub>O<sub>3</sub>/PES membrane for wastewater filtration*. Journal of Membrane Science, 2009. **341**(1-2): p. 67-75.
127. Taha, A.A., *Direct synthesis of mesostructured carbon nanofibers decorated with silver-nanoparticles as a multifunctional membrane for water treatment*. Advances in Natural Sciences-Nanoscience and Nanotechnology, 2015. **6**(4).
128. Xiao, J.L., et al., *Simultaneous regulation of morphology, crystallization, thermal stability and adsorbability of electrospun polyamide 6 nanofibers via graphene oxide and chemically reduced graphene oxide*. Rsc Advances, 2016. **6**(47): p. 41392-41403.
129. Wiener, J., S. Shahidi, and M.M. Goba, *Laser deposition of TiO<sub>2</sub> nanoparticles on glass fabric*. Optics and Laser Technology, 2013. **45**: p. 147-153.
130. Sakkas, V.A., et al., *Metolachlor photocatalytic degradation using TiO<sub>2</sub> photocatalysts*. Applied Catalysis B-Environmental, 2004. **49**(3): p. 195-205.
131. Murray, C.A. and S.A. Parsons, *Comparison of AOPs for the removal of natural organic matter: performance and economic assessment*. Water Science and Technology, 2004. **49**(4): p. 267-272.
132. Hoffmann, M.R., et al., *Environmental Applications of Semiconductor Photocatalysis*. Chemical Reviews, 1995. **95**(1): p. 69-96.
133. Daneshvar, N., D. Salari, and A.R. Khataee, *Photocatalytic degradation of azo dye acid red 14 in water: investigation of the effect of operational parameters*. Journal of Photochemistry and Photobiology a-Chemistry, 2003. **157**(1): p. 111-116.
134. Chong, M.N., et al., *Recent developments in photocatalytic water treatment technology: A review*. Water Research, 2010. **44**(10): p. 2997-3027.
135. Kaneko, M. and I. Okura, *Photocatalysis: Science and Technology*. 2002: Springer Berlin Heidelberg.
136. Pekakis, P.A., N.P. Xekoukoulotakis, and D. Mantzavinos, *Treatment of textile dyehouse wastewater by TiO<sub>2</sub> photocatalysis*. Water Research, 2006. **40**(6): p. 1276-1286.
137. El-Bindary, A.A., et al., *Adsorption of Acid Yellow 99 by polyacrylonitrile/activated carbon composite: Kinetics, thermodynamics and isotherm studies*. Journal of Molecular Liquids, 2014. **197**: p. 236-242.

138. Juang, R.S., F.C. Wu, and R.L. Tseng, *The ability of activated clay for the adsorption of dyes from aqueous solutions*. Environmental Technology, 1997. **18**(5): p. 525-531.
139. Sharma, P., et al., *Kinetics and Adsorption Behavior of the Methyl Blue at the Graphene Oxide/Reduced Graphene Oxide Nanosheet-Water Interface: A Comparative Study*. Journal of Chemical and Engineering Data, 2013. **58**(12): p. 3477-3488.
140. Singh, D., *Studies of the adsorption thermodynamics of oxamyl on fly ash*. Adsorption Science & Technology, 2000. **18**(8): p. 741-748.
141. Goel, N.K., et al., *Development of adsorbent from Teflon waste by radiation induced grafting: Equilibrium and kinetic adsorption of dyes*. Journal of Hazardous Materials, 2011. **193**: p. 17-26.
142. Tsuruta, M. and A. Koshimo, *Steam and Heat Setting of Nylon 6 Fiber .2. Effects of Heat Setting of Nylon 6 Fiber on Dyeability and Fine Structure*. Journal of Applied Polymer Science, 1965. **9**(1): p. 11-&.

## RESEARCH OUTPUTS

### Journal Publication:

1. Wang, Y., Wiener, J., Sorption kinetics for the removal of dyes from effluent onto polyamide 6 nanofibrous assembly, submitted.
2. Wang, Y., Wiener, J., Militký, J., Adsorption of Acid Blue 41 by polyamide 6 nanofibers: Isotherms, kinetics and thermodynamics studies, submitted.
3. Wang, Y., Wiener, J., Militký, J., Mishra, R., Zhu, G., Ozone effect on the properties of Aramid fabric, (2016) *Autex Research Journal*, accepted. *Impact factor: 0.460*
4. Wang, Y., Wiener, J., Zhu, G. Langmuir isotherm models applied to the sorption of acid dyes from effluent onto polyamide nanofibers, (2013) *Autex Research Journal*, 13 (3), pp. 95-98. *Impact factor: 0.460*

### Conference Publication:

5. Wang, Y., Wiener, J. Dynamic sorption process of acid dye on nanofibers assembly with TiO<sub>2</sub> nanophotocatalysis, (2016) NANOCON 2016, 8th International Conference, accepted.
6. Wang, Y., Wiener, J. Kinetics study for the removal of acid dyes from aqueous solutions using polyamide nanofibrous membranes, (2016) Aachen-Dresden-Denkendorf International Textile Conference 2016, accepted.
7. Wang, Y., Wiener, J., Surface modification of Polyamide 6 nanofibers with steam, (2016) Workshop B Iávoda 2016, 22-25.09.2016, Liberec, Czech Republic.
8. Wang, Y., Marek, J., Wiener, J., Study on the acid dye removal by polyamide 6 nanofibrous membrane, (2015) NANOCON 2015, 7th International Conference. *Thomson Reuter, Indexed in ISI Web of Knowledge.*
9. Wang, Y., Wiener, J., Zhu, G., Huang J. Sorption kinetics analysis of acid dye on polyamide 6 nanofibers under different pH, (2014) STRUTEX 20, 1-2, 12, 2014.
10. Wang, Y., Wiener, J., Zhu, G. Sorption isotherm study on two polyamide nanofibrous membranes, (2014) NANOCON 2014, 6th International Conference,

- pp. 405-410. *Thomson Reuter, Indexed in ISI Web of Knowledge.*
11. Wang, Y., Wiener, J., Stelmakh, A., Dye filtration properties of polyamide 6 nanofibrous membrane, (2014) 16-19, 9, 2014, Rokytnice nad Jizerou, czech republic.
  12. Wang, Y., Wiener, J., Zhu, G., Huang, J., Characterization of polyamide 6 membrane by BET theory, (2014) ICCE-22, 13-19, 7, 2014, Malta.
  13. Wang, Y., Wiener, J., Zhu, G., Huang, J., Constant online apparatus to investigate filtration, (2014) Fiber Society Spring 2014 Technical Conference: Fibers for Progress.
  14. Wang, Y., Wiener, J., Zhu, G., Sorption property of polyamide nanofibrous membrane on dyestuff for purifying wastewater, (2013) NANOCON 2013, 5th International Conference, pp. 329-333. *Thomson Reuter, Indexed in ISI Web of Knowledge.*
  15. Wang, Y., 3D Aramid fabrics for composite reinforcement, (2013) 18-20.09.2013, Rokytnice nad Jizerou, Czech Republic.
  16. Wang, Y., Wiener, J., Zhu, G., Huang, J., Venkataraman, M., Apparatus Assembling for Continual Filtration Study of Filter Membrane. 8<sup>th</sup> TEXSCI, 23-25.09.2013, Liberec, Czech Republic.
  17. Wang, Y., Wiener, J., Mishra, R., Zhu, G., Venkataraman, M., Huang, J., Militký, J., Study on Ozone Treatment of Aramid Fabrics. 8<sup>th</sup> TEXSCI, 23-25.09.2013, Liberec, Czech Republic.
  18. Wang, Y., Zhu, G., Mishra, R., Militký, J., The application of fly ash nanoparticles in composites reinforced by glass fabrics with different structures. 6<sup>th</sup> AESP, 02-06.06.2013, Wuhan, China. (*Poster Prize*)
  19. Wang, Y., Venkataraman, M., Zhu, G., Mishra, R., Wiener, J., Militký, J., Effect of Alkali Treatment on Thermal Insulation of PET Fabric. STRUTEX, 3-4, 12. 2012. Liberec, Czech republic, EU. ISBN: 978-80-7372-913-4. p80-81.
  20. Wang, Y., Venkataraman, M., Mishra, R., Militký, J., Study on Impact Behavior of Textile Structures and Composites. STRUTEX, 3-4, 12. 2012. Liberec, Czech

republic, EU. ISBN: 978-80-7372-913-4. p170-171.

**Book Chapter:**

21. Mishra, R., Militky, J., Baheti, V., Huang, J., Kale, B., Venkataraman, M., Bele, V., Arumugam, V., Zhu, G., Wang, Y. The production, characterization and applications of nanoparticles in the textile industry, (2014) *Textile Progress*, 46 (2), pp. 133-226.